IDŐJÁRÁS

QUARTERLY JOURNAL
OF THE HUNGARIAN METEOROLOGICAL SERVICE

CONTENTS

VOL. 123 ∗ NO. 4 ∗ OCTOBER – DECEMBER 2019

IDŐJÁRÁS

Quarterly Journal of the Hungarian Meteorological Service

Editorial Office: Kitaibel P.u. 1, H-1024 Budapest, Hungary
P.O. Box 38, H-1525 Budapest, Hungary
E-mail: journal.idojaras@met.hu
Fax: (36-1) 346-4669

Indexed and abstracted in Science Citation Index Expanded[TM] and
Journal Citation Reports/Science Edition
Covered in the abstract and citation database SCOPUS®
Included in EBSCO's databases

Subscription by mail:
IDŐJÁRÁS, P.O. Box 38, H-1525 Budapest, Hungary
E-mail: journal.idojaras@met.hu

IDŐJÁRÁS

Validation of RegCM regional and HadGEM global climate models using mean and extreme climatic variables

Ildikó Pieczka[1,*], **Judit Bartholy**[1,2], **Rita Pongrácz**[1,2], and **Karolina Szabóné André**[1]

[1] *Department of Meteorology, Eötvös Loránd University*
Pázmány P. s. 1/A, H-1117, Budapest, Hungary

[2] *Eötvös Loránd University, Faculty of Science,*
Excellence Center,
Brunszvik u. 2, H-2462, Martonvásár, Hungary

*Corresponding Author E-mail: pieczka@nimbus.elte.hu

(Manuscript received in final form October 2, 2018)

Abstract— The horizontal resolution of global climate models (GCMs) is still too coarse to evaluate regional climatic differences, therefore, to analyze regional environmental changes, it is essential to downscale the GCM simulation results. One of the methods widely and most often used for this purpose is dynamical downscaling. In the present paper we examine the ability of a specific global (HadGEM2-ES) and a specific regional climate model (RegCM) to describe present climatic conditions in different geographical areas within the Med-CORDEX domain. Our main goal with this validation is to inform researchers, who are planning to complete climate change impact studies about the major characteristics of the simulation outputs, serving as important input in such studies. So we analyzed annual and seasonal mean fields, mean error fields relative to the reference measurements, and selected climate indices. On the basis of the results, dynamical downscaling generally cools the HadGEM results, which depends on the distance from the ocean, and orography. A clear improvement can be recognized in the root-mean-square error (RMSE) of temperature indices when using finer resolution. Moreover, dynamical downscaling with higher resolution often increases the precipitation in mountains. Furthermore, in order to quantify the potential added value of RegCM simulations, a complex measure was introduced to take into account both the magnitude and spatial extent of bias. The analysis shows a general improvement in the cold-related indices in Central Europe and all temperature-related climate indices in Western Europe. The influence of model resolution is usually so strong, that it results in the underestimation of precipitation indices changing into overestimation and vice versa.

Key-words: climate model, validation, added value, RegCM, HadGEM2-ES, extreme indices, Europe, Hungary

1. Introduction

Although the resolution of climate models is continuously improving as computational capacity increases, the differences between the outputs of global climate models (GCMs) and regional climate models (RCMs) are still clearly visible. It is important to note that these differences are not exclusively due to their different resolutions (*Di Luca et al.*, 2015; *Flaounas et al.,* 2013; *Torma et al.,* 2015). Besides the evident spatial difference, another important factor is the different ultimate goals of their uses: global models are designed to simulate large-scale processes (e.g., midlatitude cyclones, anticyclones), whereas regional models should provide more details related to smaller scale phenomena (as the use of finer grids allows explicit representation of small-scale processes, e.g., mesoscale circulations, specific hydrodynamic instabilities, surface-forced processes, and the rain-shadow effect of mountains). To study regional scale changes, it is essential to downscale the GCMs, even if this might introduce additional uncertainties into the system of physical modeling through the final selection of the methods, models, parameterizations used. Either statistical or dynamical approaches, or their combination, can be used to downscale the GCM results (*Maraun et al.,* 2015), and in this paper we apply dynamical downscaling (*Giorgi*, 1990).

A general improvement of model performance can be seen through the consecutive generation of climate models (from their initial versions to the most recent developments), which is partly due to (i) the generally higher horizontal resolution that up-to-date computing capacities allow, and (ii) the associated improvement of the representation of meteorological processes in the models. Among the numerous possible measures of model quality, the most often used measure is the simple bias, when several models are considered then the difference between the multi-model mean and a reference provides an overall quick evaluation of the set of models. The multi-model mean of the annual mean temperature of the CMIP5 (Coupled Model Intercomparison Project Phase 5, which compares global coupled ocean-atmosphere general circulation models, cmip.llnl.gov) historical experiments (i.e., using the observed records of atmospheric composition including the anthropogenic influences, and the time series of solar and volcanic forcings as boundary conditions) in the Med-CORDEX area (for the 1980–2005 period) agrees well with the reanalysis (typically within 1 °C, while inconsistency within reanalysis datasets is below 0.5 °C, see *Fig. 9.2* in *IPCC*, 2013). The bias of the seasonal cycle amplitude is relatively small for Central Europe, but has a southwest-northeast gradient as larger biases correspond to the areas of large seasonal amplitude (*Fig. 9.3* in *IPCC*, 2013). Models tend to dry out the soil too effectively at high temperatures, which results in a generally enhanced warm bias in the warmer months in the cases of RCMs, and in the majority of CMIP3 and CMIP5 model simulations (- in *IPCC*, 2013). The problem may be related to the broadly used

soil data in climate models as suggested by *Anders* and *Rockel* (2009). The simulation of large-scale patterns of precipitation has somewhat improved since the CMIP3 ensemble (e.g., *Fig. 9.6* in *IPCC*, 2013; *Joetzjer et al.,* 2013; *Knutti et al.*, 2013). However, at regional scales, precipitation is still not simulated in CMIP5 as well as it is in RCMs, because the regional scale precipitation strongly depends on various local parameters. These are represented much better in RCMs than in GCMs (i.e., finer topography, better land use/land cover representation, and more precise convection parameterization are available in RCMs). Nevertheless, the well-known large-scale features are reproduced well by the multi-model mean of GCM simulations. Considering extreme climatic conditions, both temperature and precipitation extremes (e.g., 20-year return values) are simulated relatively well by the CMIP3 and CMIP5 models. Moreover, none of the major climate quantities (e.g., sea ice extent, carbon sink, temperature at different atmospheric levels, etc.) show degradation from CMIP3 to CMIP5. Besides GCM development, the capability of RCMs to describe the past and present climatic conditions in Europe, and their potential added value compared to the global models is extensively studied. There is definitely high confidence that downscaling adds value when considering small-scale phenomena, extreme events, or complex topography (*IPCC*, 2013). Examples include the improved simulation of large-scale precipitation patterns for East Asia (*Gao et al.*, 2012), convective precipitation (*Rauscher et al.*, 2010), near-surface temperature (*Feser*, 2006) and wind (*Kanamaru* and *Kanamitsu*, 2007), precipitation (*Lucas-Picher et al.*, 2012), coastal climate features (*Winterfeldt* and *Weisse*, 2009; *Winterfeldt et al.*, 2011; *Kawazoe* and *Gutowski*, 2013; *Vautard et al.*, 2013), storms (*Donat et al.*, 2010), midlatitude cyclones (*Cavicchia* and *Storch*, 2011), cutoff cyclones (*Grose et al.*, 2012) and polar lows (*Zahn* and *von Storch*, 2008), or higher statistical moments of the water budget (*Bresson* and *Laprise*, 2011). RCMs can also improve the large-scale circulation with respect to that inherent in the boundary conditions (*Veljovic et al.,* 2010).

Due to the large amount of generated data, researchers make choices when presenting their work: papers usually focus on specific features (e.g., on cyclogenesis in the Mediterranean by *Flaounas et al.,* 2013) or sub-regions (e.g., the Alps in *Torma et al.,* 2015). Another usual approach is to study several larger regions via an ensemble of numerous individual simulations (e.g., *Giorgi et al.,* 2012; *Coppola et al.,* 2014). In this case the diverse characteristics of the simulation results for different smaller subregions within the larger regions are only roughly described.

In this paper we compare and analyze a GCM simulation and a GCM-driven RCM run covering the Med-CORDEX area (defined in *Somot et al*., 2012), and validate their outputs focusing on European sub-regions for present climatic conditions. The representation of topography in the models over the

area of interest (in the case of the regional model, after removing the buffer zone from the integration domain) can be seen in *Fig. 1*. For detailed regional scale analysis, four subregions are defined within the Med-CORDEX domain: Western, Eastern, Southern, and Central Europe, as seen in *Fig. 1*. They represent regions with different climate characteristics due to their geographical locations and orographical features (i.e., oceanic, continental, Mediterranean climate, and their 'mixture', respectively). To provide a general picture, first mean temperature and precipitation outputs are validated, and then we continue with an analysis of climate indices.
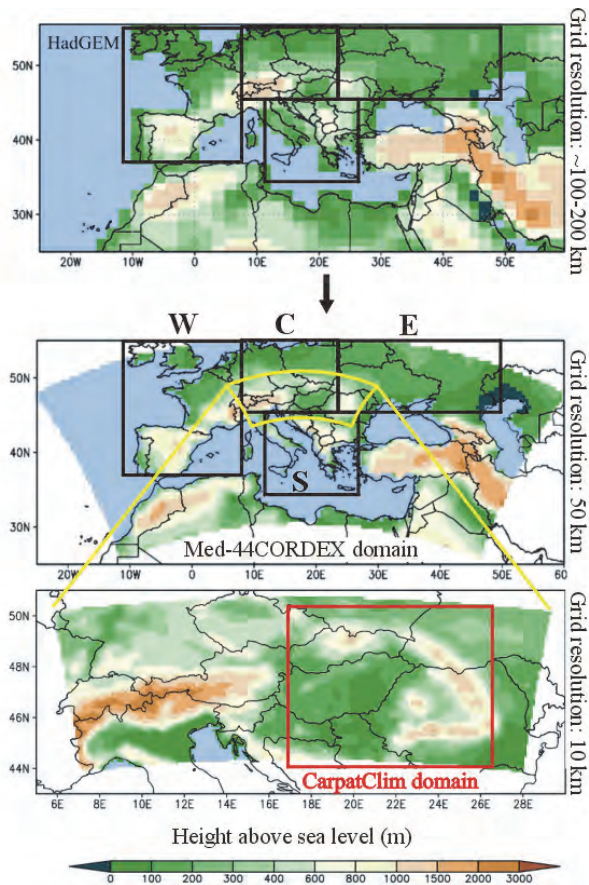
Fig. 1. Topography of the models for the domain of interest: HadGEM2-ES (top); RegCM4.3 with 50 km resolution (RegCM4.3_BATS_50km), Med-CORDEX domain (middle); RegCM4.3 with 10 km resolution (RegCM4.3_BATS_10km), Central European domain (bottom). The black rectangles represent the selected areas (Western, Central, Eastern and Southern Europe), the yellow polygon and the red rectangle represent the domain for the nested run, and the Carpatclim domain, respectively.

Afterwards, we proceed with a focus on our region of interest: we compare model outputs of a double-nested 10 km resolution simulation to the fine resolution Carpatclim database for Hungarian gridpoints, and we discuss the influence of resolution on the outputs across a chain of model simulations. The ultimate goal of the paper is to describe the weaknesses and strengths of our model simulation (performed for the past), and which may become one of the four candidate RCMs (*Krüzselyi et al.,* 2011), which were adapted and run in Hungary, when completing future national impact studies. The experiments completed with a newer version of the RegCM serve as the input of such impact studies (e.g., in hydrological studies as presented in *Kis et al.,* 2017). Both historical and scenario runs are available online (http://nater.mfgi.hu/en) for such studies in the framework of the NAGIS (National Adaptation Geographical Information System). Thus, the target audience of the paper includes researchers focusing on various climate change impacts, e.g., hydrological consequences, agricultural modeling, forestry, ecology, urban planning, etc. For such a wide range of users, the present open access journal is an ideal source of information at the start of their studies.

2. Data and methods

Our simulation was carried out using RegCM4, a limited-area, hydrostatic, compressible, sigma-p vertical coordinate model maintained at the ICTP (International Centre for Theoretical Physics), Trieste (*Elguindi et al.,* 2011). According to the user guide (*Elguindi et al.,* 2011), RegCM can use initial and lateral boundary conditions (ICBCs) from the following CMIP5 models: HadGEM, MPI, GFDL, Canadian model, EC-Earth, IPSL, EH5OM. We selected just one of these GCMs due to time and storage constraints. The entire experiment covered the period 1950–2005 with ICBCs from the HadGEM2-ES (Hadley Centre Global Environment Model version 2, Earth-System configuration, *Collins et al.,* 2011) GCM, taking historical forcings (*Jones et al.,* 2011) into account (i.e., using the historical record of greenhouse gases, aerosols, solar and volcanic changes).

Elguindi et al. (2014) found that HadGEM2-ES is characterized by a relatively good level of performance among CMIP5 models for most regions (including the Mediterranean region), which makes it a good choice for use as a driving GCM in our study. Moreover, it is a relatively high sensitivity model compared to the others, which is its advantage in use in climate change studies. This advantage is more obvious when using this climate model for estimating future climate conditions. However, since climate change studies require a reference period from the past with the same model setup, models sensitive to anthropogenic radiation forcing due to greenhouse gas concentration increase should be analyzed for the historical runs.

The atmospheric component of HadGEM2-ES uses a horizontal latitude and longitude resolution of 1.25°×1.875° with 38 vertical levels (*Collins et al.,* 2011). The oceanic component has a resolution of 1° (increasing to 1/3° at the equator) and 40 vertical levels (*Collins et al.,* 2011). HadGEM2-ES represents interactive land and ocean carbon cycles and dynamic vegetation, moreover, it employs an interactive tropospheric chemistry scheme (*Jones et al.,* 2011). The model timestep is 30 min (in case of the atmosphere and land components) and 1 h (in case of the ocean component).

Our region of interest is the Med-CORDEX domain (more specifically, the Carpathian Basin), which is the smallest among all the CORDEX domains. Here, we analyze the extent to which the RegCM is able to refine the results of the HadGEM2-ES, and the differences between the simulations using different resolutions.

2.1. Description of the RegCM settings

The default Med-CORDEX project settings were used at 50 km horizontal resolution (*Somot et al.,* 2012), which were provided by the ICTP, and the participants agreed to change only one parameter or method at a time. Our contribution to Med-CORDEX was to use RegCM with the activation of the subgrid BATS scheme (Biosphere-atmosphere Transfer Scheme), hereinafter referred to as RegCM4.3_BATS_50km. This means that the land surface processes are modeled by BATS version 1e (*Dickinson et al.,* 1993) with the treatment for subgrid variability of topography, and land cover is determined using a mosaic-type approach (*Giorgi et al.,* 2003). Each grid cell is divided into 25 subgrid cells, which results in a 10 km × 10 km land surface grid cell for intermediate calculations. This is thought to improve the model performance while keeping the computational time shorter than that required for a finer resolution model run, since only surface physics is calculated on the fine grid, but the calculations of atmospheric processes keep the coarser, original grid.

Comparing the outputs of the RegCM4.3_BATS_50km simulation to the default ICTP simulation (which does not activate the subgrid BATS scheme), the difference can be considered relatively small, mostly below 1 °C for temperature, and 15 mm/month for precipitation. However, the activation of the scheme results in slight differences, which depend on the season. In general, our simulation is a little warmer than that of the ICTP's (downloaded from https://www.medcordex.eu/ *Coppola et al.,* 2014), except in summer, when the Apennine Peninsula and the eastern regions appear to be somewhat colder. Furthermore, the precipitation difference between the two simulations on the Apennine Peninsula in summer increases to 15–30 mm/month, so our model run with the activated subgrid BATS scheme produces more precipitation.

For the second part of the study, a 10 km horizontal resolution RegCM simulation (hereinafter referred to as RegCM4.3_BATS_10km) nested into the previously described RegCM4.3_BATS_50km simulation was performed over a Central European domain (*Fig. 1*, bottom) with identical parameterization settings (which in this case means 2 km × 2 km surface tiles). RegCM was run with the mixed cumulus scheme, i.e., the MIT-Emanuel approximation (*Emanuel*, 1991; *Emanuel* and *Zivkovic-Rothman*, 1999) is used above sea surface and the *Grell* (1993) above land surface with the closure of *Fritsch* and *Chappell* (1980). The region-specific comparison of the results using the different parametrization schemes of convective processes and their detailed descriptions are presented in *Pieczka et al.* (2017).

2.2. Validation data

We use the E-OBS gridded daily database (*Haylock et al.,* 2008) to validate the ability of the models to describe present climatic conditions. This database is a gridded time-series dataset covering the period 1950–2016 for the area of 25°N–75°N, 40°W–75°E at 0.25° horizontal resolution, and contains several meteorological variables. A detailed comparison of E-OBS to other regional datasets can be found in *Prein* and *Gobiet* (2017), who highlight the uneven geographical distribution of stations included in the interpolation of available data and the production of the gridded datasets. The lack of stations can generate further problems during validation, especially in precipitation-related variables, and in the eastern European countries, including Hungary.

For the validation of the RegCM4.3_BATS_10km, we decided to use the Carpatclim data, which is a high resolution homogeneous gridded database covering the period 1961–2010 for the Carpathian Region with 0.1° horizontal resolution, and containing all the major surface meteorological variables (*Szalai et al*., 2013; *Spinoni et al*., 2015). Daily temperature (min, mean, max) and precipitation datasets were downloaded from the Carpatclim portal for the validation domain (i.e., 44°N–50°N, 17°E–27°E) and compared to the simulated values. The density of stations used for the production of the gridded dataset is five-fold of that in the E-OBS (*Prein* and *Gobiet*, 2017).

The 1986–2005 time frame covers 20 years instead of 30 years, which is the standard length of climate normals. The use of 20-year-long periods can already be considered long enough to form a climatological sample (e.g., *Arguez* and *Vose*, 2011; *Arguez et al.,* 2013). Moreover, 1986–2005 is used for the sake of consistency with the latest Assessment Report of the Intergovernmental Panel on Climate Change (e.g., Chapter 12 of *IPCC*, 2013).

3. Results and discussion

Traditional tools for evaluating the models' ability to describe regional climatic conditions include the statistical analysis of (i) annual and seasonal mean fields and mean error fields relative to the reference measurements, and (ii) climate indices. Here, we focus on temperature and precipitation as being the two most often used climatic elements in determining the local conditions. First, validation for the mean temperature and precipitation is discussed, and then validation of some selected climate indices is presented.

3.1. Validation of the mean values of temperature and precipitation

The spatial distribution of modeled annual and seasonal mean temperature and precipitation data (*Figs. 2* and *3*, respectively) is similar to that of the observed data. However, locally some differences can be identified, e.g., in the temperature values of the Alps among different datasets in winter, and in Eastern Europe in summer, and there are differences in the seasonal precipitation values of the Alps and over Turkey among different datasets. More specifically, the detailed comparison of regional bias is summarized in *Table 1*, from which the following regions can be highlighted, where both the temperature and precipitation bias decreased overall from the HadGEM to the RegCM simulations: the southern part of the British Isles, North France, the North European Plain, the Carpathian Basin (except in summer). Nevertheless, in other regions (e.g., in the Iberian Peninsula) the bias increased substantially. The amplitude of the simulated annual temperature cycle is more intense, especially in the global model: summer temperature is overestimated, while winter temperature is underestimated over most of the entire domain (*Fig. 4*). The application of RegCM generally reduces negative bias in winter, and transforms the structure of the error pattern in summer: the southern part of Western Europe becomes colder, while Central and Eastern Europe becomes warmer than in the E-OBS. This behavior is not limited to summer, and can also be identified in the other seasons, but is less emphasized.
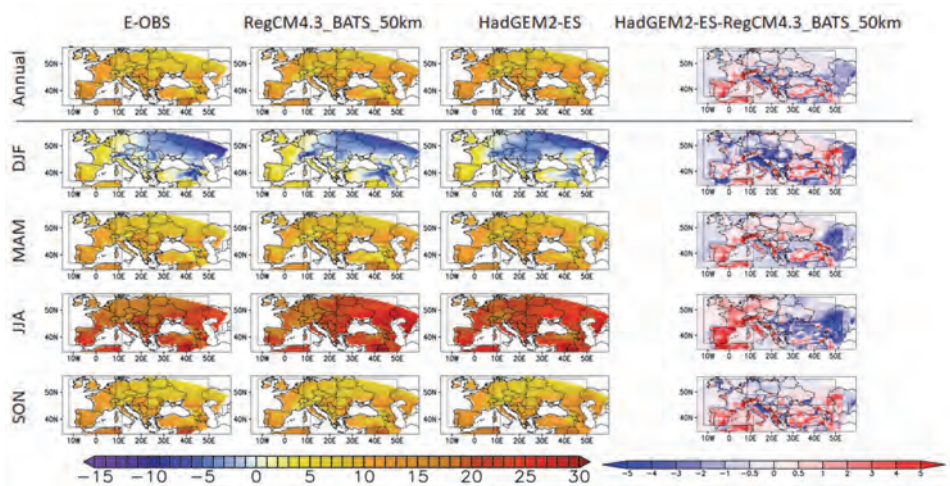
Fig. 2. Annual and seasonal mean temperature (°C) of E-OBS (left), RegCM4.3_BATS_50km (2nd column), HadGEM2-ES (3rd column), and the difference of model simulations (right), for the period 1986–2005. For the sake of visual comparison, all fields are interpolated to the grid of RegCM4.3_BATS_50km.
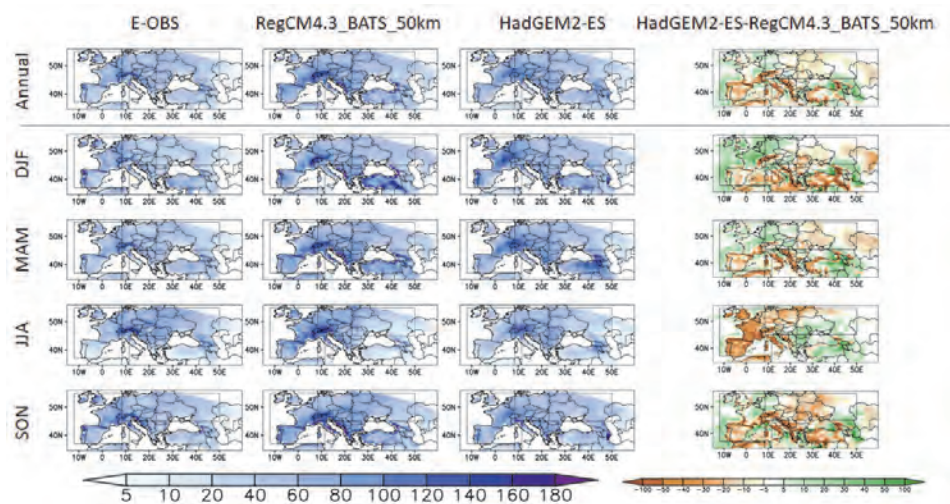

Fig. 3. Annual and seasonal mean precipitation (mm/month) of E-OBS (left), RegCM4.3_BATS_50km (2nd column), HadGEM2-ES (3rd column), and the difference of model simulations (right), for the period 1986–2005. For the sake of visual comparison, all fields are interpolated to the grid of RegCM4.3_BATS_50km.

Table 1. Visualization of the comparison of HadGEM2-ES/ RegCM4.3_BATS_50km model performance based on regional bias values relative to E-OBS reference data, for the period 1986-2005. Green: better performance of RCM, light brown: better performance of GCM, white: similar performance.

	Annual		DJF		MAM		JJA		SON	
	T	p	T	p	T	p	T	p	T	p
Southern part of the British Isles	green	green	green	green	green	green	green	brown	green	white
France	green	green	green	green	green	green	green	brown	white	green
Iberian Peninsula	brown	green	green	green	green	green	green	brown	green	green
North European Plain (in Germany and Poland)	green	brown	green	green	green	green	green	green	green	green
Alps	green	green	green	green	green	white	green	brown	green	green
Carpathian Basin	green	white	green	green	green	green	green	white	green	brown
East European Plain in Ukraine	green	brown	green	brown	green	brown	green	white	green	green
East European Plain in Russia	brown	green	green	white	green	brown	green	green	green	green
Apennine Peninsula	white	green	green	green	brown	green	green	green	green	green
Balkan Region	green	brown	green	brown	green	green	green	brown	green	brown
Greece	white	green	white	green	green	green	brown	white	green	white
Asia Minor (Turkey)	green	brown	green	brown	green	brown	green	green	white	brown

In general, higher overestimated temperature can be found in RegCM outputs in the northeastern part of the Med-CORDEX domain, while underestimation occurs in the southwestern part, with the highest gradient between the two regions existing during summer. This shift of the mean temperature bias field is an important result of the dynamical downscaling, since the application of RCM cools the GCM outputs substantially, by about 1–4 °C in general (the greatest exception is in Eastern Europe in summer). This is a known behavior of the RegCM, as similar conclusions can be seen for a completely different region, namely southeastern Asia in *Giorgi et al.* (1999). The cooling effect of RegCM on the driving GCM outputs is probably related to the treatment of cloud radiative processes (*Coppola et al.*, 2014). Clouds generally reflect some portion of incoming shortwave radiation, thus the transmitted part is reduced, which later warms the surface and the atmosphere. The emitted longwave radiation is trapped less efficiently by higher level clouds compared to lower level and thicker clouds, hence near-surface warming is less intense. Overall, thick, low level clouds have a stronger impact on temperature than high level clouds. Since the moisture-, and thus cloud-related processes are the weakest part of climate models in terms of understanding the climate system, their radiation effects cause uncertainty in the final results. Moreover, we assume that proximity to the moisture source, i.e., large water bodies, also has an important effect. As a

418

result, cooling is the most pronounced in southern Europe (which is illustrated by the red color in this area in the right column of *Fig. 2*). In case of some subregions (e.g., the Iberian Peninsula, throughout the year) the cooling effect becomes too strong, while in the eastern part (Carpathian Basin, East European Plain, Asia Minor) of the domain warm bias still remains in summer despite the present cooling effect. However, for instance, in the Carpathian Basin during winter this general cooling effect is not present at all, namely, the seasonal mean of RegCM outputs are 1–2 °C warmer than that of HadGEM2-ES outputs, which can be partly explained by the smaller interannual variability of mean winter temperature values using RegCM simulation compared to the HadGEM2-ES driving simulation.
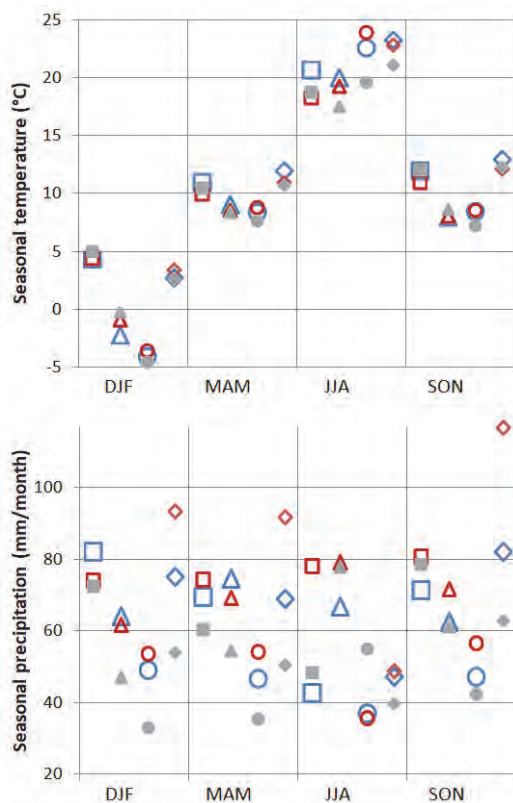
Fig. 4. Comparison of the simulated seasonal mean temperature (top) and precipitation (bottom) values over land to the E-OBS reference data for the four regions, for the period 1986–2005. (Colors and symbols are as follows: HadGEM2-ES: blue, RegCM4.3_BATS_50km: red, E-OBS: grey; Western Europe: square, Central Europe: triangle, Eastern Europe: circle; Southern Europe: diamond)

The temperature mean values of RegCM4.3_BATS_10km closely follow those of RegCM4.3_BATS_50km, but show more local details, as expected. The

differences between the simulations are greater in case of precipitation, which is the consequence of higher overall spatial variability compared to temperature. The spatial distribution of meteorological variables in the model generally reflects that of the observations, nevertheless, with excessive precipitation in the Carpathian Mountains, except in summer (*Fig. 5*).
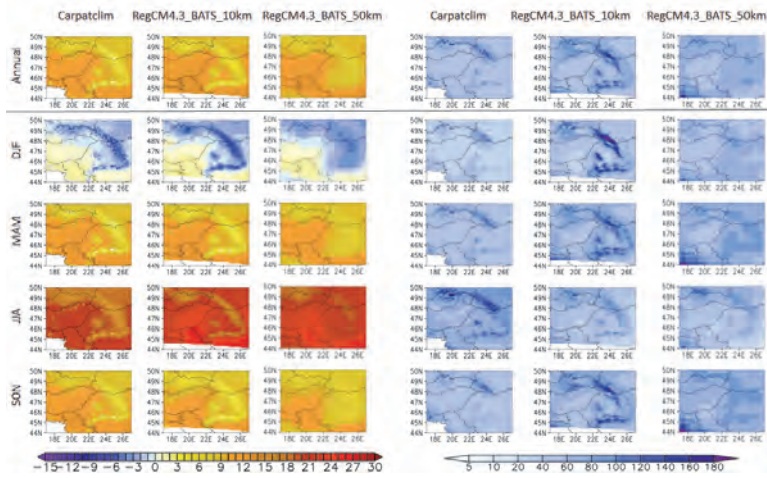
Fig. 5. Annual and seasonal mean temperature (°C) and precipitation (mm/month) of Carpatclim (left), RegCM4.3_BATS_10km (center), and RegCM4.3_BATS_50km (right), for the period 1986–2005.

In most parts of the model domain, HadGEM2-ES outputs are wetter compared to E-OBS (*Figs. 3* and *4*), except in summer, when more than half of the region is drier in the model than the observations. The exceptions (e.g., the regions with more precipitation in summer) are located in the southern part of the domain. The areas of local precipitation maximum are slightly displaced in some seasons. The location and spatial distribution of precipitation are better represented in RegCM (e.g., the local maxima in the Alps or on the shores of the Adriatic Sea is noticeable in RegCM outputs, although sometimes they are too strong) than in HadGEM2-ES outputs, which is not surprising due to the refined orography and land-sea mask. RegCM often produces excessive precipitation compared to HadGEM2-ES, resulting in overestimation, except in summer in the eastern part of the domain. Furthermore, RegCM increases the precipitation in the mountains compared to HadGEM2-ES, probably due to local orographical forcings present in the finer resolution model. In some cases (when HadGEM2-ES provides a good estimation for the amount of precipitation) this effect is too strong and causes

excessive precipitation, while in other locations it improves the modeled results. In the western part of the domain no real improvement can be seen.

3.2. *Validation of climate indices*

The use of regional models and their increasing resolution are believed to add value not necessarily to the means, but to higher order statistics, and to the tails of the distribution function. Therefore, we selected climate indices (*Table 2*) to study the exceedance of given thresholds, and duration of specific phenomena. To illustrate the model behavior, both temperature and precipitation related indices are represented, also, the left and right tails of the distribution curve are considered. Unlike the simpler annual distribution of temperature, which allows an annual analysis, precipitation requires more detailed, seasonal analysis (in this paper summer and winter are presented). For the analysis the deviation from E-OBS (and for RegCM4.3_BATS_10km from Carpatclim) was calculated, and areas with significant biases were located.

Table 2. Definition of selected climate indices

Name	Definition
SU (Summer days)	number of days per time period when T2max > 25 °C
TR (Tropical nights)	number of days per time period when T2min > 20 °C
FD (Frozen days)	number of days per time period when T2min < 0 °C
ID (Ice days)	number of days per time period when T2max < 0 °C
RX1day	highest one day precipitation amount (mm)
R10mm	number of days with daily precipitation sum exceeding 10 mm
DD (Dry days)	number of dry days (with daily precipitation amount below 1 mm)
CDD (Consecutive dry days)	maximum number of consecutive dry days (with daily precipitation amount below 1 mm)

The spatial structures of temperature index values are reproduced reasonably well by the models compared to the reference data (*Figs. 6* and *7*). The biases

already present in the summer mean temperature can be seen in the bias maps of SU and TR, too. However, although the bias of mean temperature was significant almost everywhere, this is not the case with TR, where the area with significant bias is reduced to a much smaller region north of the Caucasus (*Fig. 8*). The spatial structure of SU bias correlates well with mean temperature bias, and the impact of RegCM4.3_BATS_50km is also similar: it shifts temperature distribution to the left, but this shift (i.e., cooling effect) is too intense in some areas, causing underestimation in Western Europe, for instance. The structure and intensity of SU in Eastern Europe is similar in RegCM4.3_BATS_50km and HadGEM2-ES.
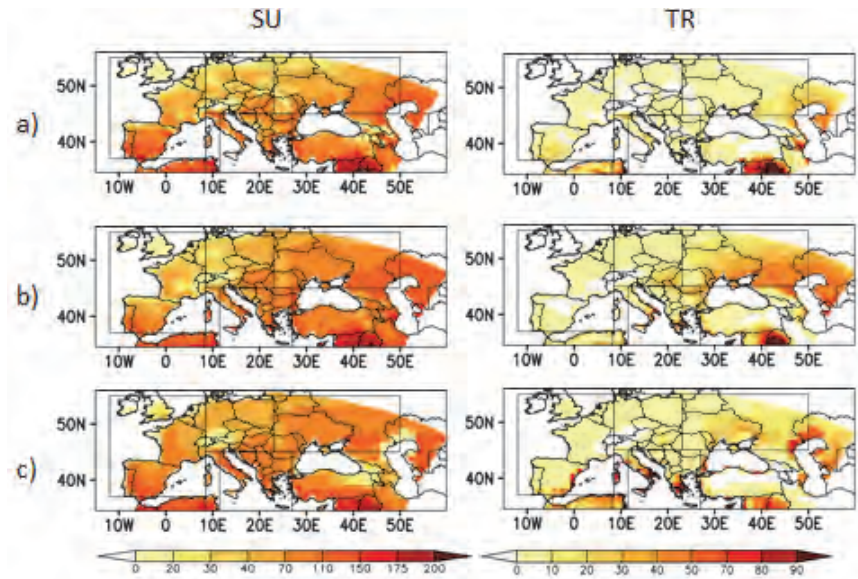

Fig. 6. Mean annual number of days of SU (left) and TR (right) in E-OBS (a, top), RegCM4.3_BATS_50km (b, middle), and HadGEM2-ES (c, bottom), for the period 1986–2005. For the sake of visual comparison, all fields are interpolated to the grid of RegCM4.3_BATS_50km.
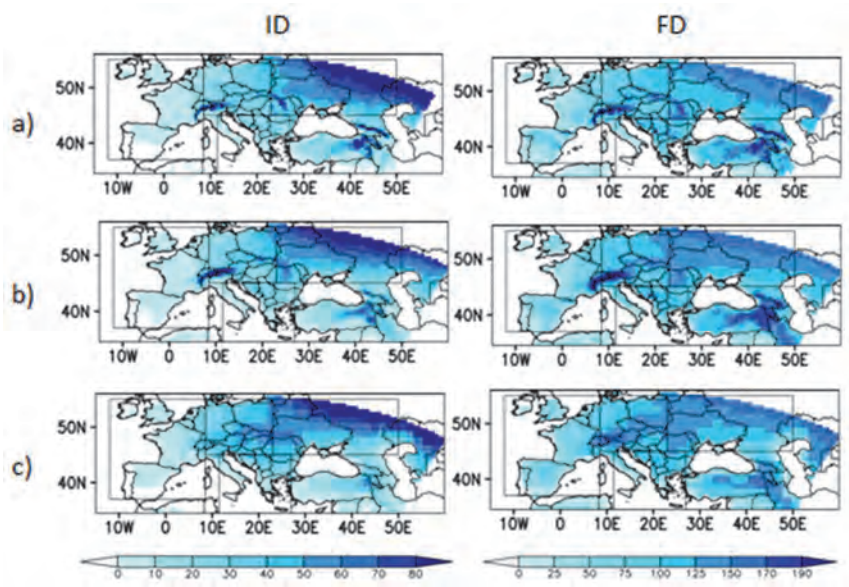
Fig. 7. Mean annual number of days of ID (left) and FD (right) in E-OBS (a, top), HadGEM2-ES (b, middle), and RegCM4.3_BATS_50km (c, bottom), for the period 1986–2005. For the sake of visual comparison, all fields are interpolated to the grid of RegCM4.3_BATS_50km.
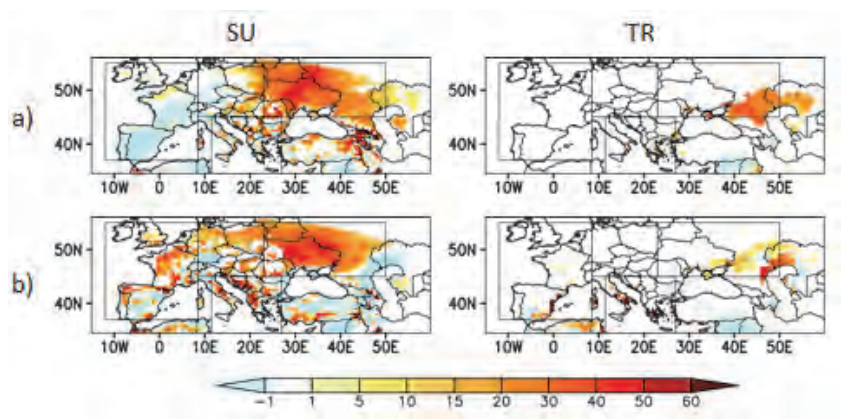
Fig. 8. Bias values (in days) of SU (left) and TR (right) in RegCM4.3_BATS_50km (a, top), and HadGEM2-ES (b, bottom), showing the significant values only, for the period 1986–2005 (reference data: E-OBS). For the sake of visual comparison, all fields are interpolated to the grid of RegCM4.3_BATS_50km.

The spatial structure of the bias of ID and FD (*Fig. 9*) shows similarities to the winter mean temperature bias: colder, therefore overestimated ID and FD in most of the domain, while warmer, therefore underestimated ID and FD around the Caspian Sea. The models seem to be more successful in simulating the indices with lower values (i.e., ID, TR) than with higher values (i.e., FD, SU) if the bias is expressed in days, which is not surprising because of the less frequent occurrence, and thus, smaller potential differences between simulated and observed frequency values. This could also be evaluated using bias expressed as relative difference; however, in case of rare events, such a measure would misleadingly magnify small differences.
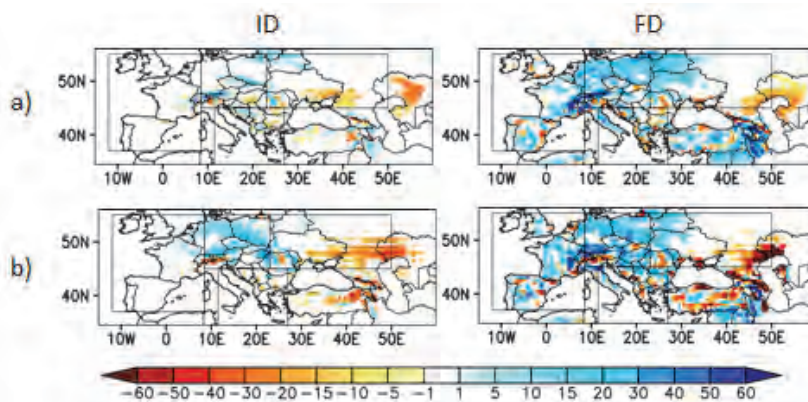
Fig. 9. Bias values (in days) of ID (left) and FD (right) in RegCM4.3_BATS_50km (a, top), and HadGEM2-ES (b, bottom), showing the significant values only, for the period 1986–2005 (reference data: E-OBS). For the sake of visual comparison, all fields are interpolated to the grid of RegCM4.3_BATS_50km.

Besides the bias maps, RMSE is another performance statistical parameter used for climate indices, e.g., *Sillmann et al.* (2013), *Razavi et al.* (2016). Since simple bias can hide differences between two spatial patterns because opposite differences can eliminate each other, RMSE adds more detail to the comparison due to its definition containing squared differences. *Chai* and *Draxler* (2014) suggest using both bias and RMSE to evaluate model performance. *Table 3* summarizes the spatial average RMSE values for indices, regions, and models. In case of temperature indices, RegCM4.3_BATS_50km clearly performs better than HadGEM2-ES, except for TR in Central and Eastern Europe. For Hungary,

RegCM4.3_BATS_10km results in similar magnitude RMSE values (compared to Carpatclim reference data), and a slight improvement can be seen between the RegCM runs with 10 km and 50 km at the left tail of the distribution (e.g., for FD and ID), whereas larger improvements appear between the RegCM and GCM results (for FD, ID, and SU). This is probably connected to the better representation of orography at the resolution used by RCM, which allows for a more realistic appearance of the barrier (or basin) effect, and which blocks cold air masses arriving from the north during winter.

Table 3. Spatial RMSE of climate indices calculated for the four regions and Hungary in case of RegCM4.3_BATS_10km (R10 – for Hungary only), RegCM4.3_BATS_50km (R50) and HadGEM2-ES (H) outputs (reference data: E-OBS for Europe and Carpatclim for Hungary). Calculations were performed on a 50-km grid.

	Western		Central		Eastern		Southern		Hungary		
	R50	H	R50	H	R50	H	R50	H	R10	R50	H
SU	26.8	29.2	21.5	28.4	30.3	37.1	28.9	35.8	24.9	21.5	26.5
TR	5.6	8.8	7.9	5.7	22.2	14.0	25.9	27.7	26.2	22.3	13.2
FD	23.4	27.1	32.4	34.3	21.8	26.8	26.8	30.7	27.6	28.5	33.6
ID	5.6	7.9	20.7	28.8	21.6	27.6	10.5	16.6	17.2	17.2	36.3
RX1day, winter	14.5	13.8	10.1	9.8	8.6	6.9	18.9	13.3	9.7	8.7	11.0
RX1day, summer	19.0	12.8	19.0	15.8	14.7	13.6	18.6	13.2	17.7	17.8	17.9
R10mm, winter	5.2	5.9	3.2	3.2	2.7	2.0	6.1	5.0	2.4	2.3	2.5
R10mm, summer	5.7	3.6	5.4	4.9	3.6	4.0	4.5	3.6	5.2	5.0	5.2
DD, winter	13.6	13.8	14.7	15.8	10.9	13.6	16.7	14.5	10.3	12.8	20.6
DD, summer	15.6	12.4	12.4	13.6	13.0	10.8	12.2	14.4	11.6	11.4	15.7
CDD, winter	10.5	10.8	11.1	10.5	8.2	9.1	12.3	11.9	11.6	11.9	13.2
CDD, summer	15.0	14.7	9.0	7.5	17.6	11.1	18.8	15.9	12.9	12.6	8.5

Precipitation in RegCM4.3_BATS_50km is too intense compared to both E-OBS and HadGEM2-ES: not only is the mean precipitation higher, but RX1day is also generally overestimated. This is a common behavior of regional models (*Soares et al.,* 2012). The difference between the RMSE of the two simulations is more pronounced in Western and Central Europe in summer,

when the contribution of local scale processes (e.g., convection) is stronger in the region than in winter. Interestingly, this seasonal difference cannot be seen in Eastern and Southern Europe. This is related, especially in Eastern Europe, to drier and warmer conditions present in the models compared to observation, probably limiting convection, and therefore reducing seasonality.

The spatial structure of R10mm is similar in the observed and modeled data, with better spatial representation of RegCM4.3_BATS_50km than HadGEM2-ES. RMSE values are smaller than for Rx1day, however, the absolute values of R10mm are also smaller. These deficiencies may partly originate from the reference database (*Prein* and *Gobiet*, 2017), e.g., precipitation undersampling in E-OBS. Results for the drought-related indices (DD, CDD) lead to less clear conclusions, and depend on region and season.

In the half of the examined indices, regions, and periods, the RMSE of RegCM4.3_BATS_50km was smaller than that of HadGEM2-ES. For Hungary this ratio is even better (10 seasonal indices out of the total 12 seasonal indices included in *Table 3* show better performance of RegCM4.3_BATS_50km). Nevertheless, RMSE values from RegCM4.3_BATS_10km and RegCM4.3_BATS_50km are close to each other with small overall differences between the estimations using different resolutions.

To decide which model performs better is a complex task, because it includes several factors, e.g., it depends on the goal of the study. However, the magnitude and spatial extent of bias are usually among the most important components. Therefore, after calculating biases and their significance (using Welch's test), we prepared the histograms for all regions. In order to keep the paper to a reasonable length, only one example is shown here from the 90 histograms prepared during the analysis, see *Fig. 10* as an illustration. Then, we introduced the measure *m* as follows:

$$m = \left| m_- \right| + \left| m_+ \right| = \left| \sum_{i=1}^{N_-} f_i \cdot b_i \right| + \left| \sum_{i=1}^{N_+} f_i \cdot b_i \right|,$$

where f_i is relative frequency of bias b_i, and the corresponding products are summed for the underestimation (with N_- different bias categories) and overestimation (with N_+ different bias categories).

Table 4 summarizes the results separately for underestimation and overestimation (on the basis of m_- and m_+, respectively) for comparing HadGEM2-ES with RegCM4.3_BATS_50km. A cell is colored green when the introduced metrics (either m_- and m_+) are better for RCM than GCM, and light brown if the opposite happens. White means that the performance of the two models using different resolutions is close to each other.

Relative frequency (%)

0   2   4   6   8

-75   -50   -25   0   25   50   75
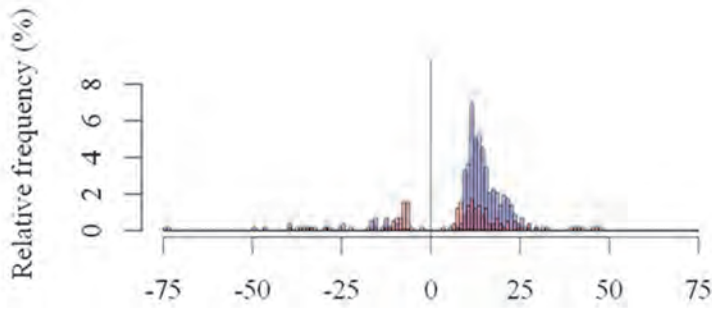
Fig. 10. Histogram of significant bias values of ID (days) in RegCM4.3_BATS_50km (red) and HadGEM2-ES (blue) for Central Europe, showing the significant values only, for the period 1986–2005 (reference data: E-OBS).

Table 4. Visualization of the comparison of HadGEM2-ES/RegCM4.3_BATS_50km model performance based on the metric defined in the text. Green: better performance of RCM, light brown: better performance of GCM, white: similar performance. U: underestimation (representing m_-, for definition see text), O: overestimation (representing m_+, for definition see text).

	Western		Central		Eastern		Southern	
	U	O	U	O	U	O	U	O
SU								
TR								
FD								
ID								
RX1day, winter								
R10mm, winter								
DD, winter								
CDD, winter								
RX1day, summer								
R10mm, summer								
DD, summer								
CDD, summer								

In case of temperature indices (the upper four lines of *Table 4*), a general improvement can be identified in Western Europe, and a clear improvement is seen in cold indices in Central Europe. The underestimation of temperature indices improved in Eastern Europe and their overestimation improved in Southern Europe.

427

In case of precipitation indices (the middle and lower four lines of *Table 4* for winter and summer, respectively) the influence of RegCM is usually too strong, and underestimation turns to overestimation and vice versa. For instance, the underestimation of the precipitation indices in summer improves (i.e., decreased) with finer resolution, however, the overall effect of overestimation increases in the regions representing Central, Eastern, and Southern Europe. A similar shift can be seen in the case of RX1day and R10mm in (i) Western Europe in summer, and in (ii) Eastern and Southern Europe in winter. Opposite changes (improved overestimation with increased underestimation) occur in the drought-related indices (i.e., DD and CDD) in Western Europe in summer. Among the precipitation-related indices, only RX1day shows clear improvement in terms of both overestimation and underestimation in Western Europe.

4. Conclusions

The novelty of the analysis stems from the unique set-up of RegCM applied to the Med-CORDEX and Carpathian regions. The CORDEX international initiative recommends completing several experiments using different regional climate models for the pre-defined 14 regions (*Lake et al.,* 2017). This paper contributes to this international effort by evaluating our RegCM simulations. In addition, the main validation results of recent RegCM4 simulations are summarized in this paper in order to facilitate and inform the researchers and users of the RegCM4 simulation outputs during their planning and performance of climate change impact studies, which strongly rely on climatological input. On the basis of the presented results, the following conclusions can be drawn.

(1) The spatial distribution of the annual and seasonal mean temperature and precipitation is sufficiently simulated by the models with all the presented resolutions.

   (i)   The highest temperature biases occur in summer in Eastern Europe. The impact of the dynamical downscaling with RegCM is not uniform throughout the region and year: although it generally cools the HadGEM results, its magnitude depends on the distance from the ocean, and orography.

   (ii)   The location and spatial distribution of precipitation is better represented in RegCM simulations than in HadGEM2-ES outputs, however, dynamical downscaling with higher resolution often increases precipitation in the mountains, and also produces excessive precipitation.

(iii) The temperature and precipitation mean values of RegCM4.3_BATS_10km closely follow the mean values of RegCM4.3_BATS_50km.

(2) Regarding the climate indices:

(i) The overall spatial structure of temperature indices is reproduced reasonably well by the models, however, the consequence of the general biases in the mean temperature can be observed in the overestimation or underestimation of the index values in certain regions. In general, the models are more successful in simulating the indices with less frequent occurrence. A clear improvement can be recognized in the RMSE of temperature indices when using finer resolution.

(ii) In case of precipitation indices, the detected deficiencies partly originate from the reference database (especially in mountainous regions: even though the reference databases are carefully created, the number of measurement sites used is not sufficient in the areas with complex topography).

(3) A complex measure was introduced, which is able to take into account both the magnitude and spatial extent of bias.

(i) A general improvement can be recognized in all temperature-related climate indices in Central Europe and Western Europe, respectively. Furthermore, the underestimation (overestimation) of temperature indices improved in Eastern Europe (Southern Europe).

(ii) The influence of downscaling using finer resolution is usually too strong in the precipitation indices, which often changes underestimation into overestimation and vice versa.

References

Anders, I. and *Rockel, B.,* 2009: The influence of prescribed soil type distribution on the representation of present climate in a regional climate model. *Clim. Dynam. 33,* 177–186. https://doi.org/10.1007/s00382-008-0470-y

Arguez, A. and *Vose, R.S., 2011:* The definition of the standard WMO climate normal: The key to deriving alternative climate normals. *Bull. Amer.Meteorol. Soc. 92,* 699–704. https://doi.org/10.1175/2010BAMS2955.1

Arguez, A., Vose, R.S., and *Dissen, J.,* 2013: Alternative climate normals: Impacts to the energy industry. *Bull. Amer.Meteorol. Soc. 94,* 915–917. https://doi.org/10.1175/BAMS-D-12-00155.1

Bresson, R. and *Laprise, R.,* 2011: Scale-decomposed atmospheric water budget over North America as simulated by the Canadian Regional Climate Model for current and future climates. *Clim. Dynam. 36*, 365–384. https://doi.org/10.1007/s00382-009-0695-4

Cavicchia, L. and *von Storch, H.,* 2011: The simulation of medicanes in a high-resolution regional climate model. *Clim. Dynam. 39*, 2273–2290. https://doi.org/10.1007/s00382-011-1220-0

Chai, T. and *Draxler, R.R.,* 2014: Root mean square error (RMSE) or mean absolute error (MAE)?– Arguments against avoiding RMSE in the literature. *Geosci. Model Dev. 7,* 1247–1250. https://doi.org/10.5194/gmd-7-1247-2014

Collins, W.J., Bellouin, N., Doutriaux-Boucher, M., Gedney, N., Halloran, P., Hinton, T., Hughes, J., Jones, C.D., Joshi, M., Liddicoat, S., Martin, G., O'Connor, F., Rae, J., Senior, C., Sitch, S., Totterdell, I., Wiltshire, A., and *Woodward, S.,* 2011: Development and evaluation of an Earth-system model – HadGEM2. *Geosci. Model Dev. Discuss. 4*, 997–1062. https://doi.org/10.5194/gmdd-4-997-2011

Coppola, E., Giorgi, F., Raffaele, F., Fuentes-Franco, R., Giuliani, G., Llopart-Pereira, M., Mamgain, A., Mariotti, L., Diro, G.T., and *Torma, Cs.,* 2014: Present and future climatologies in the phase I CREMA experiment. *Climatic Change 125*, 23–38. https://doi.org/10.1007/s10584-014-1137-9

Di Luca, A., de Elía, R., and *Laprise, R.,* 2015: Challenges in the quest for added value of regional climate dynamical downscaling. *Curr. Climate Change Rep. 1*, 10–21. https://doi.org/10.1007/s40641-015-0003-9

Dickinson, R.E., Henderson-Sellers, A., and *Kennedy, P.J.,* 1993: Biosphere-atmosphere Transfer Scheme (BATS) Version 1e as Coupled to the NCAR Community Climate Model. NCAR Technical Note NCAR/TN-387+STR. DOI: 10.5065/D67W6959

Donat, M., Leckebusch, G., Wild, S., and *Ulbrich, U.,* 2010: Benefits and limitations of regional multi-model ensembles for storm loss estimations. *Clim. Res. 44,* 211–225. https://doi.org/10.3354/cr00891

Elguindi, N., Bi, X., Giorgi, F., Nagarajan, B., Pal, J., Solmon, F., Rauscher, S., Zakey, A., and *Giuliani, G.,* 2011: Regional climatic model RegCM user manual version 4.3. ITCP, Trieste, Italy.

Elguindi, N., Giorgi, F., and *Turuncoglu, U.,* 2014: Assessment of CMIP5 global model simulations over the subset of CORDEX domains used in the Phase I CREMA. *Climatic Change 125*, 7–21. https://doi.org/10.1007/s10584-013-0935-9

Emanuel, K.A., 1991: A scheme for representing cumulus convection in large-scale models. *J Atmos Sci 48,* 2313–2335. https://doi.org/10.1175/1520-0469(1991)048<2313:ASFRCC>2.0.CO;2

Emanuel, K.A. and *Zivkovic-Rothman, M.,* 1999: Development and evaluation of a convection scheme for use in climate models. *J Atmos Sci 56*, 1766–1782. https://doi.org/10.1175/1520-0469(1999)056<1766:DAEOAC>2.0.CO;2

Feser, F., 2006: Enhanced detectability of added value in limited-area model results separated into different spatial scales. *Mon. Weather Rev. 134*, 2180–2190. https://doi.org/10.1175/MWR3183.1

Flaounas, E., Drobinski, P., and Bastin, S., 2013: Dynamical downscaling of IPSL-CM5 CMIP5 historical simulations over the Mediterranean: benefits on the representation of regional surface winds and cyclogenesis. *Clim. Dynam. 40*, 2497–2513. https://doi.org/10.1007/s00382-012-1606-7

Fritsch, J.M. and Chappell, C.F., 1980: Numerical prediction of convectively driven mesoscale pressure systems. Part I: Convective parameterization. *J. Atmos. Sci. 37,* 722–1733. https://doi.org/10.1175/1520-0469(1980)037<1722:NPOCDM>2.0.CO;2

Gao, X., Shi, Y., Zhang, D., Wu, J., Giorgi, F., Ji, Z., and Wang, Y., 2012: Uncertainties in monsoon precipitation projections over China: Results from two high-resolution RCM simulations. *Clim. Res. 52*, 213–226. https://doi.org/10.3354/cr01084

Giorgi, F., 1990: Simulation of regional climate using a limited area model nested in a general circulation model. *J. Climate 3*, 941–63. https://doi.org/10.1175/1520-0442(1990)003<0941:SORCUA>2.0.CO;2

Giorgi, F., Huang, Y., Nishizawa, K., and Fu, C., 1999: A seasonal cycle simulation over eastern Asia and its sensitivity to radiative transfer and surface processes. *J. Geophys. Res. 104*, 6403–6423. https://doi.org/10.1029/1998JD200052

Giorgi, F., Francisco, R., and Pal, J., 2003: Effects of a subgrid-scale topography and land use scheme on the simulation of surface climate and hydrology. Part I: Effects of temperature and water vapor disaggregation. *J. Hydrometeorol. 4*, 317–333. https://doi.org/10.1175/1525-7541(2003)4<317:EOASTA>2.0.CO;2

Giorgi, F., Coppola, E., Solmon, F., Mariotti, L., Sylla, M.B., Bi, X., Elguindi, N., Diro, G.T., Nair, V., Giuliani, G., Turuncoglu, U.U., Cozzini, S., Güttler, I., O'Brien, T.A., Tawfik, A.B., Shalaby, A., Zakey, A.S., Steiner, A.L., Stordal, F., Sloan, L.C., and Brankovic, C., 2012: RegCM4: model description and preliminary tests over multiple CORDEX domains. *Climate Res. 2*, 7–29. https://doi.org/10.3354/cr01018

Grell, G.A., 1993: Prognostic evaluation of assumptions used by cumulus parameterizations. *Mon. Weather Rev. 121,* 764–787. https://doi.org/10.1175/1520-0493(1993)121<0764:PEOAUB>2.0.CO;2

Grose, M., Pook, M., McIntosh, P., Risbey, J., and Bindoff, N., 2012: The simulation of cutoff lows in a regional climate model: Reliability and future trends. *Clim. Dynam. 39*, 445–459. https://doi.org/10.1007/s00382-012-1368-2

Haylock, M.R., Hofstra, N., Klein Tank, A.M.G., Klok, E.J., Jones, P.D., and New, M., 2008: A European daily high-resolution gridded dataset of surface temperature and precipitation. *J. Geophys. Res (Atmospheres) 113*, D20119. https://doi.org/10.1029/2008JD010201

IPCC, 2013: *Climate Change 2013:* The Physical Science Basis. Contribution of Working Group I to the Fifth Assessment Report of the Intergovernmental Panel on Climate Change *(Eds. Stocker, T.F., Qin, D., Plattner, G.-K., Tignor, M., Allen, S.K., Boschung, J., Nauels, A., Xia, Y., Bex, V., Midgley, P.M.).* Cambridge University Press, Cambridge, United Kingdom and New York, NY, USA.

Joetzjer, E., Douville, H., Delire, C., and Ciais, P., 2013: Present-day and future Amazonian precipitation in global climate models: CMIP5 versus CMIP3. *Clim. Dynam. 41*, 2921–2936. https://doi.org/10.1007/s00382-012-1644-1

Jones, C., Hughes, J.K., Bellouin, N., Hardiman, S.C., Jones, G.S., Knight, J., Liddicoat, S., O'Connor, F.M., Andres, R.J., Bell, C., and Boo, K.O., 2011: The HadGEM2-ES implementation of CMIP5 centennial simulations. *Geosci. Mod.Develop. 4*, 543. https://doi.org/10.5194/gmdd-4-689-2011

Kanamaru, H. and Kanamitsu, M., 2007: Fifty-seven-year California reanalysis downscaling at 10 km (CaRD10). Part II: Comparison with North American regional reanalysis. *J. Climat. 20*, 5572–5592. https://doi.org/10.1175/2007JCLI1522.1

Kawazoe, S. and Gutowski, W., 2013: Regional, very heavy daily precipitation in NARCCAP simulations. *J. Hydrometeorol. 14*, 1212–1227. https://doi.org/10.1175/JHM-D-12-068.1

Kis, A., Pongrácz, R., Bartholy, J., and Szabó, J.A., 2017: The application of RCM results to hydrological analysis. Időjárás 121, 437–452.

Knutti, R., Masson, D., and Gettelman, A., 2013: Climate model genealogy: Generation CMIP5 and how we got there. Geophys. Res. Lett. 40, 1194–1199.
https://doi.org/10.1002/grl.50256

Krüzselyi, I., Bartholy, J., Horányi, A., Pieczka, I., Pongrácz, R., Szabó, P., Szépszó, G., and Torma, Cs., 2011: The future climate characteristics of the Carpathian Basin based on a regional climate model mini-ensemble. Adv. Sci. Res. 6, 69–73.
https://doi.org/10.5194/asr-6-69-2011

Lake, I., Gutowski, W., Giorgi, F., and Lee, B., 2017: CORDEX: Climate Research and Information for Regions. Bull. Amer. Meteorol. Soc. 98, ES189-ES192.
https://doi.org/10.1175/BAMS-D-17-0042.1

Lucas-Picher, P., Wulff-Nielsen, M., Christensen, J., Adalgeirsdottir, G., Mottram, R., and Simonsen, S., 2012: Very high resolution regional climate model simulations over Greenland: Identifying added value. J. Geophys. Res. Atmos. 117, D02108.
https://doi.org/10.1029/2011JD016267

Maraun, D., Widmann, M., Gutiérrez, J.M., Kotlarski, S., Chandler, R.E., Hertig, E., Wibig, J., Huth, R., and Wilcke, R.A.I., 2015: VALUE: A framework to validate downscaling approaches for climate change studies. Earth's Future 3, 1–14.
https://doi.org/10.1002/2014EF000259

Pieczka, I., Pongrácz, R., Szabóné André, K., Kelemen, F.D., and Bartholy, J., 2017: Sensitivity analysis of different parameterization schemes using RegCM4.3 for the Carpathian region. Theor. App. Climatol. 130, 1175–1188.
https://doi.org/10.1007/s00704-016-1941-4

Prein, A.F. and Gobiet, A., 2017: Impacts of uncertainties in European gridded precipitation observations on regional climate analysis. Int. J. Climatol. 37, 305–327.
https://doi.org/10.1002/joc.4706

Rauscher, S.A., Coppola, E., Piani, C., and Giorgi, F., 2010: Resolution effects on regional climate model simulations of seasonal precipitation over Europe. Clim. Dynam. 35, 685–711.
https://doi.org/10.1007/s00382-009-0607-7

Razavi, T., Switzman, H., Arain, A., Coulibaly, P., 2016: Regional climate change trends and uncertainty analysis using extreme indices: A case study of Hamilton, Canada. Climate Risk Manage. 13, 43–63. https://doi.org/10.1016/j.crm.2016.06.002

Sillmann, J., Kharin, V.V., Zhang, X., Zwiers, F.W., and Bronaugh, D., 2013: Climate extremes indices in the CMIP5 multimodel ensemble: Part 1. Model evaluation in the present climate. J.Geophys. Res.: Atmospheres 118, 1716–1733.
https://doi.org/10.1002/jgrd.50203

Soares, P.M.M., Cardoso, R.M., Miranda, P.M.A., Viterbo, P., and Belo-Pereira, M., 2012: Assessment of the ENSEMBLES regional climate models in the representation of precipitation variability and extremes over Portugal. J. Geophys. Res. 117, D07114.
https://doi.org/10.1029/2011JD016768

Somot, S., et al., 2012: The Med-CORDEX initiative: towards fully coupled Regional Climate System Models to study the Mediterranean climate variability, change and impact. Geophys. Res. Abst. 14, 6080.

Spinoni, J., Szalai, S., Szentimrey, T., Lakatos, M., Bihari, Z., Nagy, A., Németh, Á., Kovács, T., Mihic, D., Dacic, M., and Petrovic, P., 2015: Climate of the Carpathian Region in the period 1961–2010: climatologies and trends of 10 variables. Int. J. Climatol. 35, 1322–1341.
https://doi.org/10.1002/joc.4059

Szalai, S., Auer, I., Hiebl, J., Milkovich, J., Radim, T., Stepanek, P., Zahradnicek, P., Bihari, Z., Lakatos, M., Szentimrey, T., Limanowka, D., Kilar, P., Cheval, S., Deak, Gy., Mihic, D., Antolovic, I., Mihajlovic, V., Nejedlik, P., Stastny, P., Mikulova, K., Nabyvanets, I., Skyryk, O., Krakovskaya, S., Vogt, J., Antofie, T., and Spinoni, J., 2013: Climate of the Greater Carpathian Region. Final Technical Report. http://www.carpatclim-eu.org

Torma, C., Giorgi, F., and *Coppola, E.,* 2015: Added value of regional climate modeling over areas characterized by complex terrain—Precipitation over the Alps. *J.Geophys. Res.: Atmospheres 120*, 3957–3972. https://doi.org/10.1002/2014JD022781

Vautard, R., Gobiet, A., Jacob, D., Belda, M., Colette, A., Déqué, M., Fernández, J., García-Díez, M., Goergen, K., Güttler, I., and *Halenka, T.,* 2013: The simulation of European heat waves from an ensemble of regional climate models within the EURO-CORDEX project. *Clim. Dynam. 41*, 2555–2575. https://doi.org/10.1007/s00382-013-1714-z

Veljovic, K., Rajkovic, B., Fennessy, M.J., Altshuler, E.L., and *Mesinger, F.,* 2010: Regional climate modeling: Should one attempt improving on the large scales? Lateral boundary condition scheme: Any impact? *Meteorol. Z. 19,* 237–246.
https://doi.org/10.1127/0941-2948/2010/0460

Winterfeldt, J. and *Weisse, R.,* 2009: Assessment of value added for surface marine wind speed obtained from two regional climate models. *Mon. Weather Rev. 137*, 2955–2965.
https://doi.org/10.1175/2009MWR2704.1

Winterfeldt, J., Geyer, B., and *Weisse, R.,* 2011: Using QuikSCAT in the added value assessment of dynamically downscaled wind speed. *Int. J. Climatol. 31*, 1028–1039.

Zahn, M. and *von Storch,* H., 2008: A long-term climatology of North Atlantic polar lows. *Geophys. Res. Lett. 35*, L22702. https://doi.org/10.1029/2008GL035769

IDŐJÁRÁS

Analyzing the droughts in Iran and its eastern neighboring countries using copula functions

Yousef Ramezani[*1], **Mohammad Nazeri Tahroudi**[1], and **Farshad Ahmadi**[2]

[1] *Department of Water Engineering, University of Birjand*
Birjand, Iran

[2] *Department of Hydrology and Water Resources Engineering,*
Shahid Chamran University of Ahvaz
Ahvaz, Iran

*Corresponding Author E-mail: y.ramezani@birjand.ac.ir

(Manuscript received in final form November 28, 2018)

Abstract— As a long-term water deficit condition, drought is a challenging issue in the management of water resources and has been known as a costly and less known natural disaster. Monitoring and predicting droughts, especially accurate determination of their beginning and duration are crucial in management of water resources and planning for mitigating the damaging effects of drought. In this study, the droughts in the southwestern region of Asia (Iran, Afghanistan, Pakistan, and Turkmenistan) were evaluated using the joint deficit index (JDI). Data of monthly and annual precipitation of 1392 downscaled rain gauge stations (by using the Bias Correction Spatial Disaggregation (BCSD method) within the statistical period of 1971-2014 were employed to calculate JDI. The results indicated that in recent years, the number of dry months in the studied region (especially in humid regions of Iran) has significantly increased, such that across all regions in Iran, the percentage of dry months has reached over 50%. The results also showed that in addition to scientific description of the general drought condition, JDI is also able to specify the time of beginning of droughts as well as long-term droughts, allowing investigation of the drought condition on a monthly scale. The results of investigating the trend of changes in the JDI values in the studied region revealed that the variations in these values have decreased on annual scale in the studied region. The extent of reduction in JDI and the increase in the number of dry months within the statistical period of 1971–2014 have been significant (at level of 5%) in Iran, suggesting increased drought in Iran, especially during winter. The values of monthly and annual precipitation in the studied region have been descending, where among the studied countries, Iran has experienced the maximum extent of reduction in precipitation.

Key-words: copula functions, distribution function, drought, joint deficit index, empirical copula

1. Introduction

Iran is located in one of the dry regions of the earth, and is affected by the deserts of the Middle Asia as well as dry and hot deserts of Saudi Arabia and Africa. Iran is considered one of the driest regions on the earth with the least rainfall. Climate change and global warming have intensified the droughts and their durations, causing distribution of precipitations to become non-uniform affecting water resources. Considering the importance of drought, extensive research has been conducted to study it. Every research has considered special aspects of drought. In the studies carried out across different regions of the world, various methods have been used to study drought, and in turn different results have been obtained. One of the most practical indices of drought is the standardized precipitation index (SPI), first introduced by *McKee et al.* (1993). SPI for any region is calculated based on the long-term precipitation statistics at intended scales. Although SPI has been widely accepted as a common general tool for evaluation of droughts, it has some limitations as well (*Mishra* and *Singh*, 2011). One of the limitations is that no standard duration has been introduced for SPI index sometimes presenting contradictory results under different timescales. Accordingly, for general evaluation of the droughts in a region, multiple SPIs should be investigated at the same time with different timescales (e.g., 1, 3, 6, 9, 12, 24, and 48 months) (*Kao* and *Govindaraju*, 2008). In order to eliminate the limitations in SPI, *Kao* and *Govindaraju* (2008) proposed a modified SPI. Unlike the conventional SPI which considers the general average (from beginning of the statistical period until its end) to separate wet and dry periods, in the modified SPI, the threshold limit is based on monthly average. It should be noted that although the modified SPI includes better statistical concepts, to obtain reliable marginal distributions, it needs longer recorded statistics. Further, in calculating modified SPI, as with conventional SPI, selecting different timescales (e.g., 1, 3, … 24 months) results in variable results. To resolve this problem, *Kao* and *Govindaraju* (2008) combined the modified SPIs related to each month with different timescales using copula functions and developed a joint index. This index, which is called joint deficit index (JDI) is a multidimensional index for water deficit based on probability principles (*Mirabbasi et al.*, 2012).

Copula functions were presented by *Sklar* (1959) to develop multivariate distributions. These functions were first employed in hydrology studies by *De Michele* and *Salvadori* (2003) to develop a bivariate model explaining the intensity and duration of rainfall. After that, the concept of copula functions was rapidly utilized across the various areas of hydrology including drought. Drought analysis using copula functions is a new field, which started in 2006 (*Shiau*, 2006). Considering application of copula in drought analysis, the following studies can be mentioned:

Wang et al. (2016) used JDI and monthly precipitation data within the statistical period of 1985–2011 to analyze drought in the Luanhe River basin. The

results of this evaluation indicated that the drought frequency generally increases from northwest to southeast, and the drought in winter and summer is more intense. *Nadi et al.* (2017) used JDI to investigate the droughts in the Javanrood region in Kermanshah province located in the west of Iran. Their results suggested the existence of moderate and severe drought periods with a duration of 3 to 4 years in the region.

Based on the review of literature, it can be inferred that across the studies conducted on drought, precipitation data recorded in synoptic stations have been used. On the other hand, the coverage of downscaled data across each basin is wider as compared with synoptic stations. Therefore, usage of downscaled data better represents the changes in precipitation. Based on the reviewed points and considering climate change worldwide, it seems that examining droughts in Iran as well as its neighboring countries concurrently is essential. Iran is a broad country with different climates, in which precipitation distribution differs from region to region. Furthermore, since it is affected by the incoming air masses from the neighboring countries, the precipitation across the different regions of Iran is highly influenced by the situation of the neighboring countries. The aim of this study is to investigate meteorological drought conditions (using JDI) and the trend of its changes (using the modified Mann-Kendall test) in Iran and its eastern neighboring countries on a monthly scale within the statistical period of 1971–2014.

2. Materials and methods

2.1. The studied region

In this study, the monthly data and the sum of annual precipitation of 1392 downscaled rain gauge stations in Iran and its three neighboring countries (Afghanistan, Pakistan, and Turkmenistan) within the statistical period of 1971–2014 were used for investigating the drought in the regions of interest. The selected regions are located in warm and dry climates of Southwestern Asia. This region has very hot and dry summers and relatively short winters. The northern areas of this region are covered by mountain ranges, encompassing extensive areas of Turkey, Iran, and Afghanistan. In the eastern part of these protrusions, some flatlands can be seen, which have been created with the deposits of Tigris and Euphrates and have a fertile soil. The studied region and the effective air masses upon Iran in the summer and winter seasons are demonstrated in *Figs. 1* and *2*, respectively.

*Fig. 1.* The location of Iran and its eastern neighbors
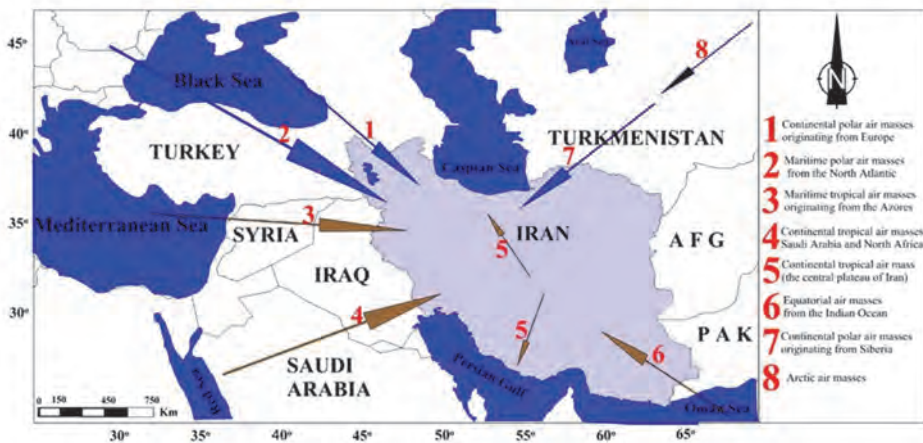
Fig. 2. Effective air masses upon Iran in the summer and winter seasons (*Khalili et al.,* 2016)

2.2. Bias correction and spatial disaggregation (BCSD)

This method was first utilized by *Wood et al.* (2002) for long-term predictions in the eastern part of the United States (*Wood et al.*, 2002). It has also been used in recent years in the majority of monthly climatic studies. This method is so important that it has been used in the output of the fourth and fifth reports by the Intergovernmental Panel on Climate Change (IPCC) alongside other methods (*Payne et al*. 2004). The three major steps this method uses for exponential downscaling of the general circulation models outputs are as follows (*Ahmed,* 2011).

1. Correcting the statistical deviation of the general circulation models outputs on a monthly scale: in this step, two correction factors are generated for temperature and precipitation of the period related to the output of climatic models. Note that this correction factor is calculated on the network points related to the output of climatic models. Further, these factors are calculated in line with the observed and historical data.

$$\begin{cases} F_t = GCM_t - OBS_t \\ F_p = \dfrac{GCM_p}{OBS_p} \end{cases} \tag{1}$$

In this relation, GCM_t and GCM_p are the monthly temperature and precipitation of the general circulation models outputs, OBS_t and OBS_P represent the monthly observed temperature and precipitation at the station of interest. Eventually, F_p and F_t denote the correction factor for precipitation and temperature of the network points of general circulation models outputs. Generally, the time period of observed data and general circulation models outputs (historical) is considered the basic period in the fifth report by the Intergovernmental Panel on Climate Change within 1990–2006. Furthermore, the accuracy of the network points in most models has been stated as 2*2.

2. After calculating the correction factors for the network points of the climatic models using interpolation instruments, these factors are estimated for higher accuracies of 1*1, 0.5*0.5, 0.25*0.25, and 0.125*0.125.

3. The correction factors obtained for higher accuracies are applied to the observed values according to Eq.(2), so that the general circulation models outputs would be estimated for the accuracy of interest. After obtaining the output values of the general circulation models for the new network points, the data around its surrounding points should be extracted considering the position of the observed station.

$$\begin{cases} GCM_t = F_t + OBS_t \\ GCM_p = F_p \times OBS_p \end{cases} \qquad (2)$$

Eventually and by accepting the assumption that the standard deviation of the basic and future periods of the general circulation models outputs is the same, the changes in the climatic components are determined for the future years.

2.3. Copula functions and Sklar theory

Copulas offer a flexible method for developing joint statistical distributions with different marginal distribution functions. Indeed, the copula is a function which links univariate marginal distribution functions for formation of a bi- or multivariate distribution function. The copulas are multivariate distribution functions whose one-dimensional margins are uniform within (0,1). The introduction and presentation of copula functions have been attributed to Sklar, who described a theory suggesting how univariate distribution functions can be combined as multivariate distributions (*Sklar*, 1959).

Sklar indicated that for continuous d-dimensional random variables $\{X_1,.....,X_d\}$ with marginal cumulative distribution functions (CDFs,) $u_j = F_{X_j}(x_j)$ where $j=1,…,d$, there is a unique d-dimensional copula, $C_{U_1,...,U_d}$, where:

$$C_{U_1,...,U_d}(u_1,...,u_d) = H_{X_1,...,X_d}(x_1,...,x_d) \;. \qquad (3)$$

u_j is the jth margin and $H_{X_1,...,X_d}$ is the joint CDF of $\{X_1,.....,X_d\}$. Since for the continuous random variables of a CDF function the margins are non-descending from 0 to 1, $C_{U_1,...,U_d}$ function can be considered as a conversion of $H_{X_1,...,X_d}$ from $[-\infty,\infty]^d$ to $[0,1]^d$. The results of this conversion is that the marginal distributions detach off $H_{X_1,...,X_d}$, and thus, $C_{U_1,...,U_d}$ become related only to the relationship between the variables, offering a complete description of the general dependence structure (*Nelson*, 2007). Although the Sklar theory had been proposed for general dimensions ($d \geq 2$), the complexity of the copulas grows rapidly with the increase in the number of variables. Therefore, most researchers use empirical copulas (especially for dimensions higher than 2) in a multivariate analysis. The concept of empirical copulas is indeed similar to the concept of the formula of plotting positions which are used in univariate statistical analysis (e.g., Weibull formula). These copulas are integral randomized cumulative probability metrics (*Nelson*, 2007). For a sample with the size of n, the d-dimensional empirical copula C_n is as follows:

$$C_n \left(\frac{k_1}{n}, \frac{k_2}{n}, ..., \frac{k_3}{n} \right) = \frac{a}{n}, \tag{4}$$

where a is equal to the number of observations $(x_1,...,x_d)$ satisfying the condition of $x_1 \leq x_{1(k_1)},...,x_d \leq x_{d(k_d)}$, in which $x_{1(k_1)},...,x_d$ with $1 \leq k_1,...,k_d \leq n$ are the sequential statistics of the sample. In a similar method, the empirical distribution function
(K_{C_n}) can be described as follows (*Genest* and *Rivest*, 1993):

$$K_{C_n}(\frac{1}{n}) = \frac{b}{n}, \tag{5}$$

where b is the number of samples $(x_1,...,x_d)$ with $C_n(k_1/n,...,k_d/n) \leq 1/n$. Eq. (5) can also be stated as follows:

$$K_{C_n}(t) = \frac{1}{n} \sum_{i=1}^{n} I(e_{jn} \leq t), \tag{6}$$

where e_{jn} is defined as follows:

$$e_{jn} = \frac{1}{n-1} \sum_{i=1}^{n} I\left(x_{1(k)} \leq x_{1(j)},...,x_{d(k)} \leq x_{d(j)} \right). \tag{7}$$

In which, n is the sample size and $I(A)$ is the indicator variable of the logical statement A. If A is true, then the value is 1, while if it is wrong, the value becomes zero. $R_{i1},..., R_{id}$ are the rank of the ith observed data $(u_1,...,u_d)$. u_w represents the values of the cumulative distribution function related to the data. The empirical copulas C_n and empirical distribution function K_{C_n} are mostly used for model validation, and are considered as the observed dependence structure (real). When a sufficiently large sample is available, empirical copulas can be used for developing nonparametric integrated empirical distributions, which are more efficient computationally.

The meaning of the model is a theoretical copula function. In order to validate the copula function for forming the bivariate distribution, after fitting the suitable marginal distribution on every variables and estimating the distribution parameters, seven copula functions used to link the marginal functions. Finally, the best fitted copula function was selected by comparing the CDF values of every copula function with the corresponding values obtained from the empirical copula. For selecting the best copula function, the Nash–Sutcliffe (NS), Akaike information criterion (AIC), Cramér–von Mises (Sn), Root Mean Square Error (RMSE), Bias and Mean Absolute Error (MAE) criteria were used.

2.4. Joint deficit index (JDI)

To specify the general condition of drought, the modified standardized precipitation index, SPI^{mod} values with different timescales were investigated. One of the comprehensive statistical processes for developing joint distribution of multiple SPI^{mod} is using copulas. *Kao* and *Govindaraju* (2008) defined *JDI* using copula distribution functions to present a scientific description (based on probability) of the general condition of drought. To develop *JDI*, Gaussian and empirical copulas can be used to develop the dependence structure of the set. Nevertheless, given the mathematical complexity of 12-dimensional Gaussian copulas, *Kao* and *Govindaraju* (2008) used empirical copula for this purpose. Since the length of the data used in this study is relatively long (481 point data which are a result of 41 years in 12 months, though for the first 11 months, u_{12} cannot be calculated), empirical copulas are reliable. Selection of $\{u_1, u_2..., u_{12}\}$ in formation of high dimensional copulas increases the dependence model complexity.

Nevertheless, as the duration of the droughts shows extensive temporal changes by only considering different durations (from one to 12 months), droughts can be described well. The reason is that the annual cycle naturally considers the seasonal effects. In addition, this structure allows for one-month evaluation for the future conditions. *Kao* and *Govindaraju* (2008) did not consider margins longer than 12 ($j>12$), since they observed that the samples utilized for $j>12$ begin to overlap, and even after using modified *SPI* process, they cause bias in the results. Therefore, in this study, to develop *JDI*, only 12 of the modified *SPI*s were considered.

One copula is indeed the cumulative probability $P[U_1 \leq u_1,...U_{12} \leq u_{12}] = t$ of the sample margins $\{u_1, u_2..., u_{12}\}$. As each margin shows the wet deficit conditions for each specific time period, the joint deficit conditions are characterized by t. Clearly, a smaller cumulative probability t denotes drier conditions (dryness across different timescales), while larger t values suggest more wet conditions. Assuming that t reflects the intensity of joint drought, the probability of incidence of events with copula values smaller than or equal to t (i.e,. events drier than a certain threshold limit) will be very useful.

For this purpose, the K_c copula distribution function is defined, as the copula distribution function is the same as the cumulative probability $K_C(t) = P[C_{U_1, U_2,...,U_{12}}(u_1, u_1,...,u_{12}) \leq t]$. The special advantage of K_c utilization is that it allows for calculating the probability criterion of the joint deficit conditions, which can be interpreted as a joint drought index.

Indeed, K_c is the same as the $C_{U_1, U_2,...,U_{12}}$ joint CDF. Thus, *JDI* was defined similarly to *SPI* (*Kao* and *Govindaraju*, 2008).

$$JDI = \phi^{-1} K_C .\tag{8}$$

As with *SPI,* positive *JDI* value ($K_c > 0.5$) suggests overall wet conditions; a negative *JDI* ($K_c < 0.5$) shows overall dry conditions, and *JDI*=0 ($K_c = 0.5$) shows normal conditions. Since *JDI* is on an inverse normal scale (as with *SPI*), classification of droughts based on *SPI* can also be used for *JDI* (*Table 1*). The most important property of *JDI* is to evaluate the general deficit conditions based on the dependence structure of the deficit indices with different time periods.

Table 1. Classification scale for the *SPI* values and corresponding event probability limits (*McKee et al.*, 1993; *Bazrafshan et al.*, 2015). It can be used for the modified *SPI*, *MSPI*, and JDI

SPI classes	*SPI* intervals	Probability limit
Extremely wet	$SPI \geq 2$	$\geq 97\%$
Severely wet	$2 > SPI \geq 1.5$	$93.3 - 97.7\%$
Moderately wet	$1.5 > SPI \geq 1$	$84.1 - 93.3\%$
Normal	$1 > SPI > -1$	$15.9 - 84.1\%$
Moderately dry	$-1 \geq SPI > -1.5$	$6.7 - 15.9\%$
Severely dry	$-1.5 \geq SPI > -2$	$2.3 - 6.7\%$
Extremely dry	$SPI \leq -2$	$\leq 2.3\%$

The trend of changes in *JDI* values was also examined using the modified Mann-Kendall test (*Rezaie et al*. 2014; *Khalili et al.* 2016; *Ahmadi et al.* 2018; *Zamani et al*. 2018). The main assumption of the Mann-Kendall test is that the sample data has no significant autocorrelation. However, some hydrological series might have a significant autocorrelation coefficient (*Khalili et al.,* 2016). When a series has a positive autocorrelation coefficient, there is an increased chance for the Mann-Kendall test to reveal existence of a trend in this series. In this case, the null hypothesis is that the lack of trend is rejected, yet this hypothesis should not actually be rejected (*Khalili et al*. 2016). In this method, the effect of all significant autocorrelation coefficients is removed from the time series and is applied to series whose autocorrelation coefficients are significant in one or more cases. Here, the modified variance *V (S)** is calculated as follows:

$$V(S)^* = V(S)\frac{n}{n^*}, \tag{9}$$

$$\frac{n}{n^*} = 1 + \frac{2}{n(n-1)(n-2)} \cdot \sum_{i=1}^{n-1}(n-i)(n-i-1)(n-i-2)r_i, \tag{10}$$

$$Var(S) = \frac{n - (n-1)(2n+5) - C}{18},$$ (11)

$$Z = \begin{cases} \dfrac{S-1}{\sqrt{Var(s)}} & \text{if } S > 0 \\ 0 & \text{if } S = 0, \\ \dfrac{S+1}{\sqrt{Var(s)}} & \text{if } S < 0 \end{cases}$$ (12)

where r_i is the i delayed autocorrelation coefficient and $V(S)$ is estimated by Eq. (11). To calculate the Z statistic in the modified Mann-Kendall test in Eq. (12), $V(S)$ is substituted by $V(S)^*$. The value of Z statistic obtained from Eq. (12) is compared with normal standard Z at α significant level.

Finally, the flowchart of proposed methodology is shown in *Fig. 3*.
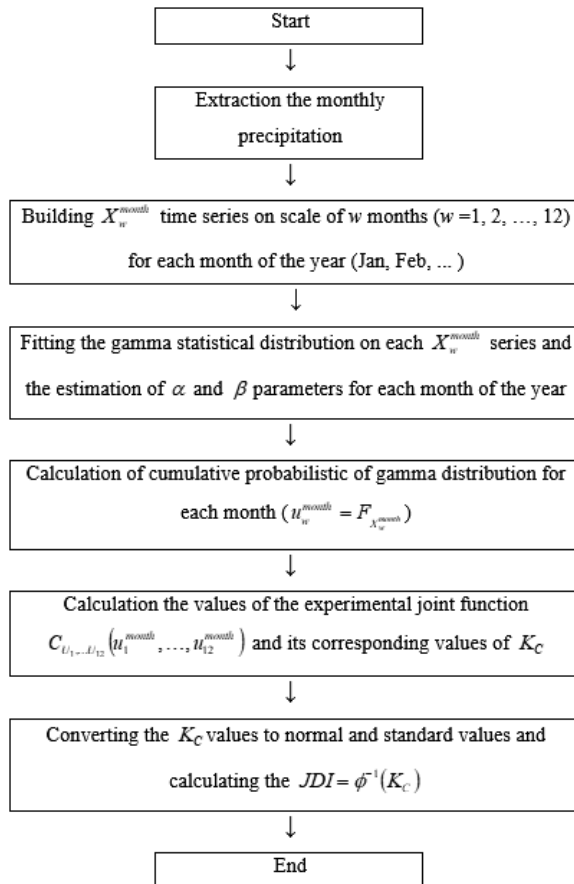
Fig. 3. Flowchart of the proposed methodology.

3. Results and discussion

In this study, the monthly data of annual precipitation of 1392 downscaled rain gauge stations in Iran and its three eastern neighboring countries were used to investigate the monthly droughts using copula functions. In this study, the monthly precipitation data of Iran, Afghanistan, Pakistan, and Turkmenistan were used. The results of calculating *JDI* values on monthly timescale in 2014 have been presented as a sample in the form of box plots (*Figs. 4–7*).
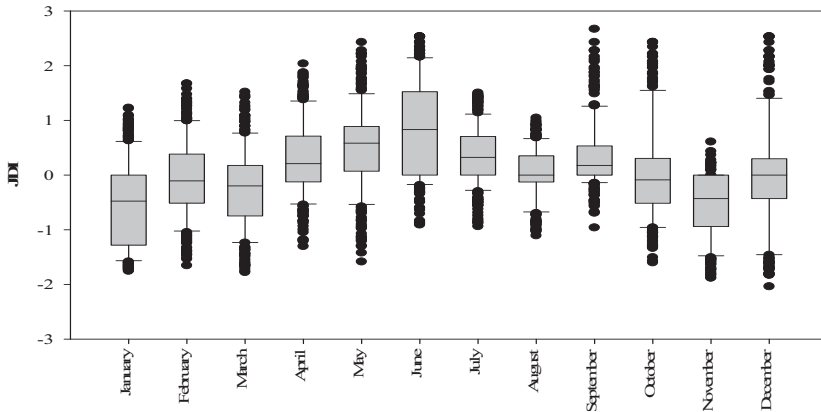
Fig. 4. Calculated monthly values of *JDI* for Iran in 2014.
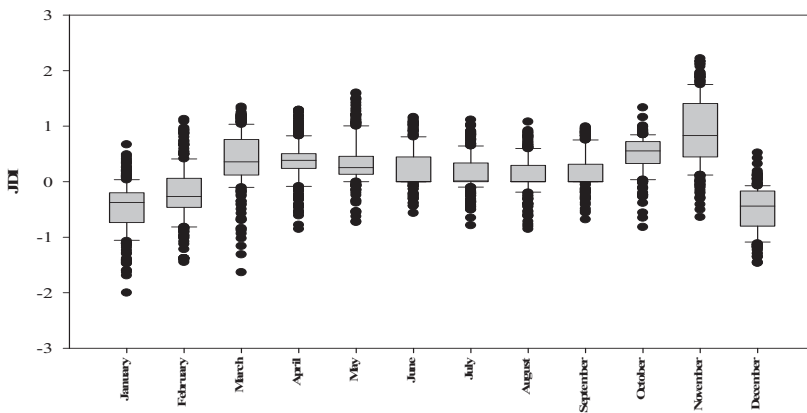
Fig. 5. Calculated monthly values of *JDI* for Afghanistan in 2014.

445
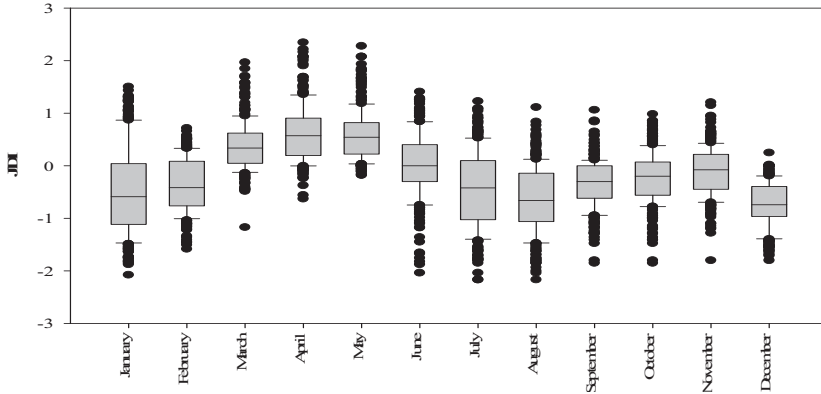
Fig. 6. Calculated monthly values of *JDI* for Pakistan in 2014.
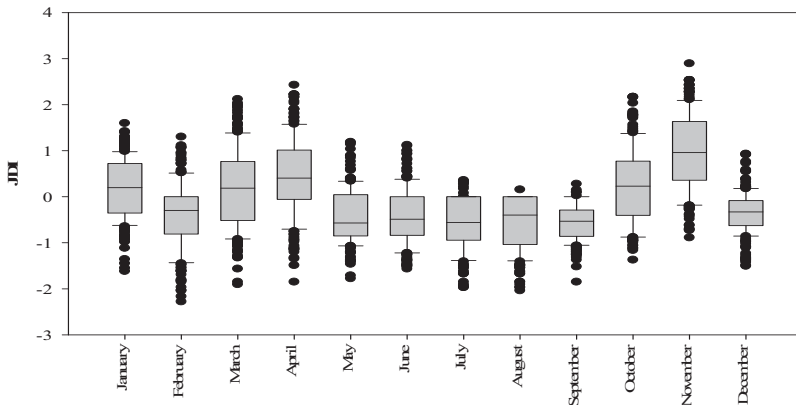
Fig. 7. Calculated monthly values of *JDI* for Turkmenistan in 2014.

3.1. *The results of investigating JDI in Iran*

The results of investigating *JDI* in Iran indicate that at the beginning of the statistical period, the major changes in *JDI* values in January, February, June, and October are negative and show normal conditions (0 to –1). In April, May, July, August, November, and December, better conditions governed the region. However, this superiority is also limited to normal conditions. The changes in monthly *JDI* values in 2014, as presented according to *Fig. 4*, suggest normal conditions in April, May, June, July, August, September, and October, as the major changes in *JDI* values are close to zero or more.

446

3.2. The results of investigating JDI in Afghanistan

The results of investigating *JDI* in Afghanistan indicate that at the beginning of the statistical period, the changes in *JDI* values varied considerably across the different months. Most of the changes in this parameter have occurred in January between –1 and –0.8, suggesting normal conditions in the region. The major changes in *JDI* values during 1971 were less than zero in all months, suggesting normal conditions across the months of the year at the beginning of the statistical period. The major changes in *JDI* values in February, March, and May are somehow similar to those of January. August, July, and June in 1971, which had the greatest range of changes in *JDI* values. In this regard, in Jul, these changes reach below 1. December, November, and September have better conditions as compared with other months, when *JDI* values are closer to zero. Several cases showed numbers above zero across different stations and in different months. The major changes in *JDI* values in this country in 1971 suggest normal conditions in the region.

At the end of the studied statistical period, the results of investigating *JDI* values suggest amelioration of drought conditions in March-November (–0.8 to 1.35). Except for Jan and December, when moderately dry conditions were experienced, other months have close to normal conditions. Based on *Fig. 5*, it can be concluded that the *JDI* values calculated in Afghanistan within the studied statistical period suggest amelioration of climate conditions in this country.

3.3. The results of investigating JDI in Pakistan

The results of investigating *JDI* in Pakistan indicate that the beginning of the statistical period shows moderately dry condition. The major changes in *JDI* values in February, March, April, and May lie in –1.5– 0, suggesting moderately dry and normal conditions. According to classification of *JDI*, almost in all months, moderately dry conditions govern the region. However, these changes in 2014 (*Fig. 6*) in March, April, and May show normal conditions. Other months have worse conditions as compared with the beginning of the statistical period, representing moderately dry and almost normal conditions.

3.4. The results of investigating JDI in Turkmenistan

The results of investigating *JDI* in Turkmenistan suggest normal conditions (–1 to 0) in the region at the beginning of the statistical period. The changes in *JDI* values are better in Apr as compared with other months. However, this superiority is also limited to normal conditions. As with other countries, the changes in *JDI* values in 2014 have progressed towards normal and sometimes moderately dry conditions (*Fig. 7*). Distribution of *JDI* values across the studied region in 2014 is presented in *Fig. 8*.
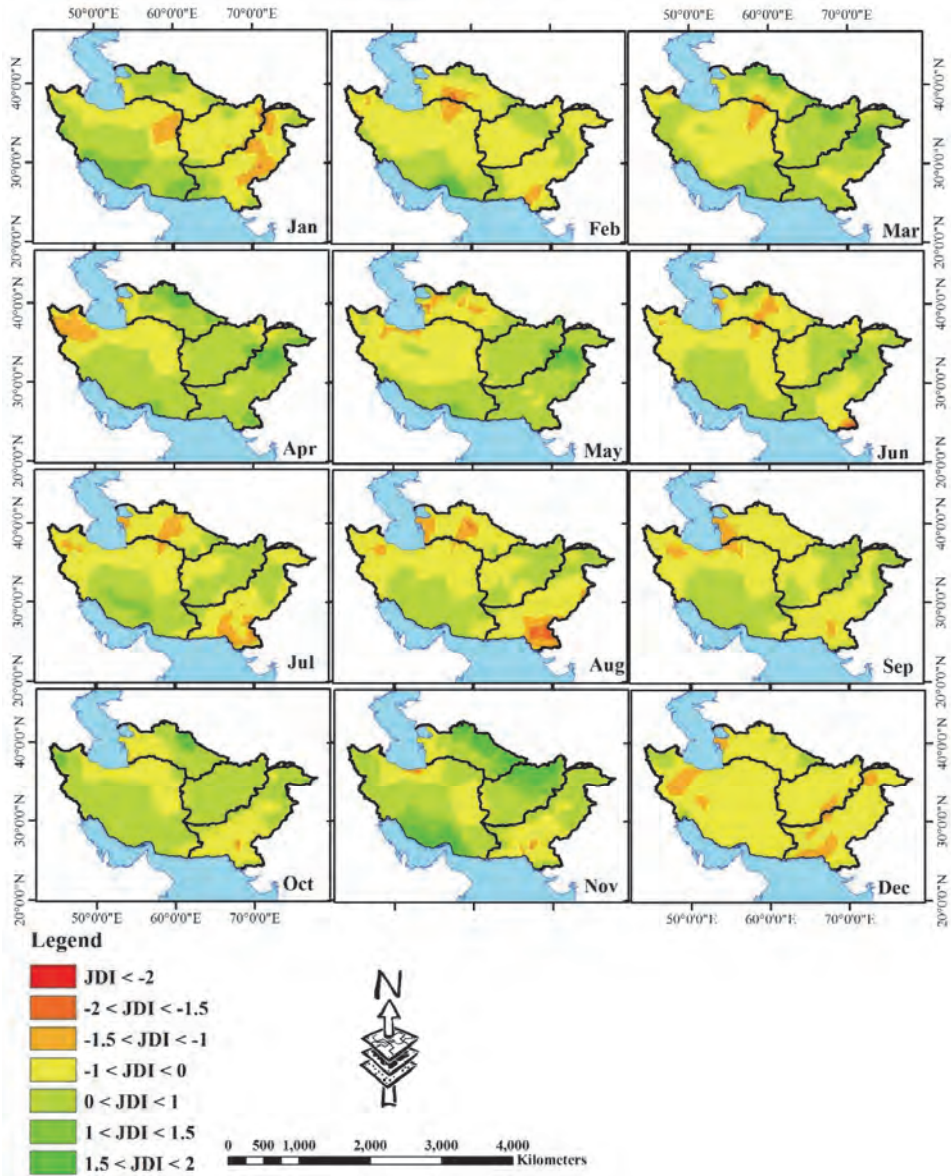
Fig. 8. Zoning of the *JDI* values across the studied region in 2014.

In 2014 and in January, most areas of Iran had a suitable status in terms of *JDI*. Also other months including May, April, March, June, October, and November experienced normal and moderately wet conditions in most areas of the studied region. However, in this year (2014) in Dec, almost all areas of the

studied region experienced moderately dry conditions. Generally, the results of zoning *JDI* values across the studied region indicated that in recent years in winter, precipitation deficit has prevailed the studied region.

Considering the dramatic changes in *JDI* parameter during the studied statistical period among the selected months, and to more accurately investigate the changes in these values (*JDI*), the trend of its monthly and annual changes should be examined within a 45-year-long statistical period (1971–2014). Based on the mentioned points, the trend of changes in *JDI* values within the 45-year statistical period was examined by the modified Mann-Kendall test. The results obtained from investigating the trend of changes in *JDI* values on an annual scale are presented in *Fig. 9*.
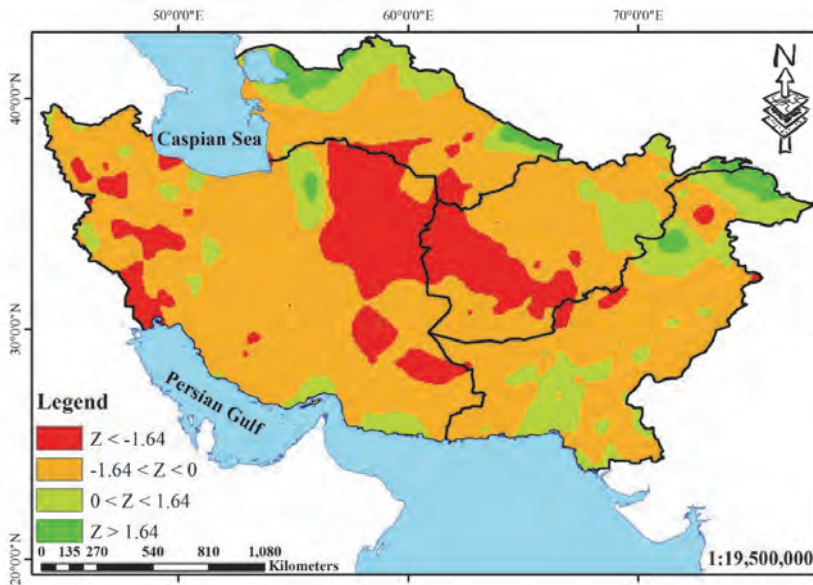
Fig. 9. Zoning of the trend of changes in *JDI* values on annual scale.

The results of investigating the trend of changes in droughts in Jan suggest increased droughts with a significant reduction in *JDI* values in the eastern and northeastern areas of Iran as well as at the Iran and Afghanistan borderline. In this month, the descending trend of *JDI* values can be observed across almost the entire studied region, which in turn shows increased droughts.

However, in February, the trend of long-term changes in monthly *JDI* values in the eastern regions of the studied zone (the eastern regions of Afghanistan and

Pakistan) as well as the northern borderline of Turkmenistan was ascending, suggesting diminished droughts in these regions. This situation of Iran became more critical in February in relation to January. The western and eastern regions of Iran have had a descending insignificant trend in *JDI* values, suggesting increased droughts.

In March, as compared with January and February, the situation of Iran became more critical. Iran suffers from more serious drought condition compared to its three eastern neighbors. In this month (March), droughts have grown significantly in Iran. However, the eastern areas of Pakistan and Afghanistan have suitable conditions in terms of precipitation. The northern regions of Turkmenistan in this month (March) have also better conditions compared to Iran.

The results of investigating the trend of changes in *JDI* values in the studied region indicated that in April, the trend of changes in *JDI* values in the northeastern, southern, and northwestern areas of Iran experienced a descending and significant trend, suggesting increased drought in these areas. In this month (Apr), the changes in *JDI* values in the central and southeastern areas of Iran have been ascending, suggesting diminished level of drought and deficit of precipitation in this month within the statistical period of 1971–2014. In April, the changes in droughts have also been descending in the northern parts of Turkmenistan as well as eastern areas of Afghanistan and Pakistan.

In May, the intensity of droughts in the central areas of Iran has decreased. However, the descending trend of *JDI* values still prevail the entire country. In this month (May), the changes of *JDI* values are ascending in the eastern areas of Afghanistan and Pakistan. This trend has also changed in June in Iran. In this month, in the central and southeastern areas of Iran, the trend changes in *JDI* values has been increasing, suggesting diminished drought and increased precipitation fluctuations. The eastern neighbors of Iran have also had a suitable situation in terms of drought. The growing changes of *JDI* values in Jul in Iran have reached the central areas of the country. The variations of *JDI* values in Jul have been decreasing and significant in parts of eastern Iran and southeastern Pakistan. From among the studied countries, the situation in Afghanistan in July is better than in other countries.

In August, the changes in *JDI* values in the studied area have been better, as compared with other months, where ascending changes are observed in *JDI* values in most areas, and these changes are also observed in September. In this month (Sep), the situation in the eastern neighbors of Iran is better than in all of the studied countries. These conditions of improved droughts in October are clear in the neighboring countries. However, in Iran in October, the predominant trend is also descending. In November, the ascending trend of *JDI* values in the neighboring countries can be clearly observed. However, across Iran, these changes are diminishing in the northwestern, western, and northeastern areas of the country.

In December, which is one of the winter months in Iran, diminishing changes of *JDI* values prevail the entire country. Apart from the eastern regions of

Afghanistan and Pakistan, as well as the northern and southern areas of Turkmenistan, other areas have experienced descending *JDI* values. These diminishing changes in this month and in winter suggest lowered precipitation and increased droughts, which is very serious.

On annual scale, the results of investigating and zoning by the aid of the Mann-Kendall Z statistic across the studied region indicated that the trend of changes in *JDI* values within the statistical period of 1971–2014 is descending and significant in the northwestern, western, southeastern, eastern, and northeastern areas of Iran, suggesting significant increase in droughts in these areas. On the annual scale, the western areas of Afghanistan and Pakistan as well as northern parts of Turkmenistan have experienced an ascending trend in *JDI* values, suggesting normal conditions in these areas. The predominant trend of *JDI* values in Iran is descending on the annual scale.

Monsoons during summer develop warm and humid tropical weather. This weather enters the southern areas of Iran in two ways: first through sea breeze which enters Iran from the Oman Sea and Persian Gulf up to a limited radius and altitude. Its area is very small and due to high pressure development of Azores High above the region, it does not have a significant effect on precipitation. The second way is the entrance of monsoon weather through low-pressure heat during summer in Pakistan and India. Nevertheless, the frequency and intensity of the summer monsoon rainfalls are low given the side of their entrance. The climatic effect of Saudi Arabia lands mostly emerges during summer. In the warm period of the year, due to establishment of Azores High over Iran, Iran's sky is devoid of cloud, thus causing the Earth's surface warming. The global warming develops a low-pressure center on the Persian Gulf. This low-pressure center pulls in the weather of Saudi Arabia Peninsula into Iran. Entrance of warm and dry weather of Saudi Arabia into Iran causes elevation of the temperature of the Khuzestan Plain cities, whereby dry and warm weather prevails this region. The increase in the droughts of the region suggests lowered level of precipitations, and the existence of a descending trend of precipitation across Iran has also been confirmed by various studies including *Kousari et al.* (2013) and *Khalili et al.* (2014).

4. Conclusion

Statistical analysis of the monthly and annual precipitation data of Iran and its neighboring countries is crucial in terms of precipitation deficit distribution climatically. Accordingly, investigating an index which can reveal this joint precipitation deficit is important. *JDI* is an index for determining changes in precipitation in a certain region, and the results of its analysis can indicate drought in an environment. In this study, *JDI* was used to analyze the drought and precipitation deficit on annual and monthly scales in Iran and its eastern neighboring countries including Afghanistan, Pakistan, and Turkmenistan within

the statistical period of 1971–2014. In addition to examining *JDI* across the studied region, the trend of changes in precipitation as well as trend of variations in *JDI* values was also investigated across the studied region. The results of investigating and zoning of *JDI* values on annual and monthly scales in the studied region showed that from among the studied countries, the drought condition and precipitation deficit is worse in Iran, and the extent of droughts in Iran is more than that of its eastern neighboring countries. The extent of droughts has also increased in recent years (up to 2014), according to the values presented by *JDI*. The results of investigating the trend of changes of precipitations in the studied region suggested a significant decrease in the precipitation in Iran within 1971–2014 on monthly and annual scales. Meanwhile, the share of Iran in terms of precipitation reduction is larger as compared with its neighboring countries including Turkmenistan, Afghanistan, and Pakistan. The results of investigating the trend of changes in *JDI* values across the studied region indicated that the variations of *JDI* values on annual scale have been descending in the studied region. Based on the obtained results, it was found that the trend of changes in *JDI* values in Iran (such as diminishing precipitations) has been more declining as compared with other countries, suggesting increased droughts in recent years. The results imply descending changes of *JDI* values across the entire Iran. Generally, the results of zoning of *JDI* values across the studied region indicated that in recent years in winter, precipitation deficit has prevailed the studied region.

References

Ahmadi, F., Nazeri Tahroudi, M., Mirabbasi, R., Khalili, K. and *Jhajharia, D.*, 2018: Spatiotemporal trend and abrupt change analysis of temperature in Iran. *Meteorol. Appl. 25*, 314–321. https://doi.org/10.1002/met.1694

Ahmed, K.F., 2011: Bias Correction and Downscaling of Climate Model Outputs Required for Impact Assessments of Climate Change in the US Northeast , Master's theses, University of Connecticut OpenCommons@UConn

Bazrafshan, J., Nadi, M. and *Ghorbani, K.*, 2015: Comparison of empirical copula-based joint deficit index (JDI) and multivariate standardized precipitation index (MSPI) for drought monitoring in Iran. *Water Resour. Manage. 29*:2027–2044. https://doi.org/10.1007/s11269-015-0926-x

De Michele, C. and *Salvadori, G.*, 2003: A generalized Pareto intensity-duration model of storm rainfall exploiting 2-copulas. *J. Geophys. Res.: Atmospheres 108,* D2. https://doi.org/10.1029/2002JD002534

Genest, C. and *Rivest, L-P.*, 1993: Statistical inference procedures for bivariate Archimedean copulas. *J. Amer. Statistic. Assoc. 88*,1034–1043. https://doi.org/10.1080/01621459.1993.10476372

Kao, S.C. and *Govindaraju, R.S.*, 2008: Trivariate statistical analysis of extreme rainfall events via the Plackett family of copulas. *Water Resour. Res. 44(2).* https://doi.org/10.1029/2007WR006261

Khalili, K., Esfandiary, S., Khanmohammadi, N. and Nazeri Tahrudi, M., 2014: Half-century air temperature trends in Iran. *J.Midd. East Appl. Sci. Technol. 8*, 208–213.

Khalili, K., Tahoudi, M.N., Mirabbasi, R. and Ahmadi, F., 2016: Investigation of spatial and temporal variability of precipitation in Iran over the last half century. *Stoch. Environ. Res. Risk Ass. 30,* 1205–1221. https://doi.org/10.1007/s00477-015-1095-4

Kousari, M.R., Ahani, H. and Hendi-zadeh, R., 2013: Temporal and spatial trend detection of maximum air temperature in Iran during 1960–2005. *Glob. Planet. Change 111*, 97–110. https://doi.org/10.1016/j.gloplacha.2013.08.011

McKee, T.B., Doesken, N.J., and Kleist, J., 1993: The relationship of drought frequency and duration to time scales. In: Proceedings of the 8th Conference on Applied Climatology, 1993. vol 22. American Meteorological Society Boston, MA.179–183.

Mirabbasi, R., Fakheri-Fard, A., and Dinpashoh, Y., 2012: Bivariate drought frequency analysis using the copula method. *Theor. Appl. Climatol. 108*, 191–206. https://doi.org/10.1007/s00704-011-0524-7

Mishra, A.K. and Singh, V.P., 2011: Drought modeling–A review. *J. Hydrol. 403*,157–175. https://doi.org/10.1016/j.jhydrol.2011.03.049

Nadi, M., Bazrafshan, J., Pourtahmasi, K., and Bräuning, A., 2017: Tree-ring based reconstruction of the joint deficit index in Javan-Roud Region, Kermanshah (Iran). *Int. J. Climatol. 37*,420–429. https://doi.org/10.1002/joc.4715

Nelsen, RB., 2007: An introduction to copulas. Springer Science & Business Media.

Payne, JT., Wood, AW., Hamlet, AF., Palmer, RN., and Lettenmaier, DP,. 2004. Mitigating the effects of climate change on the water resources of the Columbia River basin. *Climatic change. 62,*(1-3), 233-256.

Rezaie, H., Khalili, K., Khanmohammadi, N., and Nazeri Tahrudi, M., 2014. Surface air temperature trends during the last 20 years in Iran. *J. Appl. Environ. Biol. Sci. 4(1s)*, 40–46.

Shiau, J., 2006: Fitting drought duration and severity with two-dimensional copulas. *Water Resour. Manage. 20*, 795–815. https://doi.org/10.1007/s11269-005-9008-9

Sklar, A., 1959: Distribution functions of n dimensions and margins. Publications of the Institute of Statistics of the University of Paris 8, 229–231.

Wang, Y., Li, J., Feng, P., and Hu, R., 2016: Analysis of drought characteristics over Luanhe River basin using the joint deficit index. *J. Water Clim. Change 7,* 340–352. https://doi.org/10.2166/wcc.2015.108

Wood, A.W, Maurer, E.P., Kumar, A., and Lettenmaier, D.P., 2002: Long-range experimental hydrologic forecasting for the eastern United States, *J. Geophysical Research: Atmospheres. 107*, D20: ACL-6. https://doi.org/10.1029/2001JD000659

Zamani, R., Mirabbasi, R., Nazeri, M., Meshram, S. G. and Ahmadi, F., 2018. Spatio-temporal analysis of daily, seasonal and annual precipitation concentration in Jharkhand State India. *Stoch. Environ. Res. Risk Ass. 32*, 1085–1097. https://doi.org/10.1007/s00477-017-1447-3

IDŐJÁRÁS

Cyclical variability of seasonal precipitation in Poland

Jadwiga Nidzgorska-Lencewicz and **Małgorzata Czarnecka**

Department of Environmental Management
West Pomeranian University of Technology in Szczecin
Papieża Pawła VI St 3A, 71-459 Szczecin, Poland

*Corresponding Author E-mail: jnidzgorska@zut.edu.pl

Abstract— The aim of the present paper was an attempt to detect the recurring fluctuations in the course of seasonal sums of precipitation in Poland. The basic material consisted of monthly sums of atmospheric precipitation obtained from 37 IMGW-BIP weather stations from the period 1951 – 2016, excluding the mountain areas. Spectral analysis was performed concerning precipitation sums in the four calendar seasons: spring (March – May), summer (June – August), autumn (September – November), winter (December – February). The results of the spectral analyses showed that the changes in seasonal precipitation sums recorded in the analyzed multiannual period occurred in numerous, statistically significant cycles, with a clear predominance of the cycles with the following length: 4.0, 4.6, 4.9, 5.3, 5.8, 6.4, and 7.1 years. It was found that the winter season is characterized by the most pronounced cyclicality (cycles of 6.4 years), whereas the spring season is marked by the highest variability in terms of periodicity.

Key–words: seasons, variability, spectral analysis, cycle

1. Introduction

Changes occurring in the global climate system encourage deeper analysis of variability of climatic conditions on regional or local scales (*Marosz et al.,* 2011). The need for research on climate change is also indicated by the work of *Kaszewski* (2015), who developed a synthesis of studies conducted by Polish climatologists. The most commonly studied issues are the basic climatic

elements – air temperature and atmospheric precipitation. The results of numerous studies unequivocally point to the stipulation that the ongoing climate warming is in fact empirically confirmed to take place in Poland. Atmospheric precipitation, however, is not subject to such obvious changes (*Kirschenstein,* and *Baranowski,* 2005; *Kożuchowski,* 1996, 2004; *Boryczka* and *Stopa-Boryczka,* 2000*; Żmudzka,* 2009). Depending on the analyzed period, the annual precipitation sums show a statistically insignificant upward or downward trend (*Żmudzka,* 2002; *Mager et al.*, 2009; *Marosz et al.,* 2011; *Czarnecka* and *Nidzgorska-Lencewicz*, 2012; *Skowera et al.*, 2014). A similar situation is observed concerning the extreme precipitation. The study by *Marosz* (2011) showed that totals and the number of days with extreme precipitation are insignificant and spatially incoherent. *Łupikasza* (2010) presented the dominance of long–term (1951–2006) decreasing tendencies of various indices of extreme precipitation in Poland. Additionally, the changes in the values of seasonal atmospheric precipitation do not show a statistically significant linear trend (*Czarnecka* and *Nidzgorska-Lencewicz*, 2012). In spite of the above-mentioned facts, the pluvial regime in Poland has changed over the last few decades. In the south part of Poland, the number of days with very light (0.1–1.0 mm) and light precipitation (1.1–5.0 mm) showed a clear increase, and the number of days with 20.1–30.0 mm of precipitation was found to decrease (*Skowera et al.,* 2016). An upward trend of an increase in precipitation during the spring and autumn season, and the decreasing share of summer precipitation in the annual totals is the common phenomena manifested over the area of Poland (*Czarnecka* and *Nidzgorska-Lencewicz*, 2012; *Szwed*, 2018). According to *Degirmendžić et al.* (2004), this is the fundamental reason behind weakening of the continental nature of the climate. The forecasts by *Szwed* (2018) indicate that the annual totals of precipitation in Poland will increase, precipitation recorded in the warm season will continue to decrease, and precipitation in the cold season is expected to increase. Indeed, this is an extremely disadvantageous trend as there are currently many regions in Poland affected with water shortages during the growing season, and the situation is likely to aggravate. It is a recognized fact that water shortages are responsible for numerous adverse natural and economic phenomena, as well as deteriorating functioning of society (*Kędziora et al.,* 2014). Droughts result in calculable economic loss and contribute to a significant reduction in yield of cultivated plants (*Żarski et al.,* 2014*,* 2017). Recently, drought is recorded increasingly more often in Poland, particularly since 1992 (*Doroszewski et al.,* 2014).

The changes in the basic features assessed with the use of linear trend are not statistically significant due to the fact that the changes of the most labile element of the climate (assuredly, the precipitation) can be expressed as irregular fluctuations. However, studies on identifying the natural periodicity in the course of meteorological elements are not frequently conducted in Poland. Admittedly, the identified cyclicality in the course of precipitation is based on

long-term, at least century-long, measuring series, yet the results are limited to one or only few stations in Poland (*Boryczka* and *Stopa-Boryczka*, 2004; *Degirmendžić et al.*, 2004; *Miętus,* 1996; *Miler* and *Miler*, 2005*; Miler* and *Okoński*, 2011; *Twardosz* and *Cebulska* 2005; *Czarnecka* and *Nidzgorska-Lencewicz*, 2016). So far, the literature on the subject with reference to Poland is lacking in studies concerned with identifying the natural fluctuations in sums of precipitation in the whole area of Poland. The present study is an attempt to provide the missing information.

2. Materials and methods

The study is based on the monthly sums of atmospheric precipitation from the period 1951–2016 obtained from 37 meteorological stations of the Institute of Meteorology and Water Management – National Research Institute (IMGW-PIB), location of which is presented in *Fig. 1*. The analysis does not include the mountainos areas. More than half of the stations is located at an altitude below 150 m a.s.l., and only 6 stations are located at an altitude of over 200 m a.s.l. – including the two stations (Jelenia Góra and Kłodzko), which are located at an altitude of over 300 m a.s.l. The analysis considers the totals of the calendar seasons, i.e., spring (March – May), summer (June – August), autumn (September – November), and winter (December – February).

Fig. 1. Location of meteorological stations of IMGW-PIB considered in the study (mountain areas are not considered in this study).

For the purpose of identifying periodic phenomena, harmonic analysis – also known as Fourier spectral analysis, is used (*Fortuniak,* 2004; *Miler* and *Okoński,* 2011). By means of decomposition of time series, this analysis enables determination of periodicity often distorted by a random component. The condition for the application of spectral analysis is the stationarity of the analyzed series. The analyzed stochastic process was brought down to the stationary series by calculating the first increments. Then, the series was smoothed by Hamming spectral window 5, which resulted in reduction of random noise and facilitated identification of frequency range which contributes the most to the general harmonic structure of the analyzed series of atmospheric precipitation. The significance of periodicity was tested with Bartlett's Kolmogorov-Smirnov test and Fisher's Kappa. The calculations were made with the use of Statistica 10 software.

3. Results

The mean annual sum of precipitation calculated on the basis of the results obtained from 37 stations from the period 1951–2016, excluding the mountainous area, amounted to 596 mm and was almost the same as that recorded for the 60-year-long period 1951–2010 (*Czarnecka* and *Nidzgorska-Lencewicz*, 2012), and the average from 53 stations in the standard 30-year-long period 1971–2000 (*Ziernicka-Wojtaszek*, 2006). On average, the smallest total precipitation i.e., approximately 410 mm, was identified in 1982, whereas twice the amount was recorded in 2010 (*Fig. 2*). Annual precipitation, of a sum of more than 700 mm, was recorded more frequently in the first half of the analyzed multiannual period, and a longer series of precipitation of lower or comparable values to the average amount was recorded in the period 1982–1997. Mean precipitation totals from 37 stations in spring, summer, autumn, and spring were: 130, 223, 138, and 103, respectively. The maximum and minimum seasonal sums of precipitation occurred in different years, yet all of them were recorded in the 20th century. Pluvial continentalism in Poland is manifested by more than double predominance of summer precipitation over precipitation recorded in winter. Sums of precipitation in the three summer months constitute approximately 38% of the annual total, while winter precipitation – merely approximately 17% (*Fig. 3*). Nevertheless, percentage share of seasonal precipitation in the annual sum shows very high inter-annual variability – the highest in summer and the smallest in winter. For example, in the summer of 1994, precipitation amounted to only 22% of the annual total, whereas in 2011 – to as much as 51%. Although mean precipitation values in the transitional seasons are comparable, a clear dominance of autumn precipitation is evident and distinguished by not only the highest values of the coefficient of variation in the sums (Vs=27% – *Fig. 2*), but also by greater fluctuations (as compared to spring) of the percentage share in the annual total (*Fig. 3*).
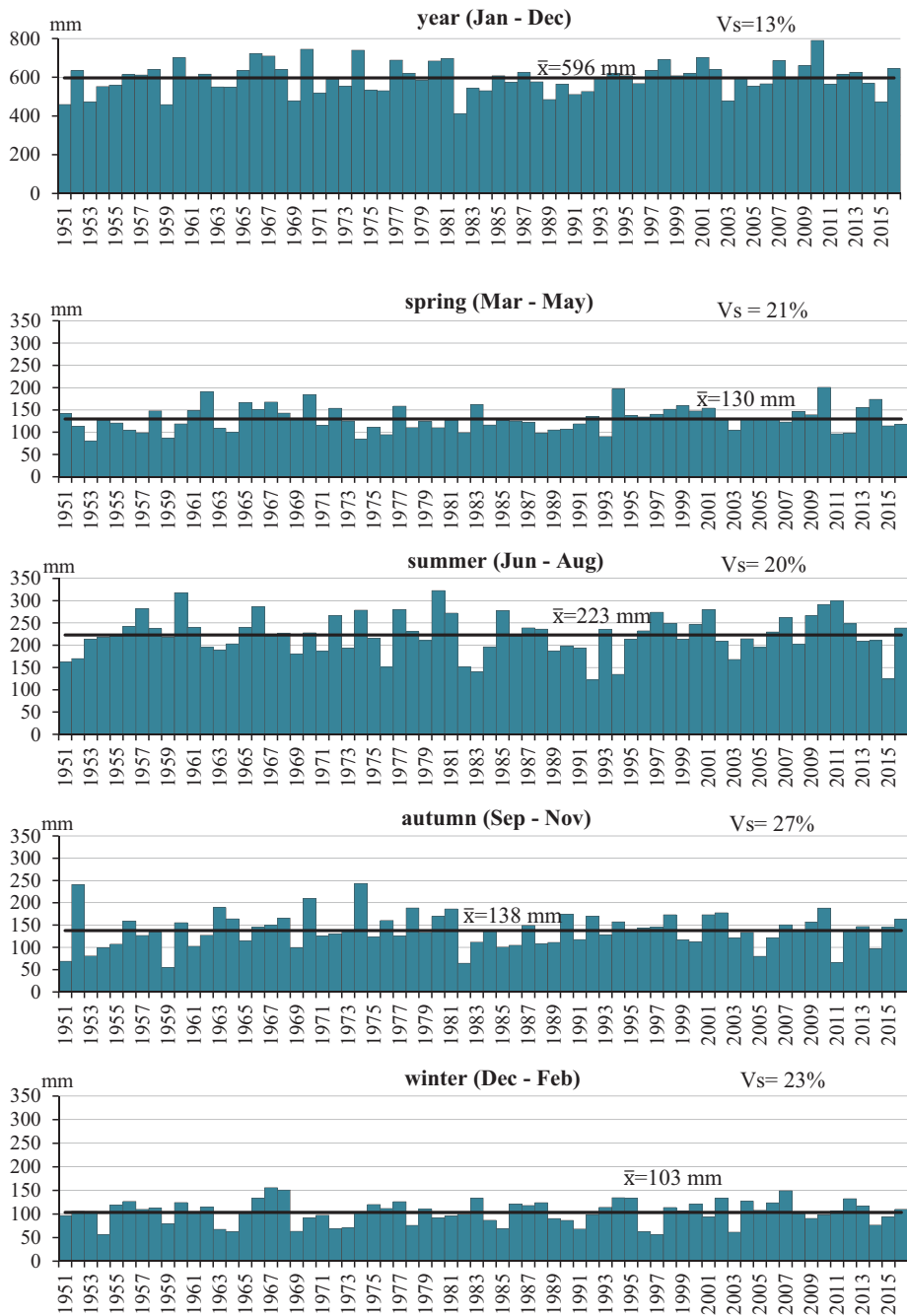
Fig. 2. Variability in the annual and seasonal precipitation sums (mm) in Poland (mean of 37 stations) in the period 1951-2016.
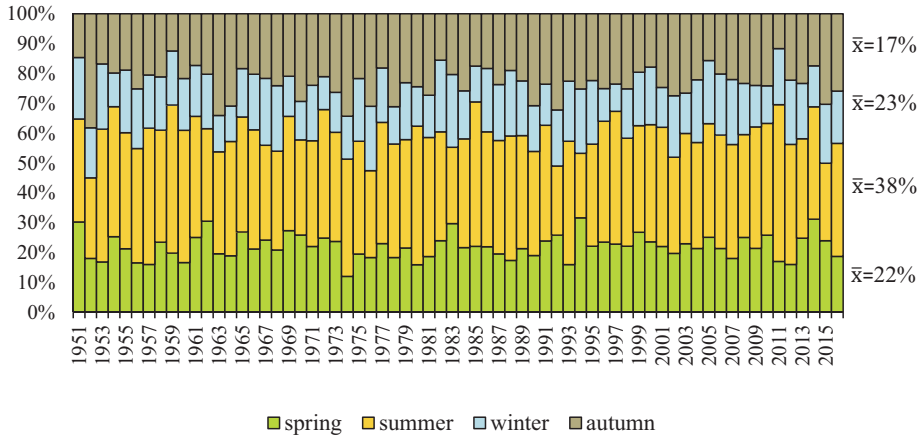
Fig. 3. Variability of percentage share of seasonal precipitation in the annual sums in Poland (mean of 37 stations) in the period 1951–2016.

The basic features of atmospheric precipitation in the 66-year-long period (1951–2016) as per individual stations are presented in *Table 1*. The values of annual and seasonal precipitation – both as regards the means and the extremes, do not differ from those determined for the 60-year-long period of 1951–2010 (*Czarnecka* and *Nidzgorska-Lencewicz*, 2012). In most of the stations, the recorded mean annual sums range from 500 to 600 mm, and the higher values were recorded in Koszalin and Tarnów. Among the 36 analyzed stations, the minimum annual sum of precipitation was recorded in Kalisz. In the analyzed multiannual period, at eight stations, the maximum annual sum of precipitation was determined in 2010, and the highest values (1200 mm) were recorded in Tarnów. At many stations, the smallest sums of precipitation occurred in 1982. The series of 1982–1984 is termed by *Doroszewski et al.* (2014) as a period of severe drought in Poland.

Table 1. Mean (a), maximum (b), and minimum (c) sum in mm and coefficient of variation (d) in % of precipitation in selected stations in Poland, in the period 1951-2016

Station number in *Fig.1*	Height in m n.p.m.	Station		Spring Mar-May	Summer Jun-Aug	Autumn Sep-Nov	Winter Dec-Feb	Year Jan-Dec
1	139	Białystok	a	128	218	140	103	590
			b	245	414	336	185	858
			c	46	94	30	46	336
			d	30	31	39	29	17
2	172	Chojnice	a	119	216	138	103	577
			b	247	489	286	211	835
			c	46	75	26	38	311
			d	33	34	37	37	19
3	38	Elbląg	a	122	238	186	121	668
			b	217	512	343	215	938
			c	52	81	63	30	354
			d	28	35	32	30	19
4	65	Gorzów Wielkopolski	a	121	191	123	112	547
			b	198	326	271	200	752
			c	46	80	47	49	337
			d	31	27	37	32	17
5	342	Jelenia Góra	a	165	283	144	105	697
			b	279	559	297	177	1007
			c	91	132	24	50	450
			d	26	30	33	30	18
8	268	Kielce	a	140	237	135	117	630
			b	296	446	324	233	1000
			c	65	122	29	48	438
			d	33	32	36	31	18
9	316	Kłodzko	a	141	258	124	75	598
			b	281	454	225	119	854
			c	59	95	38	27	339
			d	30	30	35	28	17
12	206	Kraków	a	161	267	145	107	681
			b	369	518	319	187	1021
			c	74	101	44	56	470
			d	31	28	38	27	17
15	171	Lublin	a	139	217	134	101	590
			b	337	376	299	176	821
			c	64	68	33	38	349
			d	34	26	42	29	18
16	187	Łódź	a	126	215	127	102	569
			b	256	382	230	161	780
			c	56	83	22	37	338
			d	30	30	34	31	17
18	133	Olsztyn	a	125	229	159	114	627
			b	241	374	295	196	920
			c	42	81	57	34	342
			d	34	31	31	30	19

Table 1. Continued

Station number in *Fig.1*	Height in m n.p.m.	Station		Spring Mar-May	Summer Jun-Aug	Autumn Sep-Nov	Winter Dec-Feb	Year Jan-Dec
20	86	Poznań	a	117	193	114	98	582
			b	234	306	211	177	886
			c	38	60	30	37	317
			d	34	32	38	31	20
21	189	Racibórz	a	154	254	137	92	637
			b	305	473	281	209	1006
			c	54	73	46	23	254
			d	31	33	36	33	20
23	200	Rzeszów	a	153	243	139	98	632
			b	307	460	320	167	1008
			c	60	92	39	49	340
			d	30	32	41	30	21
24	202	Sandomierz	a	133	227	123	83	566
			b	224	456	293	181	865
			c	75	116	30	32	376
			d	30	32	41	40	19
27	165	Suwałki	a	121	221	151	103	597
			b	224	463	299	188	829
			c	53	89	59	28	323
			d	30	32	35	31	17
28	5	Świnoujście	a	119	180	146	118	564
			b	249	409	313	182	761
			c	50	53	60	45	377
			d	31	33	33	30	17
29	1	Szczecin	a	120	188	127	109	543
			b	234	364	244	179	795
			c	57	70	64	43	390
			d	31	29	31	31	16
31	69	Toruń	a	108	211	118	90	528
			b	273	557	214	152	846
			c	44	86	28	31	312
			d	38	35	37	33	21
32	6	Ustka	a	116	216	219	142	693
			b	296	361	413	250	1019
			c	44	85	86	64	424
			d	36	34	36	28	18
33	106	Warszawa	a	117	207	121	88	533
			b	291	406	269	138	798
			c	36	87	17	28	345
			d	37	29	42	33	18
36	120	Wrocław	a	127	229	121	85	562
			b	211	396	213	160	776
			c	66	119	37	38	323
			d	27	30	33	32	18

The values of summer precipitation provided by most of the stations range from 200 to 250 mm, whereas the amount of winter precipitation ranges from 80 to 100 mm. The values of spring and autumn precipitation generally fall within the same range – from 100 to 150 mm. In spring and summer, the highest precipitation is recorded in the area of Tarnów and Jelenia Góra, and the lowest at the stations located in the northern regions of Poland – in Resko, Koszalin, and Ustka. In all seasons, the maximum seasonal precipitation sums were approximately two times higher than the mean sums. Greater differences, as compared to the means, were found for the minimum sums which were at least 2.5 times and in autumn even 4 times lower. For example, in Warsaw, Koło, and Kalisz, the minimum sums did not exceed 20 mm – *Table 1*. Generally, the extreme seasonal sums of precipitation were recorded at individual stations in different years – this is particularly evident as regards the maximum sums and the period of the calendar summer. In spring, by far the highest number of cases of maximum precipitation sums (11 stations) was recorded in 1970, in autumn – 1974, and in winter – 1967. In turn, the minimum precipitation, which was recorded at more stations, occurred in the summer of 2015 and in the autumn of 1959.

The spectral analysis adopted in this study showed that in the period of 1951–2016, seasonal precipitation exhibited variation in numerous cycles of various length which, according to Kolmogorov-Smirnov d Bartlett and Fisher's Kappa, meet the criteria of statistical significance. The great majority of statistically verified cycles occurred in the winter season (70%), less were recorded in summer (57%). Spring showed higher occurrence of such cycles (43%) than autumn (38%). Out of the cycles determined for each of the stations, only those which were found to be predominant in a given season are presented in *Fig. 4*. Seven basic dominant cycles characterizing the multiannual variability of precipitation in the four seasons of a year were of the following length: 4.0, 4.6, 4.9, 5.3, 5.8, 6.4, and 7.1 years. Two of the aforementioned cycles, i.e., the 5.3 and 6.4-year-long ones were manifested in binary form in a few cases.

spring (Mar - May)   **summer (Jun - Aug)**

autumn (Sep - Nov)   **winter (Dec - Feb)**

| 4.0 | 4.6 | 4.9 | 5.3 | 5.8 | 6.4 | 7.1 | 10.7 | 12.8 |
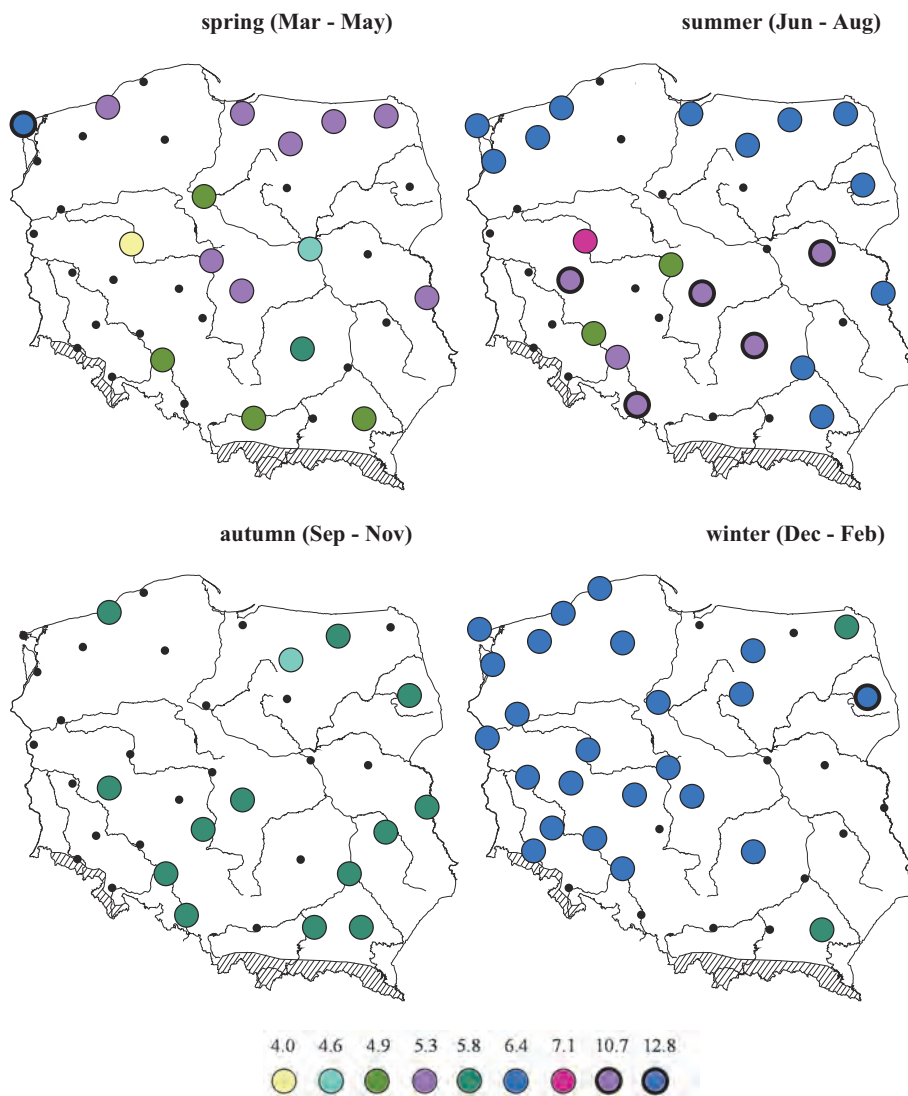
Fig. 4. Predominant cyclical elements in the distribution of seasonal precipitation in Poland, in the period 1951–2016.

Winter was the season in which the highest percentage of significant precipitation cycles was found. Moreover, in this season, the markedly dominant cycle, which occurred in most of the country, was 6.4-year-long. A relatively unified periodic variability of precipitation was determined in autumn, when the

cycles were determined to last 5.8 years. Extremely scattered results, both in terms of the length of the cycles as well as spatial distribution, were found to occur in spring and summer. In summer, a relatively unified characteristics of variability of precipitation is particularly evident in the northern part of Poland. Seasonal precipitation in this region, but also at some stations in the south-east of Poland, exhibited variability in cycles of the same length as in winter, i.e., 6.4 years. Cycles of various length – from 4.9, 5.3, 7.1 to the doubled 5.3 cycle of 10.7, which were identified at stations located in close proximity, characterise variability of summer precipitation not only in Wielkopolska – the region with the minimum recorded precipitation (among others: *Czarnecka* and *Nidzgorska-Lencewicz*, 2012, *Kędziora et al.*, 2014, *Żarski et al.*, 2017), but also on the Silesian Lowlands. Individual temporal distribution of precipitation in the period 1951–2016 was identified for Poznań – not only in the summer season, but also in spring. Spring was characterized by the highest number and span of the identified cycles, including the isolated cycles. Apart from Poznań, the characteristic spring precipitation cycles were determined in the following regions: Warsaw (4.6 years), Kielce (5.8 years), and Świnoujście (12.8 years). At a few more stations, mainly in the north-east part of Poland, the dominant cycle in the temporal course of spring precipitation sums was 5.3-year-long.

The precipitation sums characterized above are not the only ones which were positively verified in terms of statistical significance. The analysis of periodograms and spectral density graphs for individual stations showed that in each season, apart from the dominant cycle, there were other equally marked cycles of various length. This is illustrated by the estimators given in *Fig. 5*, which were developed for the four seasons, however in the unified version for 37 stations which provide a good representation for the results obtained for most of the stations. In spring, apart from the dominant 5.3-year-long cycle, a slightly shorter cycle of 4.9 years was also pronounced. In the calendar summer, there was a cycle slightly weaker than 10.7 years (binary form of 5.3 cycle), i.e., it was 6.4-year-long, which was characteristic for the stations in the north of Poland. In autumn and winter, precipitation cycles considered significant are markedly weaker as compared with the dominant ones, that is: 5.8 and 6.4, respectively. In autumn, precipitation shows even shorter cycles – 3.6 year, while in winter the cycles were longer – 9.1 years long.
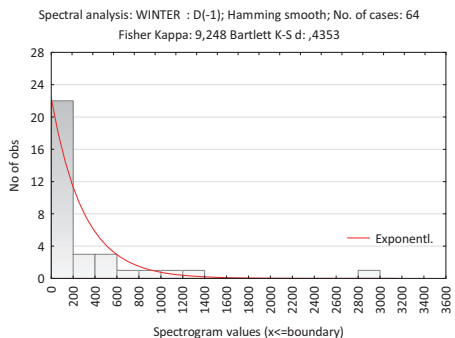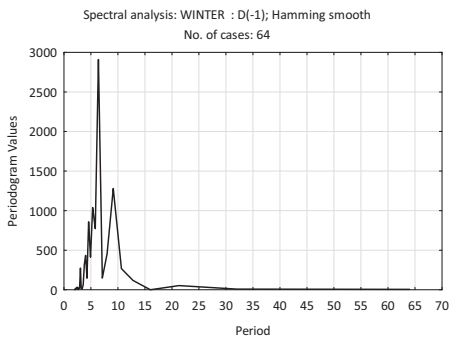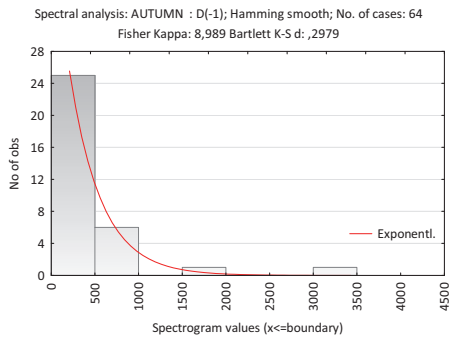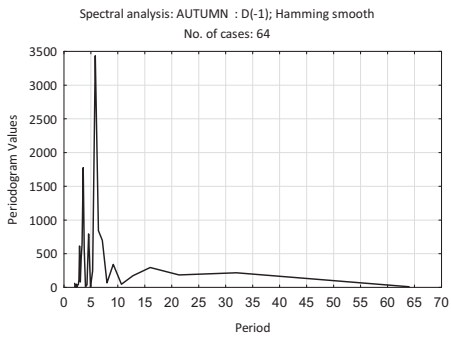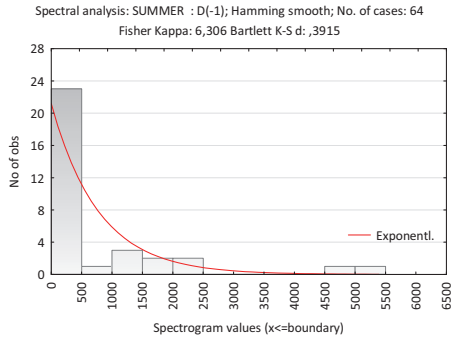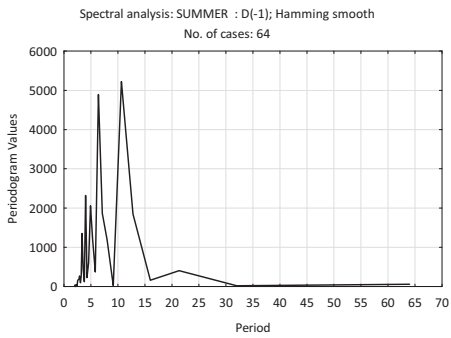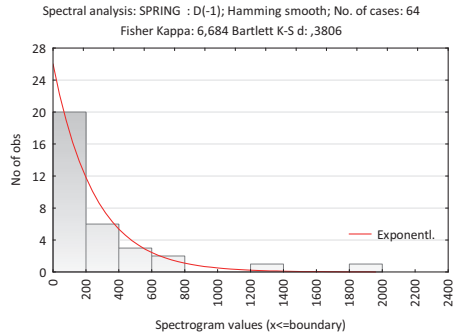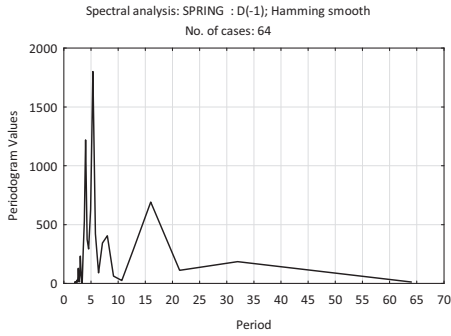
Fig. 5. Periodograms and histograms of periodogram values of seasonal total precipitation in Poland (values are averaged for 37 stations) in the period 1951–2016.

4. Conclusions

The results of the spectral analysis showed that variability of seasonal precipitation in the period 1951–2016 occurred in numerous, statistically significant cycles. The dominant cycles were of the following length: 4.0, 4.6, 4.9, 5.3, 5.8, 6.4, and 7.1 years. The identified periodicity in the course of precipitation is markedly shorter as compared with the data on the changes in air temperature, which was also evaluated using spectral analysis (*Gregorczyk* and *Michalska,* 2011*; Miętus,* 1996). Numerous and relatively short cycles confirm both the very high inter-annual variability of this element, as well as spatial variability – as for 37 stations mainly regional variability is evident, however, local variability is also present. Undoubtedly, considering the results obtained from a greater number of stations would result in even higher variation as this element is marked by discontinuity and very high variability.

The most pronounced periodicity in the course of precipitation is characteristic for the winter season, whereas least regularity was identified for spring precipitation. In many regions in the north part of Poland, variability in winter and summer precipitation occurred in 6.4-year-long cycles.

It is difficult to compare the identified periodicity in the course of seasonal precipitation in the period 1951–2016 with the scarce results presented in the literature on the subject. The principal reasons of such lack of comparability, as was clearly emphasized by *Miętus* (1996), are notably the precipitation series of various length, as well as different methods of processing basic data when using spectral analysis.

References

Boryczka, J. and *Stopa-Boryczka, M.,* 2000: Zmiany klimatu Polski w XVIII-XXI wieku. Acta UNC Toruń, Nauki Mat. Przyrod., 106, *Geografia 31*, 65–89. (in Polish)

Boryczka, J. and *Stopa-Boryczka, M.*, 2004: Cykliczne wahania temperatury powietrza i opadów w Polsce w XIX I XXI wieku. *Acta Agrophysica 3,* 21–33. (in Polish)

Czarnecka, M. and *Nidzgorska-Lencewicz, J.*, 2012: Wieloletnia zmienność sezonowych opadów w Polsce. *Woda-Środowisko-Obszary Wiejskie 12, 2(38)*, 45–60. (in Polish)

Czarnecka, M. and *Nidzgorska-Lencewicz, J.*, 2016: The cyclical nature of seasonal precipitation in Pomerania in the period 1951–2010. *Russian Meteorol. Hydrol. 4*, 27–36. https://doi.org/10.3103/S1068373916040038

Degirmendžić, J., Kożuchowski, K., and *Żmudzka E.,* 2004: Changes of air temperature and precipitation in Poland in the period 1951–2000 and their relationship to atmospheric circulation. *Int. J. Climatol. 24,* 291–310. https://doi.org/10.1002/joc.1010

Doroszewski, A., Jóźwicki, T., Wróblewska, E., and *Kozyra, J.,* 2014: Susza rolnicza w Polsce w latach 1961–2010. Instytut Uprawy Nawożenia i Gleboznawstwa Państwowy Instytut Badawczy, Puławy. (in Polish)

Fortuniak K., 2004: Wybrane metody poszukiwania okresowej zmienności w szeregach klimatycznych. In (Eds*. A. Bokwa , Z. Ustrnul*) Zastosowanie wybranych metod statystycznych w klimatologii*,* Wydawnictwo Instytutu Geografii i Gospodarki Przestrzennej, U.J., Kraków, 31–52. (in Polish)

Gregorczyk, A. and *Michalska, B.,* 2011: Zmienność temperatury powietrza w Szczecinie. *Acta Agrophysica 17,* 301–309. (in Polish)

Kaszewski, B., 2015: Zmiany klimatu Polski w pracach polskich klimatologów. *Przegląd Geofizyczny 3-4,* 217–235. (in Polish)

Kędziora, A., Kępińska-Kasprzak, M., Kowalczak, P., Kundzewicz, S.W., Miler, A.T., Pierzgalski, E., and *Tokarczyk T.*, 2014: Zagrożenia związane z niedoborem wody. *Nauka 1*, 149–172. (in Polish)

Kirschenstein, M. and *Baranowski, D.*, 2005: Sumy opadów atmosferycznych w Polsce w latach 1951-1995. Badania Fizjograficzne nad Polską Zachodnią, Seria A, Geografia Fizyczna, 56, 55–72. (in Polish)

Kożuchowski, K., 1996: Współczesne zmiany klimatyczne w Polsce na tle zmian globalnych. *Przegląd Geograficzny 68),* 79-98. (in Polish)

Kożuchowski, K., 2004: Zmienność opadów atmosferycznych w Polsce w XX i XXI wieku. In (Ed.: *K. Kożuchowski)* Skala, uwarunkowania i perspektywy współczesnych zmian klimatycznych w Polsce. Wydawnictwo Biblioteka, Łódź, 47–58. (in Polish)

Łupikasza, E., 2010: Spatial and temporal variability of extreme precipitation in Poland in the period 1951–2006. *Int. J. Climatol. 30,* 991–1007. https://doi.org/10.1002/joc.1950

Mager, P., Kasprowicz, T., and *Farat, R.*, 2009: Change o air temperature and precipitation in Poland in 1966-2006. [In: Climate change and agriculture in Poland – impacts, mitigation and adaptation measures. *Acta Agrophysica, Rozprawy i Monografie 169*, 19–38.

Marosz, M., Wójcik, R., Biernacik, D., Jakusik, E., Pilarski, M., Owczarek, M., and *Miętus, M.*, 2011: Zmienność klimatu Polski od połowy XX wieku. Rezultaty projektu klimat. *Prace i Studia Geograficzne 47,* 51–66. (in Polish)

Miętus M., 1996: Zmienność temperatury i opadów w rejonie polskiego wybrzeża Morza Bałtyckiego i jej spodziewany przebieg do roku 2030. *Materiały Badawcze IMiGW*, *Seria Meteorologia, 26,* (in Polish).

Miler, A.T. and *Miler, M.*, 2005: Trendy i okresowości zmian temperatury oraz opadów dla Poznania w latach 1848-2000. Zeszyty Naukowe Wydziału Budownictwa i Inżynierii Środowiska Politechniki *Koszalińskiej, Inżynieria Środowiska 22*, 945–956. (in Polish)

Miler, A.T. and *Okoński, B.,* 2011: Zmiany klimatyczne w Puszczy Zielonka od 1848 roku. *Infrastruktura i Ekologia Terenów Wiejskich 2,* 193–203. (in Polish)

Skowera, B., Kopcińska, J., and *Kopeć, B.,* 2014: Changes in thermal and precipitation conditions in Poland in 1971–2010. *Ann. Warsaw Univ. of Life Sci. – SGGW, Land Reclamation 46*, 153–162. https://doi.org/10.2478/sggw-2014-0013

Skowera, B., Kopcińska, J., and *Bokwa, A.*, 2016: Changes in the structure of days with precipitation in Southern Poland in 1971-2010. *Időjárás 120,* 365–381.

Szwed, M., 2018: Variability of precipitation on Poland under climate change. *Theor. Appl. Climatol.135,* 1003–1015. https://doi.org/10.1007/s00704-018-2408-6

Twardosz, R. and *Cebulska, M.,* 2005: Periodical changes of precipitation and the number of precipitation days in Cracow. *Prace Geograficzne 115,* 49–56.

Ziernicka-Wojtaszek, A., 2006: Zmienność opadów atmosferycznych na obszarze Polski w latach 1971-2000. In (Eds.: *J. Trepińska, Z. Olecki*]) Klimatyczne aspekty środowiska geograficznego. Instytut Geografii i Gospodarki Przestrzennej Uniwersytetu Jagiellońskiego, Kraków, 139–148. (in Polish)

Żarski, J., Dudek S., Kuśmierek-Tomaszewska, R., Bojar, W., Knopik, L., and *Żarski, W.*, 2014: Agroklimatyczna ocena opadów atmosferycznych okresu wegetacyjnego w rejonie Bydgoszczy. Infrastruktura i Ekologia Terenów Wiejskich, II/3, 643–656 (in Polish). http://dx.medra.org/10.14597/infraeco.2014.2.2.047

Żarski, J., Dudek, S., Kuśmierek-Tomaszewska, R., and *Żarski, W.,* 2017: Effects of agricultural droughts in the province of kujawsko-pomorskie and possibilities of minimizing their impact. *Infrastruktura i Ekologia Terenów Wiejskich, II/2,* 813–824. http://dx.medra.org/10.14597/infraeco.2017.2.2.063

Żmudzka E., 2002.: O zmienności opadów atmosferycznych na obszarze Polski nizinnej w drugiej połowie XX wieku. *Wiadomości IMGW 25(46),* 4, 23-38 (in Polish).

Żmudzka E., 2009: Współczesne zmiany klimatu Polski. *Acta Agrophysica 13,* 555–568. (in Polish)

IDŐJÁRÁS

Modeling the impact of climate change on yield, water requirements, and water use efficiency of maize and soybean grown under moderate continental climate in the Pannonian lowland

Milena Jancic Tovjanin [1]*, **Vladimir Djurdjevic**[2], **Borivoj Pejic** [1], **Nebojsa Novkovic** [1], **Beba Mutavdzic** [1], **Monika Markovic** [3], and **Ksenija Mackic** [1]

[1] *University of Novi Sad, Faculty of Agriculture*
Department of Field and Vegetable Crops
Dositej Obradovic Sq 8, 21000 Novi Sad, Serbia

[2] *University of Belgrade, Faculty of Physics*
Institute of Meteorology
Dobracina 16, 11000 Beograd, Serbia

[3] *University of Osijek, Faculty of Agriculture*
Kralja Petra Svacica 1d, 31000, Osijek, Croatia

* *Corresponding Author e-mail: milena.jancic@polj.uns.ac.rs*

(Manuscript received in final form September 4, 2018)

Abstract— In Central and Eastern Europe, climate changes have been predicted (*Trnka et al.*, 2009). These changes are expected to have a great impact on field crops during the spring-summer growing season. The aim of this paper is to estimate the impact of climate change on the main field crops (maize and soybean) in the Republic of Serbia. The AquaCrop model was used as a tool to quantify climate change impact on yield and net irrigation using results from the ECHAM climate model (SRES A2 scenario for the 2041–2070 and 2071–2100 periods) and data from two experimental fields located in the southern part of the Pannonian lowland. The analyzed results for the 2041–2070 and 2071–2100 periods showed an increase in maize (1 and 1.3 t/ha) and soybean (1.9 and 2.8 t/ha) yields and a very significant increase in the net irrigation of 151.4 and 183.1 mm in maize production and 179.3 and 227.3 mm in soybean production under climate change conditions compared to the 1961–1990 period. Additionally, irrigation water use efficiency was calculated to estimate the importance of irrigation, because crop production is usually conducted under rainfed conditions. It was concluded that maize and soybean production should benefit from climate changes but with higher water quantities.

Key-words: AquaCrop model, climate change impact, crop water requirement; maize, soybean, yield

1. Introduction

Climate patterns with soil conditions play a fundamental role in shaping environmental ecosystems for agriculture production. Some short-term climate variations are natural, but long-term trends observed in recent decades indicate a changing climate on global (*Downing et al.,* 2000; *Harrison et al.,* 1995; *Houghton et al.,* 1996; *Rosenzweig* and *Iglesias,* 1994; *Sathaye et al.,* 1997; *Wolf* and *Van Diepen,* 1995) and regional (*Alexandrov et al.,* 2002; *Lalic et al.* 2012) levels. Many projects (ADAGIO, COST 704) and research networks (AgMIP, MACSUR) are designed to assess and predict climate change impact on agriculture production (*Bindi et al.* 2015). Results published from the European Environmental Agency (EEA) regarding climate change, vulnerability, impacts, and adaptation in Europe (*EEA,* 2004, 2005, 2007a, 2007b) have shown a negative impact on agriculture in the southern and eastern European countries. The aim of climate change research was to integrate decision makers' feedback to assess potential production risks and limitations at the local and regional levels for fundamental field crops. Under future climate conditions, higher temperatures, water shortages, and irrigation need are expected (*Trnka et al.,* 2009).

In the research community, many crop models have been used (DSSAT, WOFOST, MARS, STICS SORKAM) to simulate the yield and phenology of main field and vegetable crops. Analyzed yield results in many previous studies expect to have lower yields under climate change conditions. Additionally, in recent studies in our region, a lower yield is expected for the main field crops (maize, wheat, and soybean) under rainfed conditions with climate change using the DSSAT crop model (*Jancic,* 2016a, 2016b). The FAO AquaCrop model was chosen for future simulations, because it was developed to simulate crop yield response to environmental stress (*Farahani et al.,* 2009). It is a crop water productivity model that evaluates the yield response to water and salinity stress, and may be successfully used in locations where water may be a key limiting factor in crop production.

The model was calibrated and validated (*Abedinpour et al.,* 2012; *Ahmadi et al.,* 2015; *Paredes et al.,* 2014; *Stricevic et al.,* 2011) in many studies for yield and various irrigation conditions. The model was also successfully calibrated and validated under our environmental conditions for past climate and soil conditions and various different field management (*Stricevic et al.,* 2011), and a previous research verified the use of the AquaCrop model in further studies to simulate yield and net irrigation under future climate conditions for main field crops.

Serbia is an emerging country where agriculture plays an important role in the national economy. Field crops are vulnerable to climate changes, especially spring-summer crops, which have huge water requirements during the summer months (*Pejić et al.,* 2011a, 2011b). In this study, Rimski Sancevi in Vojvodina,

the southern part of the Pannonian lowland with great agricultural potential, climatic and soil conditions, was chosen for high production. This study is important for assessing the risk of climate change impact on maize and soybean yield and irrigation water use efficiency (IWUE) to maintain economically high production under optimum irrigation and for estimating potential limitations under future conditions. Both crops have a growing season from April to September (AS period), during which less precipitation, higher temperature, and more days with extreme high temperatures were predicted (*Jancic,* 2017; *Jancic et al.,* 2015; *Mihailović et al.,* 2014).

In Serbia, maize and soybean are mostly cultivated under non-irrigated conditions on 1.77 million ha with a production of 872.1 million t and on 171000 ha with a production of 540859 t, respectively (Statistical Office of the Republic of Serbia [*RSSS*], 2012). The largest production area is in the Vojvodina region (*RSSS,* 2012).

The aim of this paper is to quantify the impact of climate change on the water requirements, yield and irrigation water use efficiency of maize and soybean under favorable agricultural conditions using an AquaCrop model, and to analyze the possibilities and limitations to the production of these two crops under future conditions.

2. Materials and methods

2.1. Location and experimental data

Experimental fields were in Rimski Sancevi, located in the southern part of the Pannonian lowland (latitude 45° 20' N, longitude 19° 51' E, altitude 84 m). The experimental field location was characterized by a moderate continental climate (*Mihailović et al.,* 2014) with an annual maximum temperature of 16.3 °C, minimum temperature of 5.9 °C, relative humidity of 74.8%, and precipitation of 576.8 mm (Rimski Sancevi station records for 1961–1990). The fields are the property of the Institute for Field and Vegetable Crops. Maize and soybean experimental fields were cultivated for six years, from 1998 to 2003 for mid-season maize and from 1989 to 2004 for soybean first maturity groups.

Soil type was classified according to the International Use of Soil Science Working Group (WRB) as a calcareous chernozem by the WRB classification (*IUSS Working Group WRB,* 2007). Mechanical, chemical, and hydrological characteristics of the soils were obtained from field samplings and are given in T*ables 1* and *2*. The soil's texture class was silty clay. Soil analyses were performed for two layers: the upper 30 cm and the lower 53 cm, at which the maize and soybean roots are most developed. The chemical properties for crop production were characterized as very favorable. The carbon content was 1.51% in the upper layer and 0.98% in the deeper layer, and the nitrogen content was 0.19 to 0.15%. *Table 2* shows the hydrological properties. The total available

water in the active rhizosphere of maize was 200 mm/m, and the bulk density was 1.21 g/cm^3. Soil moisture for irrigation needs was monitored by the standard gravimetric method every seven days. Samples were collected by means of a drill from two layers: 0–30 and 30–53 cm. The field capacity was defined at 33 vol%, permanent wilting point at 13 vol%, and saturation at 46 vol%.

Table 1. Mechanical and chemical characteristics of the soil at Rimski Sancevi

Location	Profile depth (cm)	Clay (%)	Silt (%)	Sand (%)	Organic carbon (%)	Nitrogen (%)
Rimski Sancevi	30	27.49	35.76	36.75	1.51	0.19
	53	26.55	34.31	39.14	0.98	0.15

Table 2. Hydrological characteristics of the soil at Rimski Sancevi

Bulk density (g/cm^3)	Field capacity (vol %)	Permanent wilting point (vol%)	Saturation (vol%)	Total available water (mm/m)
1.21	33	13	46	200

2.2. Past and future climate data

The daily weather data used for current climate conditions were observed at the weather station at Rimski Sancevi (*Fig. 1*), near the experimental field. The dataset included maximum and minimum temperature (°C), precipitation (mm), vapor pressure (mbar), and wind speed (m/s). The reference evapotranspiration rates were calculated by applying the FAO Penman-Monteith method (*Allen et al.,* 1998). The time period included years from 1961 to 1990. The data for future climate conditions were assumed from the integrated coupled model ECHAM developed at the Max Planck Institute for Meteorology (*Roeckner et al.,* 2003). The resulting data were dynamically downscaled for two periods from 2041 to 2070 and from 2071 to 2100. The A2 scenario determined by the Intergovernmental Panel on Climate Change (*IPCC*, 2001) was used for greenhouse gas (GHG) emissions for the two integration periods mentioned above. All simulations were performed considering the CO_2 effect. The average CO_2 concentration for the 1961–1990 period was 333.4 ppm, for the 2041–2070 period it was 560 mm, and for the 2071–2100 period it was 734.5 ppm. The absolute change in air temperature and relative change in precipitation for future conditions for the April – September growing season and June – July – August (JJA period) summer period were analyzed as the most limited agroclimatic parameters in field crop production (*Olesen et al.,* 2011).

Fig. 1. The location of the study area at Rimski Sancevi (latitude 45°20'N and longitude 19°51'E).

2.3. Field crop and management data

Maize phenology, yield, irrigation data, and crop management were observed for six years, from 1998 to 2003 from a field experiment in Rimski Sancevi.

In maize production, sowing was performed from April 16 to 22, depending on the weather conditions for each season. The mid-season maize NSSC 640 usually requires approximately 10 days after sowing to emerge, with a maximum canopy of approximately 40 days. Flowering was observed from the end of the first week of July to mid-July and maturity from the 14th to the 29th of September (*Table 3*). The plant density was maintained at 5.7 to 6.3 plants/m^2, with 0.9 m row spacing. Crop management was as practices with no specific changes.

In soybean production, sowing was performed in approximately April 20, with soybean maturity group I. The plant density was 4.0 to 4.3 plants/m^2, with a row spacing of 0.9 m. The phenology was also observed, and the soybean I maturity group usually required 10 to 15 days after sowing to emerge, with a maximum canopy cover of approximately 78 days. Flowering was observed at the end of June and beginning of July and maturity from the 1st to the 8th of September. The observed phenology for each year is presented in *Table 3*.

Table 3. Plant density, sowing/emergence/flowering/harvesting dates, precipitation, and irrigation

Year	Plant density (plants/ha)	Sowing	Emergence	Flowering	Harvesting	Precipitation (mm)	Irrigation (mm)
Maize							
1998	57000	Apr 21	May 1	Jul 16	Sep 14	412.3	60
1999	57000	Apr 22	May2	Jul 14	Sep 17	477.9	0
2000	60000	Apr 18	Apr 28	Jul 11	Sep 18	123.0	180
2001	63000	Apr 16	Apr 30	Jul 10	Sep 19	605.8	60
2002	60000	Apr 16	Apr 29	Jul 7	Sep 23	212.3	120
2003	63000	Apr 22	May 1	Jul 7	Sep 29	220.3	240
Soybean							
1989	42000	Apr 21	May 3	Jul 1	Sep 5	305.8	120
1990	40000	Apr 22	May 7	Jun 30	Sep 3	140.0	180
1991	43000	Apr 22	May 7	Jul 2	Sep 8	414.8	0
1992	42000	Apr 19	May 2	Jun 28	Sep 1	171.3	180
1993	42000	Apr 21	May 4	Jul 4	Sep 2	181.3	240
1994	42000	Apr 22	May 7	Jul 5	Sep 6	258.1	180

2.4. *AquaCrop model parameters, calibration and validation, and input data*

For simulations, the AquaCrop model requires input data based on the observed climate, soil, and crop management data. *Steduto et al.,* (2009) provide a detailed description and present the architecture of the model.

AquaCrop version 5.0 offers files that contain parameters suitable for the simulation of maize and soybean production, but the default values for maize and soybean were chosen only as a starting point, and the final key parameters were modified to fit the local crop management. All crop parameters were calibrated for the NSSC 640 maize hybrid, thus the crop model can simulate and present the real crop production under our local conditions. *Table 4* presents the final parameters used in the AquaCrop model calibration for maize and soybean production. The initial canopy cover was 0.37%, with a maximum canopy cover of 96% (*Table 4*). The base temperature, under our conditions, was set to 8 °C, and the upper temperature was set to 30 °C. Water productivity was 35 g/m^2, and the harvest index was 48% (*Table 4*). The crop management was as usual under our conditions, and soil fertility was considered as sufficient amounts added to set ideal conditions for yield genetic potential and for estimated climate change conditions. Applied net irrigation and precipitation observed for each year during the growing season for maize and soybean are presented in *Table 3*.

Table 4. Default and final parameters for AquaCrop model calibration for maize and soybean production

Description	Maize default	Maize final	Soybean default	Soybean final	Units/meaning
Base temperature	8	8	5	8	°C
Upper temperature	30	30	30	30	°C
Initial canopy cover (CC$_o$)	0.49	0.37	1.65	2	%
Canopy expansion (CGC)	16.3	26.1	1.6	10.2	% /day
Maximum canopy cover (CCx)	96	96	98	98	%
Canopy decline coefficient (CDC) at senescence	11.7	11.7	2.9	2.9	% /day
Water productivity, (WP*)	33.7	35	16	19	as fraction of TAW %
Reference harvest index (HI$_o$)	48	48	40	35	%

The AquaCrop model was calibrated for maize production using daily weather data from the Rimski Sancevi weather station, soil characteristics, and crop management data for the 1999 experimental field (*Table 5, Fig. 2*).

The relative deviation between the observed and simulated dry matter yields was 1%, and the absolute change in net irrigation was 0 mm. The validation was performed for a six-year period from 1998 to 2003 at the same location (*Table 5, Fig. 2*). The relative deviation (*Tornqvist et al.,* 1985) between the simulated and observed dry matter yields was calculated for each year to show how the model fits in various climate conditions under the same or similar crop management activity. The relative deviation between the simulated and observed yields varied from 1 to 10%, except in one year, 2000. The absolute change in net irrigation varied from 0 to 15 mm, except in 2000 and 2001. The highest deviation in yield, 13%, and the absolute change in net irrigation, 117.6 mm, occurred in 2000; the latter was 60 mm in 2001, when the number of dry days was greater than the long-term average, with significant low precipitation in the growing season. This significant difference between the simulated and observed yield values is a consequence of the model's inability to simulate the plant reaction to stress under extreme conditions, such as high variations in daily air temperature and precipitation in short time intervals (*Lalic et al.,* 2011). The coefficient of determination (R^2) calculated for yield was 0.7823, and the coefficient of correlation (R) was 0.8845, which improves high agreement between the simulated and observed yields.

Table 5. Calibration (for 1999) and validation of maize grain yield (dm t/ha) for the 1998–2003 period

Year	Observed yield (dm t/ha)	Simulated yield (dm t/ha)	Relative deviation in yield (%)	Observed IWUE (kg/m³)	Simulated IWUE (kg/m³)
1998	8.8	9.7	10	14.7	14.1
1999	9.8	9.9	1	0.0	0.0
2000	11.6	10.1	−13	6.4	3.4
2001	9.3	9.7	5	15.5	0.0
2002	11.7	10.6	−9	9.8	7.9
2003	11.6	10.7	−8	4.8	4.6
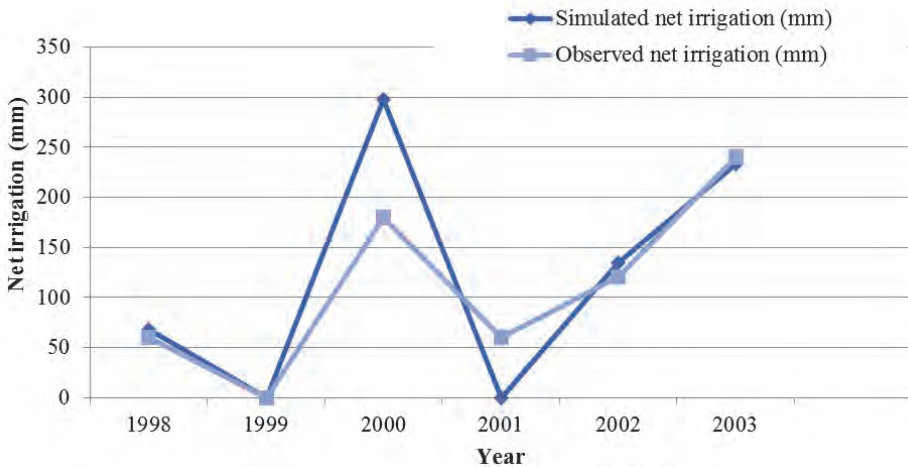
Fig. 2. Validation of net irrigation (mm) in the maize production.

The AquaCrop model was also calibrated for soybean I maturity group production for 1994 (*Table 6, Fig. 3*). The default and final crop parameters are presented in *Table 4*. All parameters were calibrated to fit the soybean yield production and phenology under local conditions. The base temperature was set to 8 °C, and the maximum temperature was 30 °C. The initial canopy cover was 2%. Water productivity was 19 g/m², and the harvest index was 35% (*Table 4*).

476

Table 6. Calibration (for 1994) and validation of I group maturity soybean grain yield (dm t/ha) for the 1989–1994 period

Year	Observed yield (dm t/ha)	Simulated yield (dm t/ha)	Relative deviation (%)	Observed IWUE (kg/m³)	Simulated IWUE (kg/m³)
1989	3.9	4.4	12	0.3	0.4
1990	4.5	4.6	2	0.3	0.2
1991	4.3	4.5	4	0.0	0.0
1992	4.5	4.7	5	0.3	0.2
1993	4.5	4.6	2	0.2	0.2
1994	4.6	4.7	2	0.3	0.2
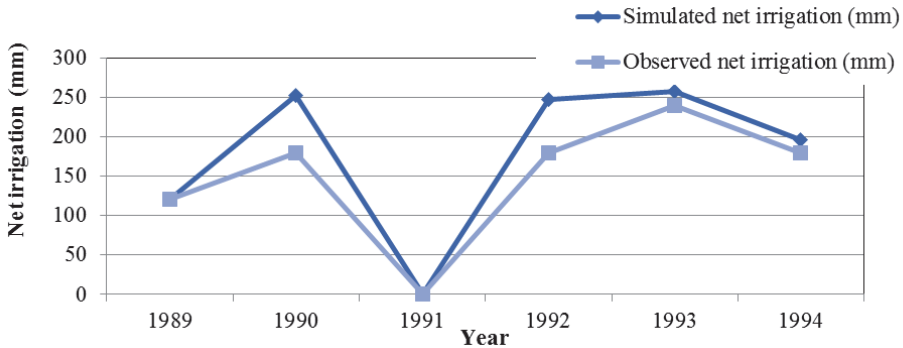
Fig. 3. Validation of net irrigation (mm) in the I group maturity soybean production.

The relative deviation between the simulated and observed dry matter yields was 2%, and the absolute change in net irrigation was 16.9 mm. The model was validated for a 6-year experiment at the same location (*Table 6, Fig. 3*). The relative deviation between the simulated and observed yields varied from 2 to 5%, except in 1989, when the relative deviation was 12%. The absolute change in net irrigation varied from 0 to 16.9 mm, except in 1990 and 1992, when the precipitation was significantly lower than the long-term average. In years with significant dry weather conditions, the model gave higher net irrigation from 66.9 to 70 mm, which is two applications more than under our agroclimatic conditions. The coefficient of determination calculated for yield was 0.8529, and the coefficient of correlation was 0.9235, which implies a high agreement between the simulated and observed yields.

For past climate conditions, from 1961 to 1990, and future climate conditions, 2050, some crop management operations in AquaCrop model simulations had to be set and fixed to ensure that the model simulates only the climate impact on the current crop production. In the model, for maize and soybean production for the 1961–1990 period and future conditions, sowing and phenology were set at the average sowing, emergence, maximum canopy cover, flower appearance, and maturity dates (*Table 7*). Additionally, under irrigated conditions, the readily available water was set at 80%, below which the soil water content in the root zone may not drop, as in our experimental fields. This irrigation method in the model, including defined and set local soil hydrological characteristics, gave similar net irrigation quantities to the measured net irrigation from the field experiments.

Table 7. Calendar days of maize and soybean by growth phases for crop simulations for 1961 – 1990 period and expected climate conditions

Phenological phase	Maize (calendar days)	Soybean (calendar days)
To emergence	10	15
Maximum canopy cover	41	78
Maximum rooting depth	86	98
Start of canopy senescence	106	109
Maturity	146	135
Start of flowering	85	78
Length building up of harvest index	61	59
Duration of flowering	20	13

The irrigation water use efficiency was calculated as follows:

$$IWUE = yield / irrigation, \tag{1}$$

where IWUE is the irrigation water use efficiency (kg/m^3), while yield (kg/ha) and irrigation (m^3/ha) are measured/simulated from the field experiments.

3. Data analyses

Three statistical methods were used to analyze and compare observed yield data from field experiments and simulation yield results.

The first statistical parameter was the relative deviation (*Tornqvist et al.,* 1985) calculated between the simulated and observed dry matter yields for each year. The method was chosen to show how the model works and its sensitivity to various climate conditions each year under the same or similar crop management activities:

$$r = (S - M) / M * 100 ,$$ (2)

where *r* is the relative deviation (%), *M* is the observed yield (dm t/ha), and *S* is the simulated yield (dm t/ha). The crop model fits when *r* is less than 15% (*Tsuji et al.,* 1998).

The second calculated statistical parameter was the coefficient of determination, R^2:

$$R^2 = \frac{\sum (Mi - \overline{M})(Si - \overline{S})}{\sqrt{\sum (Mi - \overline{M})^2 \sum (Si - \overline{S})^2}} ,$$ (3)

where $\overline{S}$ and $\overline{M}$ are the mean values of the simulated and observed data. The coefficient provides information on how much the variation in simulated yield results is defined by the impact of input data, which shows the model's ability to simulate real crop production. The model fits when R^2 tends to be 1.

The third statistical parameter was the coefficient of correlation *R*. It describes the relative measure of the degree of agreement between the measured and simulated values, a linear connection between these two variables.

4. Results

4.1. Current and future climate conditions

The analyses for current climate conditions (1961–1990) included observed daily weather data for air temperature and precipitation for growing seasons April-September (AS) and June-July-August (JJA) (*Table 8*). The average air temperature was 18.9 °C for the AS period and 20.4 °C in the summer months. The precipitation was 286.4 mm for the AS period and 199.0 mm for the driest period JJA. Absolute change in temperature and relative change in precipitation were calculated for 2041–2070 and 2071–2100, according to the current period 1961–1990.

For future conditions, in the AS period, the increase in temperature was predicted to be 2.3 °C in the 2041–2070 period and 4.1 °C in the 2071–2100 period. The highest increase in temperature is expected during the summer months (JJA) for 2.3 °C in 2041–2070 and 4.4 °C in 2071–2100. At the same time, the predicted precipitation is expected to be lower in the AS period, by 6.4% in 2041–2070 and 19.4% in 2071–2100, and significantly lower in the JJA period, by 19.7% in 2041–2070 and 21.9% in 2071–2100 (*Table 9*).

Table 8. Climate conditions for the 1961-1990 period at Rimski Sancevi (t - temperature; p - precipitation)

	April - September		June-July-August	
	t (°C)	p (mm)	t (°C)	p (mm)
1961–1990	18.9	286.4	20.4	199.0

Table 9. Absolute change in temperature (°C) and relative change in precipitation (%) for 2041–2070 and 2071–2100 using ECHAM model under A2 scenario (t – temperature; p – precipitation).

	April - September		June-July-August	
	t (°C)	p (%)	t (°C)	p (%)
2041–2070	2.3	−6.4	2.3	−19.7
2071–2100	4.1	−19.4	4.4	−21.9

4.2. *Climate change impact on maize and soybean yield, net irrigation, and IWUE*

Using current climate data for the 1961–1990 period, soil characteristics, current crop management, and fixed crop parameters from the AquaCrop model calibration, as well as dry matter yield and net irrigation were simulated for the mid-season maize and soybean I maturity groups under the current climate conditions for 30 years.

Table 10a shows the simulated dry matter yield (kg/ha) for the mid-season maize and I maturity group soybean for the current period 1961–1990.

The analyzed results showed a very high yield for soybean and maize production for the current period, similar to the real production in the northern part of Serbia. The net irrigation varied from year to year, according to various weather conditions. The average net irrigation was 521 m^3/ha, and IWUE was also calculated as 18 kg/m^3.

For future conditions, the average yield, IWUE, and calculated absolute change in yield and net irrigation for the 2041–2071 and 2071–2100 periods under the A2 scenario were shown, according to the 1961–1990 period (*Table 10b*).

Table 10a. Yield (dm kg/ha), net irrigation (mm), and IWUE (kg/m^3) in maize and soybean production

	Average maize yield (dm kg/ha)	IWUE in maize production (kg/m^3)	Maize net irrigation (m^3/ha)	Average soybean yield (dm kg/ha)	IWUE in soybean production (kg/m^3)	Soybean net irrigation (m^3/ha)
1961–1990	9400	18.0	521	4300	3.6	1187

Table 10b. Average yield (dm kg/ha), absolute change in net irrigation (mm), and IWUE (kg/m^3) in maize and soybean production using ECHAM model under A2 scenario

	Average maize yield (dm kg/ha)	IWUE in maize production (kg/m^3)	Absolute change in maize net irrigation (m^3/ha)	Average soybean yield (dm kg/ha)	IWUE in soybean production (kg/m^3)	Absolute change in soybean net irrigation (m^3/ha)
2041–2071	10400	5.1	1514	6254	2.1	1793
2071–2100	10700	4.5	1831	7090	2.0	2273

The simulated maize yield was 10400 kg/ha in the 2041–2070 period, which is higher than the 1000 kg/ha grain yield in the past climate conditions. The minimum simulated yield in the 2041–2070 period was 9900 kg/ha, and the maximum was 10800 kg/ha. In 2071–2100, the simulated yield showed a higher value of 10700 kg/ha. The minimum simulated yield was 10400 kg/ha, and the maximum was 10900 kg/ha. The production is expected to be higher under future conditions according to the 1961–1990 period, but at the same time, the net irrigation showed significantly higher norms of 1514 m^3/ha in 2041–2070 and 1831 m^3/ha in 2071–2100. The IWUE calculated was 5.1 kg/m^3 for the 2041–2070 period and 4.5 kg/m^3 for the 2071–2100 period.

The simulations for soybean production showed a significantly higher yield of 6254 kg/ha in the 2041–2070 period, which is 1900 kg/ha higher than the grain yield according to the 1961-1990 period. The minimum simulated yield was 5800 kg/ha, and the maximum was 6700 kg/ha. For the 2071–2100 period, the model simulated a grain yield of 7090 kg/ha. A 2800 kg/ha higher grain yield is expected according to the past climate conditions. The minimum simulated yield was 6700 kg/ha, and the maximum was 7500 kg/ha. The AquaCrop model simulated benefits in soybean production under future climate conditions, and the net irrigation was expected to be significantly higher, 1793 m^3/ha in the 2041–2070 period and 2273 m^3/ha in the 2071–2100 period, than in the past climate conditions. The IWUE calculated for the 2041–2070 period was 2.1 kg/m^3 and 2.0 kg/m^3 for the 2071–2100 period.

5. Discussion

5.1. The climate and the maize and soybean production in 1961–1990

Maize and soybean are temperate crops with widespread aerial production, especially maize. The base temperature for emergence is 8 °C for both crops (*Djordjevic et al.,* 2015; *Kotorac,* 2014; *Miladinović et al.,* 2008).

Maize root and morphology are well developed, and this crop does not have a high demand for water. The mid-season maize NSSC 640 was developed in 1989 as a hybrid at the Institute of Field and Vegetable Crops, Novi Sad. It has high genetic potential in yield, is very resistant to diseases and highly tolerant to drought. This hybrid is very adaptable under various agroecological conditions (*Stojaković et al.,* 2015).

Soybean is more vulnerable to drought and erosion at the beginning of the growing season, with a less developed root system and crop cover. However, toward the end of the vegetative phase, the crop has a strong root system and has approximately 500 mm water requirement during the growing season (*Djordjevic et al.,* 2015).

For both crops, the critical period for water is from the flowering to grain filling in the summer months, a period when the temperature is highest with a low relative humidity and the lowest precipitation in Serbia.

From 1961 the 1990, temperature and precipitation were analyzed as decisive agrometeorology parameters that may limit crop production. The temperature was observed from 12.1 to 28.2 °C in the JJA period, and the average precipitation varied from 102.6 mm to 368.6 mm in the same JJA period. The temperature did not exceed critical limits, while the precipitation varied from year to year. The temperature conditions were favorable for both maize and soybean productions; s it was necessary to irrigate crops only in several dry year during the JJA period.

5.2. Climate change impact on yield, net irrigation, and IWUE for 2041–2070 and 2071–2100

The analyzed results for temperature and precipitation under future conditions confirm previous researches (*Jancic,* 2017; *Jancic et al.,* 2015; *Olesen et al.,* 2011) and reports (Central and Eastern Europe Climate Change Impact and Vulnerability Assessment *[CECILIA],* 2006; *IPCC,* 2001), that temperature is expected to increase, especially during summer months, with lower precipitation. The higher temperatures, more days with extreme high temperatures, and lack of precipitation lead to the simulated lower yields for maize and soybean when irrigation is not included (*Jancic,* 2016b; *Jancic et al.,* 2015), and to stable and higher yields when the crop is under irrigated conditions (*Jancic et al.,* 2015). Simulations with the CO_2 effect also gave higher yields, as in previous studies, for soybean (*CECILIA,* 2006; *Jancic et al.,*

2015; *Mihailović et al., 2014; Southworth et al., 2002; Wittwer,* 1995) and maize (*Jancic, 2016a; Mihailović et al., 2014; Wang et al.,* 2011). The expected increase in temperature and lack of precipitation caused higher net irrigation and lower IWUE values in the simulated maize and soybean crop productions under optimum available water conditions. Previous research in various regions has also reported and expected higher water demands in future conditions (*FAO Water Reports,* 2011).

6. Conclusions

- Higher temperatures are expected during the AS growing period, especially during summer months (JJA).

- Precipitation is expected to be significantly lower in the future conditions during all months of the growing season (AS), especially in the summer JJA period.

- In future conditions, the expected benefit is higher yield in maize and soybean production.

- Significantly higher net irrigation is expected with the same total available water conditions under current crop management and lower IWUE values.

The crop simulation results showed higher yield production for both maize and soybean crops under future conditions. On the basis of the crop model results, maize and soybean production is expected to benefit from climate changes and increases in CO_2, which make it possible to increase these crop production areas in Serbia. Additionally, it is necessary to note that the AquaCrop model gave high yield production results under very significant higher net irrigation in future conditions. The AquaCrop model has a solution to fix the percent of total available water for crops and gives the possibility to estimate and test various irrigation methods and quantities through simulations and their impact on yield using climate scenarios. It is also noticeable that irrigation water efficiency is lower. Water is a natural resource that has limitations, and it is necessary in further researches to test limited irrigation conditions as a sustainable water use, their impact on yield, and the limit of water use to maintain a high yield in maize and soybean production under future conditions. Additionally, it is necessary to estimate various adaptation measures, such as earlier sowing date, mulching, sustainable fertilization, various genetic varieties of crops, and most adaptable crops in future climate conditions.

References

Abedinpour, M., Sarangi, A., Rajput, T.B.S., Singh, M., Pathak, H. and *Ahmad, T.*, 2012: Performance evaluation of AquaCrop model for maize crop in a semi-arid environment. *Agric. Water Manage. 110*, 55–66. https://doi.org/10.1016/j.agwat.2012.04.001

Ahmadi, S.H., Mosallaeepour, E., Kamgar-Haghighi, A.A. and *Sepaskhah, A.R.*, 2015: Modeling maize yield and soil water content with AquaCrop under full and deficit irrigation managements. *Water Res. Manage. 29*, 2837–2853. https://doi.org/10.1007/s11269-015-0973-3

Alexandrov, V., Eitzinger, J., Cajic, V. and *Oberforster M.*, 2002: Potential impact of climate change on selected agricultural crops in north-eastern Austria. *Glob. Change Biol. 8*, 372–389. https://doi.org/10.1046/j.1354-1013.2002.00484.x

Allen, R.G., Pereira, L.S., Raes, D. and *Smith, M.*, 1998: Crop Evapotranspiration. Guidelines for computing crop water requirements. Irrigation and drainage paper 56. FAO, Rome.

Bindi, M., Palosuo, T., Trnka, M. and *Mikhail, A.*, 2015: Modelling climate change impacts on crop production for food security. *Climate Res. 65*, 3–5. https://doi.org/10.3354/cr01342

Central and Eastern Europe Climate Change Impact and Vulnerability Assessment (CECILIA), 2006: Climate change impacts in central-eastern Europe: Crop yield and forest tree growth changes influenced by climate change effects, regional conditions and management systems (Project No. 037005, Report: D6.1). National Forest Center, Forest Research Institute, Zvolen, Slovakia.

Djordjevic, V., Malidža, G., Vidić, M., Milovac, Ž. and *Šeremešić, S.*, 2015: Priručnik za gajenje soje – Danube Soya. Novi Sad, Srbija. (In Serbian)

Downing, T.E., Harrison, P.A., Butterfield, R.E. and *Lonsdale, K.G.*, 2000: Climate Change, climatic variability and agriculture in Europe. An integrated assessment (Research Report 21, Contract ENV4-CT95-0154). Commission of the European Union, Brussels, Belgium.

EEA, 2004: Impacts of Europe`s changing climate: An indicator – based assessment (EEA Report no. 2/2004). EEA, Copenhagen.

EEA, 2005: Climate change and river flooding in Europe (Briefing No. 1). EEA, Copenhagen.

EEA, 2007a: Climate change: The costs of inaction and the cost of adaptation (Technical Report 13/2007). EEA, Copenhagen.

EEA, 2007b: Climate change and water adaptation issues (Briefing Document 2007: 01). EEA, Copenhagen.

FAO Water Reports, F. W., 2011: Climate change, water and food security. Food and Agricultural Organization of the United Nations, Rome.

Farahani, H.J., Izzi, G. and *Oweis, T.Y.*, 2009: Parameterization and evaluation of the AquaCrop model for full and deficit irrigated cotton. *Agronomy J. 101*, 469–476. https://doi.org/10.2134/agronj2008.0182s

Harrison, P., Butterfield, R. and *Downing, T.*, 1995: Climate change and agriculture in Europe assesment of impacts and adaptation. University of Oxford, Oxford, UK.

Houghton, J.T., Filho, L.G.M., Callander, B.A., Harris, N., Kattenberg, A. and *Maskell, K.*, 1996: Climate change. The science of climate change. Cambridge University Press, Cambridge, UK.

Intergovernmental Panel on Climate Change (IPCC), 2001: Fourth Assessment Report 2001 Report of working group III Mitigation. https://www.ipcc.ch/ipccreports/tar/wg3/index.htm

IUSS Working Group WRB, 2007: World Reference Base for Soil Resources 2006; First Update 2007. World Soil Resources Reports 103. FAO, Rome.

Jančić, M., Lalic, B., Mihailovic, D.T. and *Jacimovic, G.*, 2015: Impact of climate change and carbon dioxide fertilization effect on irrigation water demand and yield of soybean in Serbia. *J. Agric. Sci. 153*, 1365–1379. https://doi.org/10.1017/S0021859615000179

Jančić, M., 2016a: Climate change adaptation in maize production in Serbia (FACCE MACSUR Reports 2: SP9 – 3). MACSUR, Tromso-Trondheim.

Jančić, M., 2016b: Uticaj klimatskih promena na biljnu proizvodnju (PhD thesis), University of Novi Sad, Novi Sad.

Jančić, M., 2017: The use of Agriclim model in agriculture production analyses in Novi Sad. Proceedings of the 45th International Symposium on Agricultural Engineering, Actual Tasks on Agricultural Engineering, 21-24, Opatija, Croatia.

Kotorac, F., 2014: Utjecaj obrade tla i gnojidbe dušikom na prinos kukuruza (Batchelor work), Poljoprivredni fakultet, Sveučilište Josipa Jurja Strossmayera, Osijek.

Lalic, B., Eitzinger, J., Mihailovic, D. T., Thaler, S. and *Jancic, M.*, 2012: Climate change impacts on winter wheat yield change – which climatic parameters are crucial in Pannonian lowland? *J. Agric. Sci. 151*, 757–774. https://doi.org/10.1017/S0021859612000640

Lalic, B., Eitzinger, J., Thaler, S., Nejedlik, P., Kazandjiev, V., Vucetic, V., and *Eckersten, H.*, 2011: Using results of modelled yield deviation and indices of weather extremes towards a better yield assessment – current state of research. the Abstracts, International Conference on Current Knowledge of Climate Change Impacts on Agriculture and Forestry in Europe, 3.-6.5.2011, Topolcianki, Slovačka.

Mihailović, D. T., Lalić, B., Dresković, N., Mimić, G., Djurdjević, V. and *Jančić, M.*, 2014: Climate change effects on crop yields in Serbia and related shifts of Köppen climate zones under the SRES-A1B and SRES-A2. *Int. J. Climatol. 35*, 3320–3334. https://doi.org/10.1002/joc.4209

Miladinović, J., Hrustić, M. and *Vidić, M.*, 2008: Soja, monografija. Institut za Ratarstvo i Povrtarstvo, Novi Sad i Sojaprotein, Bečej. (In Serbian)

Olesen, J. E., Trnka, M., Kersebaum, K. C., Skjelvåg, A. O., Seguin, B., Peltonen-Sainio, P., and *Micale, F.*, 2011: Impacts and adaptation of European crop production systems to climate change. *Eur. J. Agronomy 34*, 96–112. https://doi.org/10.1016/j.eja.2010.11.003

Paredes, P., de Melo-Abreu, J. P., Alves, I. and *Pereira, L.S.*, 2014: Assessing the performance of the FAO AquaCrop model to estimate maize yields and water use under full and deficit irrigation with focus on model parameterization. *Agric. Water Manage. 144*, 81–97. https://doi.org/10.1016/j.agwat.2014.06.002

Pejić, B., Maheshwari, B., Šeremešić, S., Stričević, R., Pacureanu-Joita, M., Rajić, M. and *Ćupina, B.*, 2011b: Water-yield relations of maize (Zea mays L) in temperate climatic conditions. *Maydica 56*, 315–323.

Pejic, B., Maksimović, L., Cimpeanu, S., Bucur, D., Milić, S. and *Ćupina, B*., 2011a: Response of soybean to water stress at specific growth stages. *J. Food Agric. Environ. 9,* 280–284.

FAO Water Reports, F. W., 2011: Climate change, water and food security. Food and Agricultural Organization of the United Nations, Rome.

Roeckner, E., Bäuml, G., Bonaventura, L., Brokopf, R., Esch, M., Giorgetta, M., and *Tompkins, A.,* 2003: The atmospheric general circulation model ECHAM-5: Model description (Report No. 349). Max-Planck-Institut fur Meteorologie, Hamburg, Deutschland.

Rosenzweig, C. and *Iglesias, A.*, 1994: Implication of climate change for international agriculture, crop modeling study (EPA 230-B-94-. 003). Environmental Protection Agency, Washington, DC, US.

Sathaye, J.A., Dixon, R.K. and *Rosenzweig, C.,* 1997: Climate change country studies. Applied Energy, 56(3), 225–235. https://doi.org/10.1016/S0306-2619(97)0007X-4

Southworth, J., Pfeifer, R., Habeck, M., Randolph, J., Doering, O., Johnston, J. and *Rao, D.G.*, 2002: Changes in soybean yields in the midwestern United States as a result of future changes in climate, climate variability, and CO 2 fertilization. *Climatic Change 53*, 447–475. https://doi.org/10.3354/cr022073

Statistical Office of the Republic of Serbia (RSSS), 2012: Statistical yearbook of the Republic of Serbia 2012. Statistical Office of the Republic of Serbia, Belgrade, Serbia.

Steduto, P., Hsiao, T. C., Raes, D. and *Fereres, E.,* 2009: AquaCrop—The FAO crop model to simulate yield response to water. I. Concepts and underlying principles. *Agronomy J. 101*, 426–437. https://doi.org/10.2134/agronj2008.0139s

Stojaković, M., Jocković, Đ., Bekavac, G., Nastasić, A., Mitrović, B., Stanisavljević, D. and *Zorić, M.*, 2015: Prinos NS hibrida kukuruza iz različitih perioda selekcije. *Selekcija i Semenarstvo 21*, 93–102. (In Serbian) https://doi.org/10.5937/SelSem1502093S

Stricevic, R., Cosic, M., Djurovic, N., Pejic, B. and *Maksimovic, L.*, 2011: Assessment of the FAO AquaCrop model in the simulation of rainfed and supplementally irrigated maize, sugar beet and sunflower. *Agric. Water Manage. 98*, 1615–1621. https://doi.org/10.1016/j.agwat.2011.05.011

Tornqvist, L., Vartia, P. and *Vartia, Y.O.*, 1985: How should relative changes be measured? *Amer. Statistic 39*, 43–46. https://doi.org/10.1080/00031305.1985.10479385

Trnka, M., Zalud, Z., Semeradova, D., Ventrella, D., Anastasiou, D. P., Medany, M., Altaher, S., Olejnik, J., Lesny, J., Nemeshko, N., Nikolaev, M., Simota, C. and *Cojocaru, G*., 2009: Final report, including recommendations on adaptation measures considering regional aspects. Final scientific report of the ADAGIO Project: "Adaptation of agriculture in European regions at environmental risk under climate change"; Specific Support Action, FP6-2005-SSP-5-A, Proj.No.044210, Sixth Framework Programme, European Commission, Ed.: Institute of Meteorology, University of Natural Resources and Applied Life Sciences, Vienna.

Tsuji, G., Hoogenboom, G. and *Thornton, P.K.,* 1998: Understanding options for agricultural production. Kluwer Academic Publishers, Dordrecht, Netherlands. https://doi.org/10.1007/978-94-017-3624-4

Wang, M., Li, Y., Ye, W., Bornman, J.F. and *Yan, X.*, 2011: Effects of climate change on maize production, and potential adaptation measures: a case study in Jilin Province, China. *Climate Res. 46*, 223–242. https://doi.org/10.3354/cr00986

Wittwer, S.H., 1995: Food, climate, and carbon dioxide – the global environment and world food production. NewYork, NY: Lewis Publishers.

Wolf, J. and *Van Diepen, C*., 1995: Effects of climate change on grain maize yield potential in the European Community. Climatic Change, 29(3), 299–331. https://doi.org/10.1007/BF01091866

IDŐJÁRÁS

Change of maximum snow cover depth in Poland – trends and projections

Małgorzata Szwed[1*], **Andreas Dobler**[2], **Abdelkader Mezghani**[2], and **Tuomo Mikael Saloranta**[3**]

[1] *Institute for Agriculture and Forest Environment
of Polish Academy of Sciences
Bukowska 19, 60-809 Poznań, Poland*

[2] *The Norwegian Meteorological Institute
Henrik Mohns plass 1, 0313 Oslo, Norway*

[3] *The Norwegian Water Resources and Energy Directorate,
Middelthuns gate 29, 0368 Oslo, Norway*

* Corresponding Author e-mail: mszwed@man.poznan.pl

**Contact person for the seNorge model, e-mail: tus@nve.no

(Manuscript received in final form December 31, 2018)

Abstract— The present paper examines the observed variability of maximum depth of snow cover in Poland and its projections for near (2021–2050) and far (2071-2100) future. The study makes use of a set of 43 time series of observation records from stations in Poland, from 1951 to 2013. For the future, two downscaling experiments were conducted with the aim of producing reliable high-resolution climate projections of precipitation and temperature for Poland. The results of these projections were used as the input data to the *seNorge* snow model in order to transform bias-adjusted daily temperature and precipitation into daily snow conditions. Observed behavior of time series of snow is complex and not easy to interpret. The changes (if any) are dominated by strong inter-winter and intra-winter variability, rendering trend detection difficult. Projected seasonal snow cover depth (for winter as well as spring and autumn) as simulated by the snow model for the near and far future show decreases. The rate of decreasing maximum snow depth is expected to at least double by 2071–2100.

Key-words: snow cover, observations, projections, snow model, Poland

1. Introduction

In the conditions of overwhelming warming, intuitively, one can expect smaller snowfalls (by virtue of the increase in liquid winter precipitation due to warming) and, consequently, occurrence of a reduced snow cover (both shorter-lying and thinner). Yet, there is a strong natural variability of snow cover depth, also between consecutive winters or consecutive intervals within a single winter. Snow cover is, in fact, a very sensitive variable, because its formation and maintenance in the landscape depends on many factors.

In any case, thinking about global warming, one usually thinks of average conditions getting warmer. However it does not mean that in the future in the middle of a warm and snowless winter, there is no chance for one or a few frosty and snowy spells. In this context, it seems interesting to analyze what changes (if any) in the snow cover depth have been observed in past-to-present and what projections are developed for the future.

2. Data and methodology

For analyzing the present situation, the study makes use of a set of 43 time series of observation records from stations in Poland, from 1951 to 2013. The data was provided by the Polish Institute of Meteorology and Water Management - State Research Institute (Polish acronym: IMGW-PIB). The basic criteria for selection of stations were: (i) the length of the available time series of record, and (ii) the spatial distribution of stations with the goal of covering the whole territory of Poland and its climate regions, in a possibly uniform way. The studied data started on October 1, 1951 (38 meteorological stations) or later (5 stations) and continued until December 31, 2013. The meteorological stations used in the present study are listed in *Table 1* and mapped in *Fig. 1*. While for the future, the snow projections are based on gridded snow data produced from gridded precipitation and temperature.
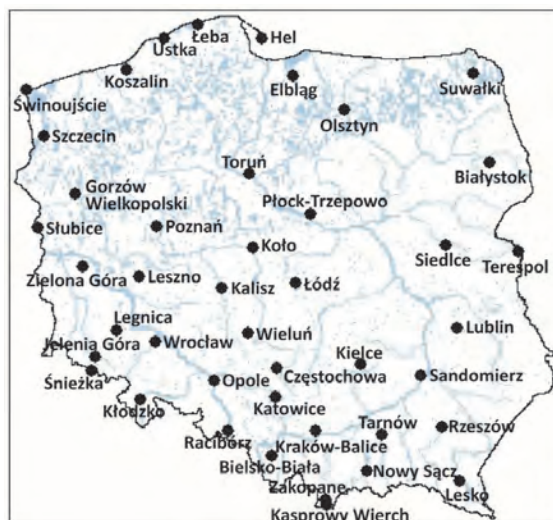
Fig. 1. Map of locations of meteorological stations used in the study.

Table 1. List of meteorological stations used in the study

Station	Lati-tude N	Longi-tude E	Eleva-tion [m.a.s.l.]	Station	Lati-tude N	Longi-tude E	Eleva-tion [m.a.s.l.]
Białystok	53°06'	23°10'	148	Olsztyn	53°46'	20°25'	133
Bielsko-Biała-Aleksandrowice	49°48'	19°00'	398	Opole	50°40'	17°58'	176
Częstochowa	50°49'	19 °06'	295	Płock-Trzepowo	52°35'	19°44'	106
Elbląg-Milejewo	54°10'	19°26'	38	Poznań	52°25'	16°50'	86
Gorzów Wielkopolski	52°45'	15°17'	72	Racibórz-Studzienna	50°05'	18°13'	190
Hel	54°36'	18°49'	1	Rzeszów-Jasionka	50°06'	22°03'	200
Jelenia Góra	50°54'	15°48'	342	Sandomierz	50°42'	21°43'	217
Kalisz	51°44'	18°05'	140	Siedlce	52°11'	22°16'	146
Kasprowy Wierch	49°14'	19°59'	1991	Słubice	52°21'	14°36'	21
Katowice	50°29'	19°05'	317	Suwałki	54°08'	22°57'	184
Kielce-Suków	50°51'	20°37'	268	Szczecin-Dąbie	53°24'	14°37'	1
Kłodzko	50°26'	16°39'	316	Śnieżka	50°44'	15°44'	1603
Koło	52°12'	18°40'	116	Świnoujście	53°55'	14°14'	6
Koszalin	54°12'	16°09'	33	Tarnów	50°02'	20°59'	209
Kraków-Balice	50°05'	19°48'	237	Terespol	52°04'	23°37'	133
Legnica	51°13'	16°10'	122	Toruń	53°03'	18°35'	69
Lesko	49°28'	22°20'	386	Ustka	54°35'	16°52'	6
Leszno-Strzyżewice	51°50'	16°32'	91	Wieluń	51°13'	18°35'	195
Lublin-Radawiec	51°13'	22°24'	238	Wrocław	51°06'	16°53'	120
Łeba	54°45'	17°32'	2	Zakopane	49°18'	19°57'	857
Łódź-Lublinek	51°44'	18°24'	187	Zielona Góra	51°56'	15°30'	180
Nowy Sącz	49°37'	20°42'	292				

For the present two characteristics, namely: (i) mean value of snow cover depth for winter (December-January-February), in cm, where the mean value is computed for all days in the given period, including days with no snow cover, and (ii) maximum value of snow cover depth for winter (December-January-February), in cm, were extracted from the time series of daily depth of snow cover.

To describe the observed temporal changes in snow cover characteristics for every station, the rate of change per year for the whole analyzed period was calculated, using linear regression, and the Mann-Kendall statistic. In order to detect existing changes/trends in time series of snow cover data, the Hydrospect 2.0 software was used (*Radziejewski* and *Kundzewicz*, 2000).

Few studies have been carried out for Poland based on the newest generation of climate model simulations, i.e., the fifth generation of the Coupled Model Intercomparison Project (CMIP5) and the European domain of the Coordinated Downscaling Experiment Initiative (Euro-CORDEX). In this paper a set of regional climate model simulations (*Table 2*) from the Euro-CORDEX experiment (*Jacob et al.,* 2014) was selected to provide climate projections. These projections can be seen as an update of old scenarios. With the aim of producing reliable high-resolution climate projections of precipitation and temperature for Poland, the output of the projections were bias-adjusted and downscaled to 5 km. They were then used as input data to the snow model in order to transform daily temperature and precipitation into daily snow conditions. More details on these bias-adjusted climate projections are given in *Mezghani et al.* (2016). The data is publicly available at http://dx.doi.org/10.4121/uuid:e940ec1a-71a0-449e-bbe3-29217f2ba31d.

Projected seasonal snow cover depth (for winter as well as spring and autumn) was simulated by the snow model for the near (2021–2050) and far (2071–2100) future horizon. In order to produce unbiased snow cover projections across Poland, two experiments assumed to the two targeted radiative forcing values of +4.5 Wm^{-2} and +8.5 Wm^{-2} in 2100 (RCP4.5 and RCP8.5) relative to pre-industrial values were used.

Table 2. List of available GCM-run-RCM combinations composing the multi-model ensemble, based on EURO-CORDEX, used in determination of projections

GCM	RCM
CNRM-CERFACS-CNRM-CM5	CLMcom-CCLM4-8-17
CNRM-CERFACS-CNRM-CM5	SMHI-RCA4
ICHEC-EC-EARTH	CLMcom-CCLM4-8-17
ICHEC-EC-EARTH	SMHI-RCA4
ICHEC-EC-EARTH	KNMI-RACMO22E
ICHEC-EC-EARTH	DMI-HIRHAM5
IPSL-IPSL-CM5A-MR	SMHI-RCA4
MPI-M-MPI-ESM-LR	CLMcom-CCLM4-8-17
MPI-M-MPI-ESM-LR	SMHI-RCA4

The *seNorge* snow model has been developed since 2004 at the Norwegian Water Resources and Energy Directorate (NVE), in cooperation with the Norwegian Meteorological Institute (MET Norway), and the Norwegian Mapping Authority (*Engeset et al.*, 2004; *Saloranta*, 2014). It simulates different snow-related variables, such as snow water equivalent, snow depth, bulk snow density, and the amount of liquid water in the snow-pack. No optimization of the *seNorge* snow model was made for the Polish conditions, so the default set of model parameters (the same as for Norway) was used. The description of the *seNorge* model and a statistical evaluation of simulating snow maps for Norway in *Saloranta* (2012) showed that a first model version generally overestimated the snow water equivalent and the snow bulk density. In this work, we are using an updated model version (v1.1.1), where the significant biases in snow water equivalent and bulk density have been removed (*Saloranta*, 2014, 2016). However, only the snow depth is analyzed in this study and a separate validation based on observed snow depth in Poland is carried out.

3. Validation

For validation purposes, the snow model was used to simulate past snow depth across Poland, based on daily mean temperature and precipitation. The mean daily temperature values were calculated as the average of the daily minimum and maximum temperatures.

Figs. 2a and 2b show the average and the total winter maximum snow depth over Poland taken from the gridded observational data set CPLFD-GDPT5 (*Mezghani et al.*, 2016). The patterns and values agree with observation-based data for the time period 1948–49 to 1997–98 given in *Falarz* (2004) with the lowest average maximum depths in western Poland (≤ 15 cm), growing towards the northeast to 30 cm, and exceeding 150 cm in the Tatra Mountains. The absolute simulated maximum winter snow depth ranges from below 40 cm in the west (and around Legnica) to more than 80 cm in the northeast, and finally, to more than 200 cm in the high mountains. Again, these values are in good agreement with those given in *Falarz* (2004) and *Szwed et al.* (2017).
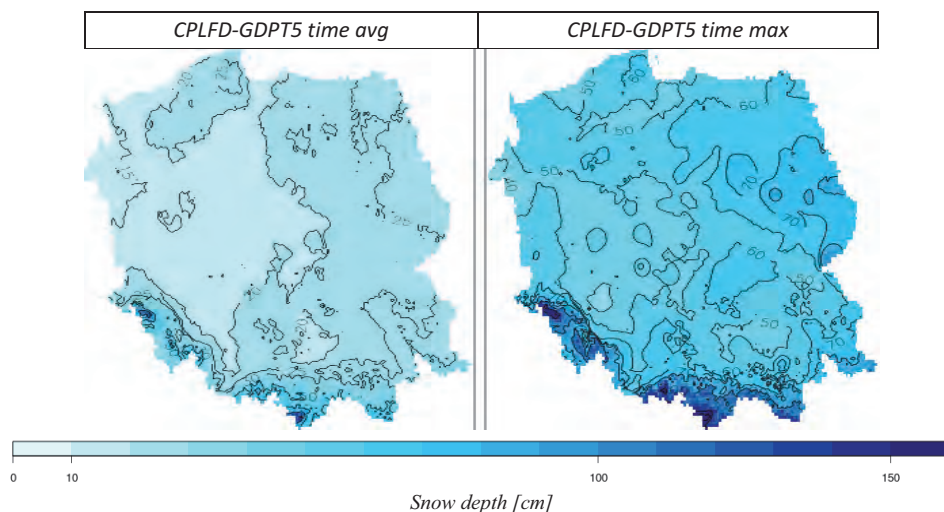
Fig. 2. Winter maximum of snow depth [cm] modeled by the *seNorge* model with input from the gridded CHASE-PL data set for the historical period. a) shows the time averages, while b) depicts the maximum values over all winters.

The *seNorge* snow model was also used with bias-adjusted precipitation and temperature values from all nine historical GCM/RCM (General Circulation Models, Regional Climate Models) runs (*Table 2*). *Figs. 3a* and *3b* show the average and the total winter maximum snow depth over Poland for the resulting multi-model ensemble mean for 1971–2000. For the average maximum depths, the patterns and values agree again with the observation-based data shown in *Fig. 2* and in *Falarz* (2004). The absolute maximum winter snow depth in the

multi-model ensemble mean shows values below 40 cm in the west and above 200 cm in the Tatra Mountains as well, but has a less pronounced increase towards the northeast. However, using the mean of several climate models is expected to smooth out some of the local gradients, which can be clearly seen for a single model (not shown). As expected, the mean pattern resembles the results from the CPLFD-GDPT5-driven snow model, as the same data has been used to bias-adjust temperatures and precipitation in the model data. However, the agreement of the simulations of past conditions via RCM and the observation-driven snow depth provide a simple test for physically-consistent sequences of precipitation and temperature data in the bias-adjusted RCM data, since non-physical combinations are expected to yield unrealistic snow depths. This also demonstrates that the dependency between precipitation and temperature has been well captured by the simulations (e.g., sequence of consecutive warm dry days and cold wet days that may have a strong influence on the snow simulations) and not critically altered by the bias-adjustment methods used.
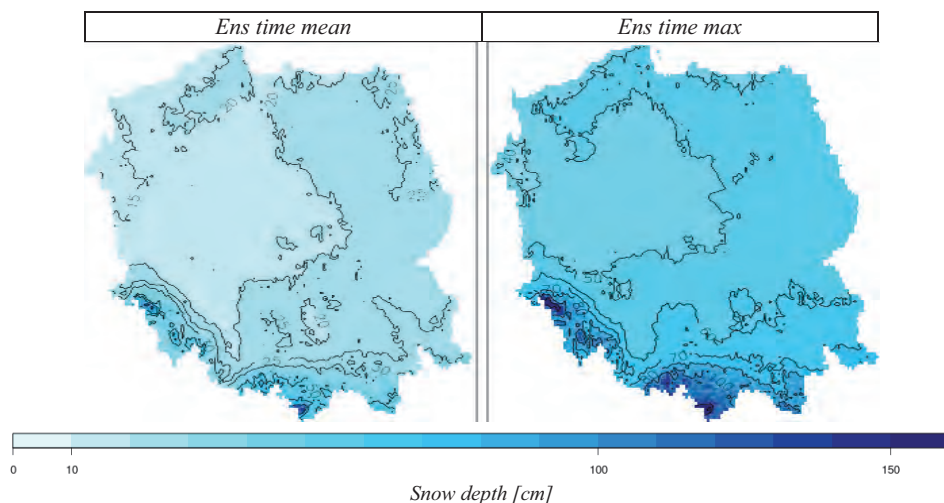
Fig. 3. Winter maximum of snow depth [cm] modeled by the *seNorge* model with input from the nine DD models for the historical period. Only the multi-model ensemble mean is shown. a) depicts the time averages, while b) shows the maximum values over all winters.

493

4. Present parameters of snow cover

Strong inter-winter and intra-winter variability of snow cover is typical for the Polish climate. A single year can make a real difference. This statement is correct for the average snow cover, but for the maximum cover it is even more expressed. The graphs of mean and maximum depth of snow cover in winter (DJF) in Toruń, Poland (*Fig. 4* and *5*) can serve as interesting examples. The difference between the lowest and the highest value in the time series of maximum snow cover depth is almost twice higher than for the time series of average depth of snow cover.

In the period of 1952–2013, the spatial variability of the maximum depth of snow cover in DJF in Poland changed on the east-west axis, generally increasing from the west to the east (northeast). The maximum depth of snow cover in winter (DJF) in the period 1952–2013 in Poland varied from 34 cm in Poznań and Słubice to 85 cm in Kraków (while in mountain areas, the maximum depth of snow cover exceeded 300 cm).
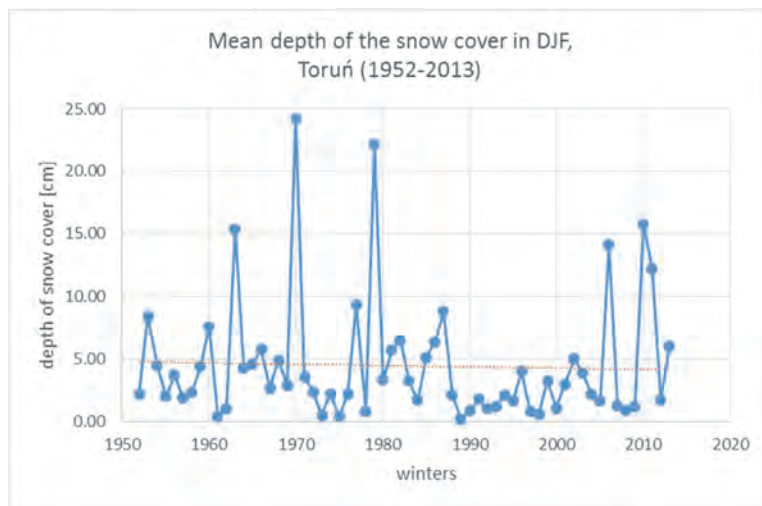
Fig. 4. Mean depth of snow cover in winter (DJF) in Toruń in the period 1952–2013.
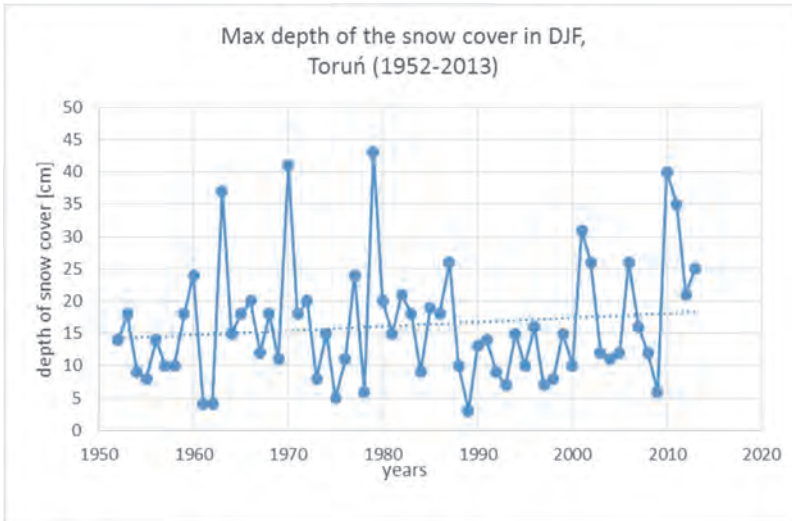
Fig. 5. Maximum depth of snow cover in winter (DJF) in Toruń in the period 1952–2013.

Observed behavior of time series of snow cover depth is complex and not easy to interpret. All tendencies are overshadowed by strong natural inter-annual variability, making trend detection unlikely. Indeed, no significant trend on the 0.05 level was detected for all part of the country (based on Mann-Kendall test). The weak tendencies in the snow-cover depth are location-specific, the value of change per year is positive at some locations, while negative at others. However, as expected in the warming climate, there are many more locations with a negative tendency (25) than with a positive one (15). In general, after 1990, a cluster of years with shallow snow cover have occurred. Nevertheless, more snowy winters (with higher depth of mean and maximum snow cover) have also appeared more recently. The winter of 1963 and 1979 (i.e., December 1962 - February 1963, and December 1978 - February 1979, respectively) are the absolute record holders. In these years, maximum of snow cover depth occurred for 13 and 12 stations (of 43), respectively. Temporal changes in maximum depth of snow cover in winter (DJF) in the period 1952–2013, expressed by the rate of change per year and the statistical significance level are presented in *Fig. 6*.
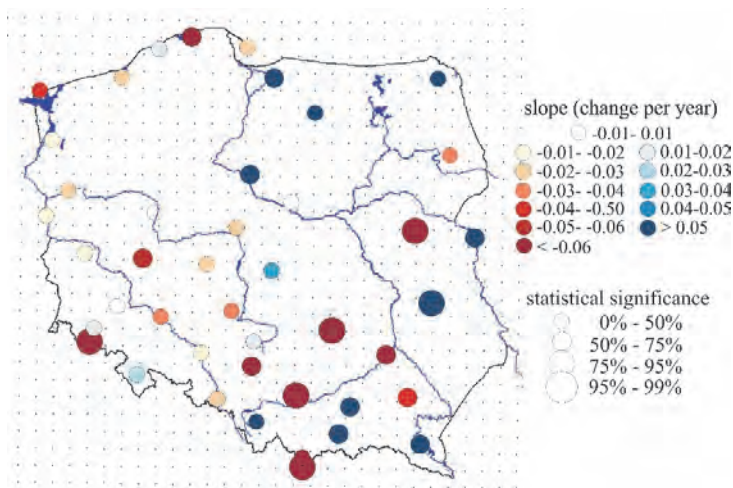
Fig. 6. Temporal changes in maximum depth of snow cover in winter (DJF) in the period 1952–2013 expressed by the rate of change per year and the statistical significance level.

5. Projection of snow cover

Table 3 summarizes the projected seasonal snow depth (for winter DJF as well as spring MAM and autumn SON) as simulated by the *seNorge* snow model by using the bias-adjusted daily projections in the near (NF) and far (FF) future. As an indicator of snow change conditions, the maximum seasonal snow depth is used and analyzed hereafter.

Table 3. Relative changes in maximum seasonal snow depth (%) from snow modeling based on bias-corrected RCM data. The corresponding ensemble mean absolute values in centimeters are also given. Confidence limits are presented in parentheses.

RCP	Future horizon	DJF	MAM	SON
RCP4.5	NF 2021-2050	-15; -10 cm (-27; 5)	-14; -9 cm (-33; 9)	-25; -5 cm (-37; -11)
	FF 2071-2100	-28; -18 cm (-44; -13)	-34; -21 cm (-56; -15)	-18; -4 cm (-50; 10)
RCP8.5	NF 2021-2050	-20; -12 cm (-33;-9)	-21; -13 cm (-45; -1)	-20; -4 cm (-47; 3)
	FF 2071-2100	-44; -27 cm (-64; -24)	-60; -37 cm (-87; -33)	-48; -10 cm (-81; -23)

Fig. 7 shows the maximum annual snow depth projections by the two future horizons: NF 2021–2050 and FF 2071–2100 (rows) in comparison to the reference interval 1971–2000, following two RCPs (representative concentration pathways) 4.5 and 8.5 (columns). Projections suggest that the maximum snow depth is expected to decrease by the two future horizons and following two RCPs. This decreasing rate is expected to be about 15% and about 20%, under RCP4.5 and RCP8.5 by 2021–2050, respectively.

This rate of decreasing maximum snow depth is expected to double by 2071–2100, regardless the RCP, and may go down to more than 40% under RCP8.5, compared to reference values. Nevertheless, even if most areas in Poland are expected to get affected, changes in central areas are less pronounced. This may be explained by the convergence of different physical processes influencing the snow conditions in those areas. In addition, small areas of increases may also occur in the near future, mainly in high mountainous regions. This is understandable in the light of increased precipitation in the warming climate. This can mean more snow fall if the increased temperature does not substantially exceed 0 °C.
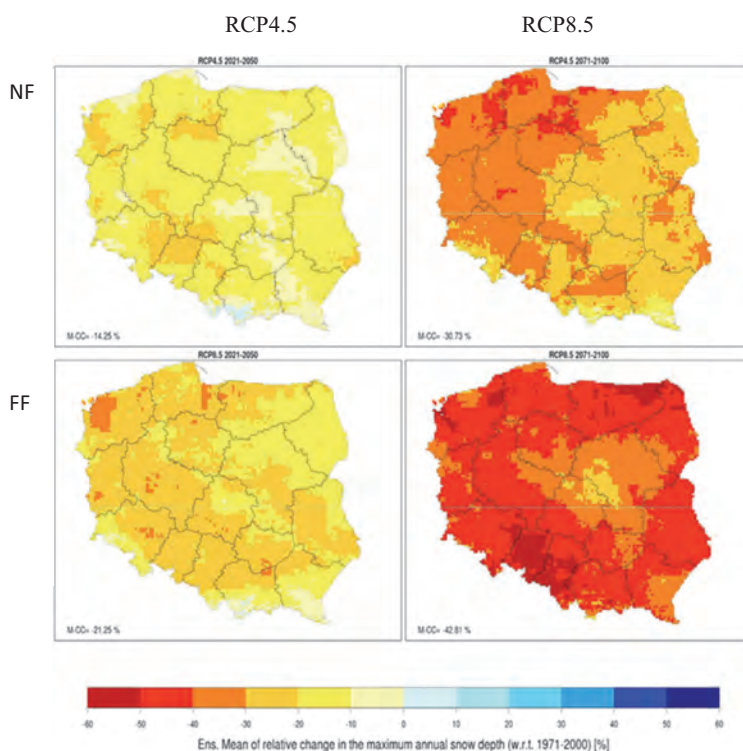
Fig. 7. Maximum snow depth projections for two horizons:NF 2021–2050 and FF 2071–2100 (in the rows) under two RCPs: 4.5 and 8.5 (in the columns).

6. Conclusions

Observed variability of maximum depth of snow cover in Poland, based on a set of 43 time series of station records, as well as projections for two future horizons were examined. Snow projections were obtained with the help of the *seNorge* snow model, fed with high-resolution climate (precipitation and temperature) projections.

Even if decrease of total annual snowfall and snow cover depth are expected in the warming climate, observed behavior of time series of records is complex and not easy to interpret. Eventual tendencies are overshadowed by the strong natural inter-annual variability, making significant trend detection unlikely. There were some winters with very high or very low snow cover depth. For instance, winter of 1963 and 1979 (i.e., December 1962 - February 1963 and December 1978 - February 1979, respectively) are the absolute record holders, because maximum of snow cover depth occurred there for 13 and 12 stations, respectively.

There are weak and location-specific tendencies in snow-cover depth, but no significant trend on the 0.05 level was detected for all part of the country (based on Mann-Kendal test). However, as expected in the warming climate, there are many more locations with a negative tendency than with a positive one. This corresponds with many other research studies concerning Europe, which report large variability between individual seasons, and the lack of distinct, statistically significant trends, e.g., for Estonia (*Jaagus,* 1997) or Slovakia (*Brown* and *Petkova,* 2007). A slight decreasing trend of snow cover depth was observed in most areas of Poland during the second half of the 20th century, but no change was distinguished for the longer periods (*Falarz* 2004; *Nowosad* and *Bartoszek* 2007; *Czarnecka* 2012).

Maximum depth of snow cover in winter (DJF) in the Polish high mountains is going to decrease. *Lapin* and *Fasko* (2005) reveal for a decrease in snow cover conditions in the Little Carpatians after 1990. Similar conclusions were reached by *Brown* and *Petkova* (2007) for Bulgarian mountainous regions. Research for central and north Tyrol identifies a minor decreasing snow depth trend during 1895–1991 (*Fliri* and *Baumkirchen,* 1991), while *Beniston* (1997) confirms a considerable decrease of snow cover since the mid-1980s in the Swiss Alps. *Falarz* (2004) quotes that an increasing trend in snow cover has been noted during the second half of the 20th century in Polish mountainous regions.

Projected seasonal snow cover depth, as simulated by the *seNorge* snow model show ubiquitous decreases for both the near and far future. The rate of decreasing maximum snow depth is expected to at least double by 2071–2100.

However, small areas of increases of snow cover depth may still occur in near future in high mountainous areas in the south part of Poland, accompanying precipitation increase in the warming climate. If the increased temperature does

not substantially exceed 0 °C, snow can be the essential component of increased winter precipitation.

References

Beniston, M., 1997: Variations of snow depth and duration in the Swiss Alps over the last 50 years: links to changes in large-scale climatic forcings. *Climatic Change 36*, 281–300. https://doi.org/10.1007/978-94-015-8905-5_3

Brown, R.D. and *Petkova, N.,* 2007*:* Snow cover variability in Bulgarian mountainous regions, 1931–2000. *Int. J. Climatol., 27,* 1215–1229. https://doi.org/10.1002/joc.1468

Czarnecka, M., 2012*:* Częstość występowania i grubość pokrywy śnieżnej w Polsce. *Acta Agrophysica, 19,* 501–514. (In Polish)

Engeset, R., Tveito, O.E., Udnæs, H.-C., Alfnes E., Mengistu, Z., Isaksen, K., and *Førland E.J.,* 2004: Snow map validation for Norway. XXIII Nordic Hydrological Conference. Tallinn, Estonia. NHP report, 48(1), 122–131.

Falarz, M., 2004: Variability and trends in the duration and depth of snow cover in Poland in the 20th century. *Int. J. Climatol*. *24*, 1713–1727. https://doi.org/10.1002/joc.1093

Fliri, F. and *Baumkirchen, H.,* 1991: Die Schneeverhaltnisse in Nord- und Osttirol in der Periode 1895–1991. *Mitteilungen der Osterreichischen Geographischen Gesellschaft 133*, 7–25. (In German)

Jacob, D., Petersen, J., Eggert, B., Alias, A., Christensen, O.B., Bouwer, L.M., Braun, A., Colette, A., Déqué, M., Georgievski, G. and Georgopoulou, E., 2014: EURO-CORDEX: new high-resolution climate change projections for European impact research *Reg. Environ. Change 14*, 563-578. https://doi.org/10.1007/s10113-013-0499-2

Jaagus, J., 1997: The impact of climate change on the snow cover pattern in Estonia. *Climatic Change 36*, 65–77. https://doi.org/10.1023/A:1005304720412

Lapin, M., and *Faško, P.,* 2005: Snow cover changes in the Little Carpathians in Slovakia. In Online Proceedings of ICAM2005, 28th International Conference on Alpine Meteorology, Zadar, Croatia, 23–27 May 2005, s. 658–661. http://meteo.hr/ICAM2005/

Mezghani, A., Dobler, A., and *Haugen, J.H.,* 2016: CHASE-PL Climate Projections: 5-km Gridded Daily Precipitation & Temperature Dataset (CPLCP-GDPT5). Norwegian Meteorological Institute. Dataset. http://dx.doi.org/10.4121/uuid:e940ec1a-71a0-449e-bbe3-29217f2ba31d

Nowosad, M. and *Bartoszek, K.,* 2007: Wieloletnia zmienność grubości pokrywy śnieżnej w okolicy Lublina. In: K. Piotrowicz, R. Twardosz (reds) Wahania klimatu w różnych skalach przestrzennych i czasowych. Instytut Geografii i Gospodarki Przestrzennej UJ Kraków, 411–421. (In Polish)

Radziejewski, M., and *Kundzewicz Z.W.,* 2000: Hydrospect - Software for detecting changes in hydrological data. In (eds.: *Robson, A.* and *Kundzewicz Z.W.*) Detecting trend and other changes

in hydrological data, App. 2. World Climate Programme-Applications and Services, World Meteorological Organization, Geneva.

Saloranta, T.M., 2012: Simulating snow maps for Norway: description and statistical evaluation of the seNorge snow model, *The Cryosphere 6*, 1323–1337. https://doi.org/10.5194/tc-6-1323-2012

Saloranta, T.M., 2014: New version (v.1.1.1) of the 'seNorge' snow model and snow maps for Norway. Norwegian Water Resources and Energy Directorate, *NVE report 6*, 36.

Saloranta, T.M., 2016: Operational snow mapping with simplified data assimilation using the seNorge snow model. *J. Hydrol. 538*, 314–325. https://doi.org/10.1016/j.jhydrol.2016.03.061

Szwed, M., Pińskwar, I., Kundzewicz, Z.W., Graczyk D. and *Mezghani A.,* 2017: Changes of snow cover in Poland. *Acta Geophysica 65*, 65–76. https://doi.org/10.1007/s11600-017-0007-z

IDŐJÁRÁS

Methodology for deriving synthetic meteorological droughts and its application for Budapest

Ognjen Gabrić[*,1] and **Jasna Plavšić** [2]

[1]*University of Novi Sad, Faculty of Civil Engineering Subotica*
Department of Hydraulic and Environmental Engineering,
Kozaračka 2a, 24000 Subotica, Serbia

[2]*University of Belgrade, Faculty of Civil Engineering Belgrade*
Department of Hydraulic and Environmental Engineering
Bulevar kralja Aleksandra 73, 11000 Beograd, Serbia

*Corresponding Author E-mail: ogabric@gf.uns.ac.rs

Abstract— In the recent years, nearly every part of Central Europe and the Balkans has experienced periods of reduced precipitation that can lead to droughts. Because of the complexity of the phenomenon and the different points of view from which the problem can be studied, it is difficult to decide when the drought started or when it ended. This paper presents a methodology for a stochastic analysis of meteorological droughts. This method is applied to precipitation and temperature data observed at a meteorological station of Budapest for the period of 1900–2000. The drought is defined as a consequence of a combined effect of temperature and prolonged dry period – consecutive days with daily precipitation below a chosen threshold for precipitation. The statistical analysis of the maximum meteorological droughts is performed by means of the peaks-over-threshold (POT) method. The proposed methodology provides probability distributions of the magnitude of droughts in terms of dry period duration and air temperatures, which can then be used to formulate synthetic design droughts for selected return periods.

Key-words: Budapest, drought, stochastic process, synthetic design drought, peaks-over-threshold (POT) method

1. Introduction

There are many different definitions of drought. Roughly, droughts can be defined as the temporary reduction in the rainfall, runoff, and soil moisture amounts, and they are related to the climatology of the region (*Sen,* 2015). Usually, the reduction in rainfall is referred to as a meteorological drought. Although there is no universal definition of drought, partly because of the complexity of the phenomenon and partly because of the point of view from which the problem is studied (hydrological, geological, environmental, agricultural, etc.), droughts can be classified into four categories *(Mishra* and *Singh,* 2010): meteorological, agricultural, hydrological, and socio-economic droughts. Lack of precipitation is the main cause of drought which leads to runoff deficit, soil moisture deficit and, at the end, to the food deficit.

From the beginning of the 16th century until the mid-18th century, summer weather was fairly warm and wet (*Rácz,* 1999). The trend of summers becoming drier made its appearance in the last third of the 18th century and continued until the 1860s. Summers became again wet in the last third of the 19th century, and a drier period commenced again at the turn of the 20th century. Wet summer weather prevailed again from the 1910s through the 1970s, and this trend ended when dry summers made a comeback in the 1980s and 1990s.

Up to the authors' best knowledge, there were four great droughts in Hungary in the medieval time (1474, 1479, 1494, and 1507) (*Kiss* and *Nikolić,* 2015). The long-lasting severe shortage of precipitation resulted in extremely low water levels of major rivers, border security problems, harvest failures, severe food shortage, and danger of mass extinction of domestic animals.

Droughts are a recurrent feature of Hungary's climate and can cause substantial damages to the nation's agriculture (*Wilhite* and *Svoboda,* 2000). It is estimated that 36% of all agricultural losses are caused by drought, followed by hail, floods, and frosts.

There is a wide range of methods used to describe drought, and new ones are being introduced depending on the purpose of analysis. Some of them are Palmer indices, standardized precipitation index (SPI), De Martonne index, Palfai aridity index (PAI), and regional models like REMO and ALADIN (*Blanka et al.,* 2013).

This paper analyzes meteorological droughts during the growing season (from April 1 to September 30) for the meteorological station of Budapest. The analysis is based on precipitation and temperature data published on the website of the Hungarian Meteorological Service (OMSZ) for the period of 1901–2000 ("CLIMATE DATA SERIES / BUDAPEST," n.d.). The applied method is primarily intended for the needs of agriculture and meteorology, and it was developed by Fabian and Zelenhasic (*Fabian*, 2015; *Fabian* and *Zelenhasic,* 2016). The methodology is based on the stochastic processes and probabilistic assessment of the number and magnitude of droughts, where the drought is considered to be a consequence of a combined effect of prolonged dry periods and

high air temperatures. Dry periods are defined as consecutive days with daily precipitation below a chosen threshold for precipitation. Also, only dry periods with a duration exceeding the certain temporal threshold are considered in the methodology. The precipitation and duration thresholds can be selected to describe critical conditions for crops of interest. The proposed methodology provides probability distributions of the magnitude of droughts in terms of dry period duration and air temperatures, which can then be used to formulate synthetic design droughts for selected return periods.

The original methodology by Fabian and Zelenhasic (*Fabian* and *Zelenhasic*, 2016) proposed three probability functions to describe the magnitude of meteorological droughts: (1) double exponential distribution with two parameters, (2) adjusted empirical distribution, and (3) polynomial of degree 4. In this paper, a modification of the methodology is adopted so that the statistical analysis of the maximum meteorological droughts is performed by means of the peaks-over-threshold (POT) method (*Plavšić*, 2007; *Todorovic* and *Zelenhasic*, 1970; *Vukmirović* and *Petrović*, 1998, 1997), which considers all extreme values of the meteorological droughts that exceed a given threshold. Generally, this is an advantage of this method over the annual maxima method, with which only the annual maximum values are included in the statistical analysis, thereby neglecting the fact that there can be more than one extreme value in some year that exceeds annual maxima in other years. The proposed methodology for describing the meteorological droughts was applied in a previous paper (*Gabrić et al.,* 2017) to two meteorological stations in Vojvodina, the northern part of Serbia, but with a shorter data record of about fifty years.

2. Methodology

2.1. Definition of meteo-drought

The meteorological drought, or meteo-drought, Z (day°C), is defined here as the product of drought duration, D (days), and mean air temperature over the drought duration T (°C) (*Fabian* and *Zelenhasic*, 2016):

$$Z = D \cdot T. \tag{1}$$

The drought duration is the duration of a dry spell in which days with precipitation smaller than a certain threshold are treated as dry days. In this study, a threshold of 5 mm is selected, because such a small amount of precipitation is insignificant for the roots of most crops. It is also assumed that dry spells lasting for 25 or more days are critical for crops, so a 25-day period is adopted as the threshold for drought duration.

The stochastic process of the meteorological droughts is conceived as a marked point process characterized by the following variables: time of the

beginning of meteo-drought τ_b, time of the end of meteo-drought τ_e, drought duration $D = \tau_e - \tau_b$, mid-point $\tau = (\tau_b + \tau_e)/2$, mean air temperature T throughout the drought duration, meteo-drought $Z = D \cdot T$, total number k of meteo-droughts in growing season ($k = 0, 1, 2,...$), and ordinal number n of meteorological drought in growing season ($n = 1, 2, 3,..., k$). Of particular interest is the greatest meteorological drought in growing season (Z_{am}), $X=Z_{am}=\sup\{Z_n, n=1, 2,…,k\}$, the distribution of which provides an assessment of design droughts, and which is the subject of this paper. With the described setup, it is also possible to analyze distributions of other variables, such as the time of occurrence τ_X of the greatest meteorological drought X.

2.2. Distribution of the maximum meteo-drought

To obtain the distribution of the greatest meteo-drought in the growing season, the peaks-over-threshold (POT) framework is used. This framework is based on the analysis of all extreme events that exceed the certain threshold within a fixed time interval. In this context, both the number of events and their magnitude are random variables. The statistical analysis of meteo-droughts within this framework is performed in three steps: (1) fitting the distribution of the number of exceedances of meteo-drought over the chosen threshold during the growing season, (2) fitting the distribution of the meteorological drought exceedances, and (3) combining the two above-mentioned distributions into the distribution of the greatest meteorological drought in the growing season.

2.2.1. The POT theoretical model

The number of meteo-droughts, k, in the growing season is a discrete random variable with a probability mass function

$$p_j = P\{k = j\}. \tag{2}$$

The Poisson distribution is the most frequently used distribution for the number of exceedances above a threshold. Alternatively, binomial and negative binomial distributions can also be used. Theoretical distribution for the number of exceedances can be chosen based on the value of the dispersion index I, defined as the ratio between the variance and mean of k: for the Poisson distribution $I = 1$ (in practice the Poisson distribution is a good fit for $0.8 < I < 1.2$), for the binomial distribution $I < 1$, and for the negative binomial distribution $I > 1$. Generally, the number of meteo-droughts decreases with increasing threshold the and consequently the number of years in which no meteorological droughts occur in the growing season increases.

The exceedance of meteo-drought Z over the chosen threshold Z_b is a continuous random variable defined as $U = Z - Z_b$. Cumulative distribution function of the exceedances, $H(u)$, is given with:

$$H(u) = H(Z - Z_b) = P\{U \le u\}. \tag{3}$$

Different theoretical distributions can be used to fit the distribution of exceedances. The most commonly used are the exponential, Weibull, and general Pareto distributions. In this study, exponential and Weibull distributions are considered.

The annual maximum meteo-drought during the growing season is a random variable Z, defined as the maximum of a random number k of exceedances U in the growing season:

$$Z_{am} = sup\{Z_n, n = 1,2, \dots, k\} = Z_b + sup\{U_n; n = 1,2 \dots k\}. \tag{4}$$

The cumulative distribution function of the annual maximum meteo-droughts, $F(z)$, is given with:

$$F(z) = P\{Z \le z\}, \tag{5}$$

and is defined only for the values of z above the threshold, i.e. for $z > Z_b$. The general expression for $F(z)$ is derived by combining the distributions of the number and magnitude of exceedances (*Todorovic*, 1970):

$$F(z) = p_0 + \sum_{k=1}^{\infty} p_k [H(z - Z_b)]^k . \tag{6}$$

Depending on the type of distribution for the number of exceedances and type of distribution for the magnitude of exceedances, the above general expression can be simplified. For the Poisson-Weibull combination, the above equation reduces to:

$$F(z) = \exp\left\{-\lambda \exp\left[-\left(\frac{z-z_b}{\alpha}\right)^{\beta}\right]\right\}, \tag{7}$$

and for the binomial-Weibull combination one obtains:

$$F(z) = \left[1 - p \exp\left\{-\left(\frac{z-z_b}{\alpha}\right)^{\beta}\right\}\right]^m . \tag{8}$$

In the last two equations, λ is the parameter of the Poisson distribution, p and m are the parameters of the binomial distribution, and α and β are the parameters of the Weibull distribution. Equations for the combination of the same discrete distributions with the exponential distribution for the exceedances are obtained for $\alpha = 1$.

2.2.2. The empirical distribution of the maximum meteo-drought

The number of droughts within the growing season depends on the threshold set for the duration of the dry spell. Over the record of N years, some years may not contain any meteo–droughts during the growing season. From the statistical point of view, a sample of N experiments in which only the values exceeding the given detection threshold are recorded, while the values below the threshold are not recorded, is referred to as the censored data sample. A distribution of the censored data sample is obtained from the total probability theorem considering the probability p_0 that a recorded value would be below the threshold. If N' out of N experiments yield data above the detection threshold, then:

$$p_0 = \frac{N-N'}{N}. \tag{9}$$

If $G(z)$ denotes the conditional distribution function obtained from N' data values above the detection threshold, the unconditional distribution function is then given with:

$$F(z) = p_0 + (1 - p_0)G(z). \tag{10}$$

Similarly, the empirical distribution function of the greatest meteo-drought in the growing season is then estimated with:

$$F_{emp}(z) = p_0 + (1 - p_0) \cdot F'_{emp}(z), \tag{11}$$

where F'_{emp} is the empirical distribution of the observed droughts that have a duration longer than the chosen threshold. When fitting the distribution of N' maximum droughts, the Weibull plotting position formula is used:

$$F'_{emp}(z_i) = \frac{i}{N'+1}, \quad i = 1, 2, \dots, N', \tag{12}$$

where N' is the number of years with at least one meteo-drought, and i is the rank of data in the ordered sample of N' data.

2.3. Distributions of the maximum drought duration and maximum mean drought temperature

Drought duration, D, and mean air temperature, T, of a meteorological drought are also random variables. Their distributions are needed to construct design meteo-droughts for the selected probability of occurrence. Analysis of maximum duration D or temperature T is performed here also by means of the peaks-over-

threshold method, analogously to identifying the distribution of the maximum meteo-droughts Z in the growing season.

2.4. Deriving design meteo-droughts

A design meteo-drought is the meteo-drought of a given probability of occurrence or return period R, obtained from the distribution of maximum meteo-droughts as the quantile Z_R for the probability of exceedance of $1/R$. Since the meteo-drought is the product of duration D and temperature T, the drought with the magnitude Z_R might occur with different combinations of durations and temperatures. Fabian and Zelenhasic (*Fabian* and *Zelenhasic*, 2016) proposed to consider two combinations of duration and temperature that lead to the drought Z_R: (1) duration D_R of return period R and the corresponding temperature $T_c = Z_R/D_R$, and (2) temperature T_R of return period R and the corresponding duration $D_c = Z_R/T_R$. Geometrically, these values define two rectangles shown in *Fig. 1*. Average rectangle ABCD, representing the R-year design meteo-drought, is obtained from the condition that the areas of two grey rectangles, A1 and A2, are equal. It can be shown that the sides D_d and T_d of the average "design" rectangle are equal to:

$$D_d = \sqrt{D_c D_R}, \ T_d = \sqrt{T_c T_R} \tag{13}$$
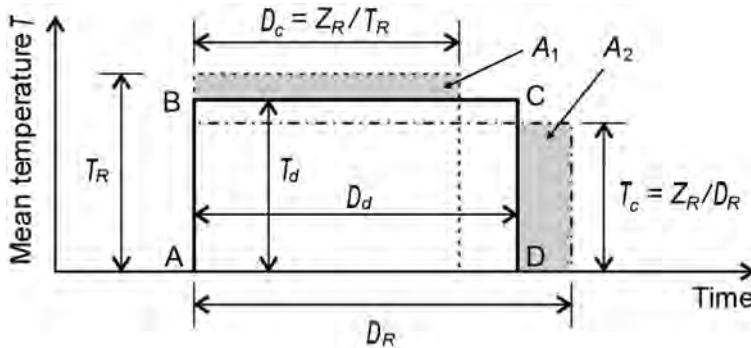
Fig. 1. Construction of the R-year design meteo-drought as proposed by *Fabian* and *Zelenhasić* (*Fabian* and *Zelenhasic*, 2016)

2.5. *Application of the methodology*

The practical application of the methodology for developing distribution of the maximum meteo-drought during the growing season includes three steps: (1) a preliminary analysis with statistical tests that are applied to the available data sets to test their randomness and homogeneity, (2) an identification of the distribution of the meteorological droughts Z, (3) an identification of distributions of drought duration D and mean temperature T, and (4) construction of the synthetic meteo-droughts.

To demonstrate the methodology, mean daily temperature and daily precipitation data from a meteorological station in Budapest (from 1900 – 2000) are used.

Fig. 2 presents the series of the mean annual temperature and *Fig. 3* presents the annual precipitation for Budapest, as well as the corresponding series for the growing season, which begins on April 1 and ends on September 30. Figures show that the annual series exhibit some persistence.

The sample for the statistical analysis is created by extracting the drought events and their parameters during the growing season in each year of observations. The threshold for the drought duration is set at 25 days.
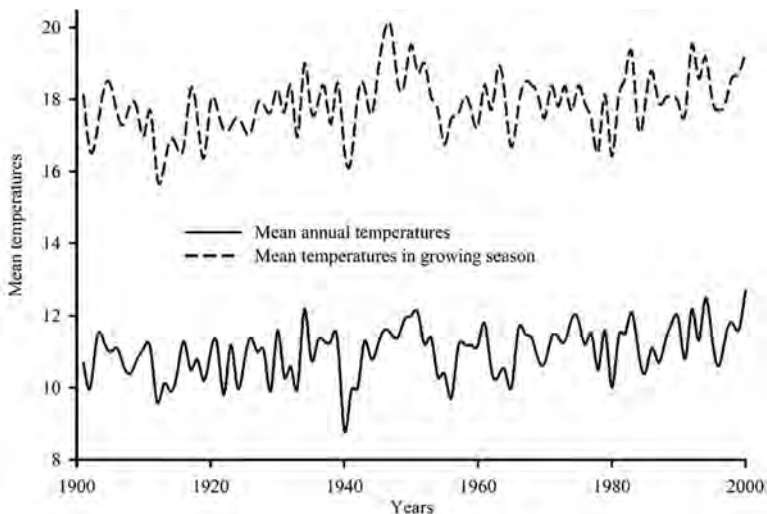
Fig. 2. Mean annual and growing season temperatures
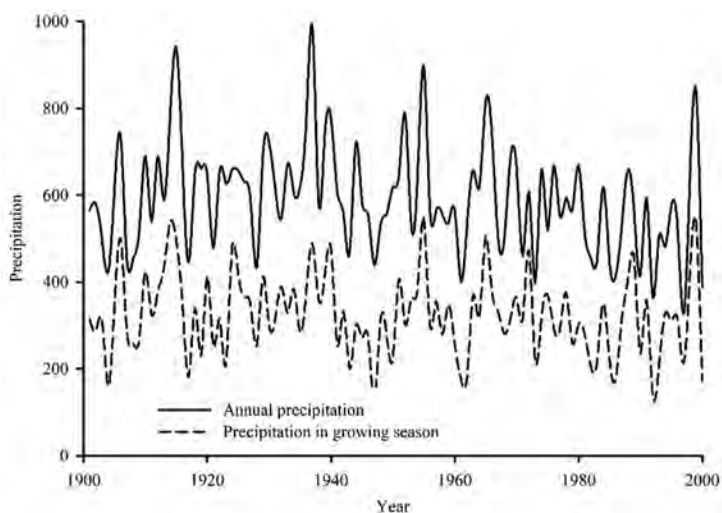
Fig. 3. Annual and growing season precipitations

A total number of extracted meteo-droughts is 141. *Table 1* shows some basic characteristics of the extracted drought events.

Table 1. Basic characteristics of 141 meteo-drought events

Statistic	Duration [day]	Average temperature [°C]T	Meteo-drought [day°C]
Minimum	80	25.1	1749.6
Maximum	25	9.6	258.0
Mean	36.8	18.9	706.2
Standard deviation	9.97	3.6	258.7

2.6. Tests for homogeneity and randomness

The POT framework assumes that the sample consists of independent and identically distributed variables, and therefore, the appropriate statistical tests need to be undertaken to confirm these assumptions.

We applied the statistical tests of homogeneity to the annual mean temperature series and annual precipitation series and found that the hypothesis on homogeneity should be rejected. We also conducted the same tests for mean

temperatures and precipitation sums during the growing season. With these series we rejected the hypothesis on homogeneity of mean temperatures, but we could not reject it for precipitation in the growing season at the 5% significance level.

The series of durations of extracted meteo-droughts and its mean temperatures are also tested for homogeneity, and we found that we could not reject the homogeneity hypothesis at the 5% significance level. The same conclusion was made after testing durations of dry periods in the growing season, and we concluded that the homogeneity assumption is valid for our analysis.

The sample of extracted meteo-droughts is tested for homogeneity by two nonparametric tests (Mann-Whitney and Kolmogorov-Smirnov tests). The runs test is applied to test the randomness of sample data *(Sheskin*, 2004), and Bartlett's test is used to test independence by testing the lack of serial correlation. All tests are applied at the 5% significance level.

For the homogeneity testing, original samples were split into two subsamples of similar size. Both Mann-Whitney and Kolmogorov-Smirnov tests have shown that the null hypothesis of homogeneity of the sample cannot be rejected at the 5% significance level (*Table 2*). The runs test has confirmed the assumption of randomness of data. The hypothesis of data independence is also confirmed by the Bartlett's test.

Table 2. Results of homogeneity and randomness tests

Test	Value of test statistic	Critical region of test statistic at the 5% significance level
Mann-Whitney	$U = -0.13$	$|U| > 1.96$
Kolmogorov- Smirnov	$D = 0.091$	$D > 0.229$
Runs test	$U = -0.04$	$|U| > 1.96$
Bartlett's test	$r_1 = -0.150$ $r_2 = 0.073$ $r_3 = -0.005$	$|r_k| > 0.170$

3. Results and discussion

3.1. Distribution of meteo-droughts

In the process of fitting distributions of the number and magnitude of meteo-droughts, several different thresholds Z_b are assumed. Based on goodness of fit and visual inspection of probability plots, the threshold value for meteo-droughts of $Z_b = 450$ day°C was selected (*Fig. 4*). The results shown in this section are the results for the selected threshold.
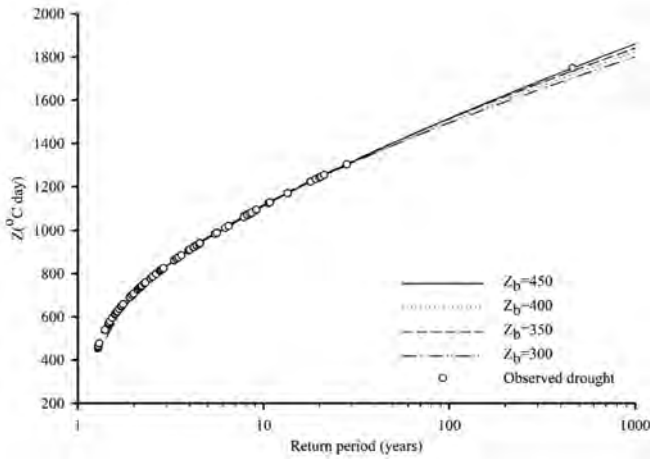
Fig 4. Observed meteo-droughts against probability plots for different Z_b

The number of meteo-droughts during the growing season that exceeds the chosen threshold is fitted with the Poisson and binomial distributions, because the dispersion index for all samples in this study was smaller than 1. Both binomial and Poisson distributions showed a good fit with the empirical distributions of the observed samples (*Fig. 5*). The application of the χ^2 test has shown that none of the theoretical distributions can be rejected at the 5% significance level, as shown in *Table 3*. The binomial distribution is in better accordance with the observed data. Fabian and Zelenhasic (*Fabian* and *Zelenhasic*, 2016) showed that the Poisson distribution can be used for distribution of exceedances. On the other hand, there are cases (*Gabrić et al.,* 2017) where only binomial distribution provides a good fit with the observed data.

Table 3. Chi-square test results for the number of exceedances (α=5%)

Distribution	Value of the test statistic	Critical region at the 5% significance level
Poisson	$\chi^2 = 4.588$	$\chi^2 > 7.815$
Binomial	$\chi^2 = 1.524$	$\chi^2 > 9.488$
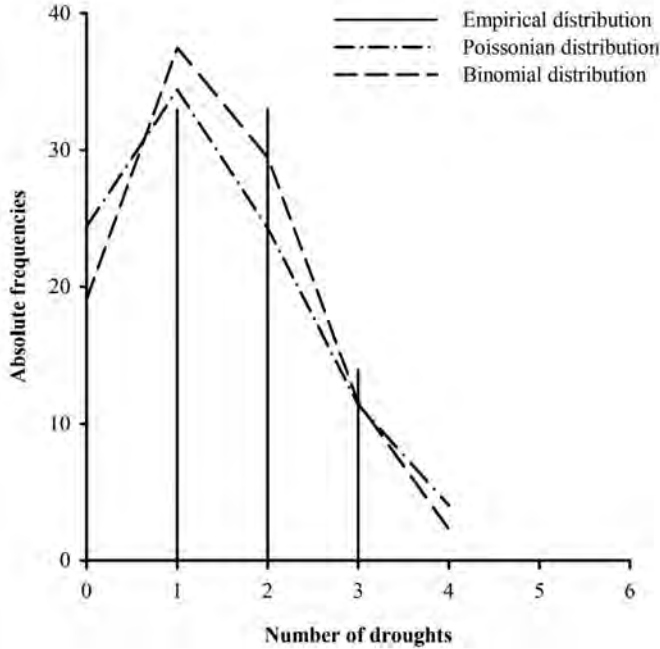
Fig. 5. Distribution of the number of exceedances of meteo-droughts above the threshold $Z_b = 450$ day°C.

The exceedances of meteo-droughts above the chosen threshold are fitted with the exponential and Weibull distributions (*Fig. 6*). The goodness-of-fit testing is carried out by the Cramer-von Mieses and Kolmogorov-Smirnov tests at the 5% significance level (*Table 4*). Unlike the results for Vojvodina in the previous paper (*Gabrić et al.,* 2017) where both exponential and Weibull distributions could be used as theoretical distributions, for the Budapest data in this paper only the Weibull distribution can be accepted as the model for the meteo-drought exceedances. Fabian and Zelenhasic (*Fabian* and *Zelenhasic,* 2016) tried several solutions, including double exponential distribution, "by eye" adjusted empirical distribution, and 4th degree polynomial as the distribution of exceedances obtained by the Lagrange interpolation formula. Only the 4th-degree polynomial passed the Kolmogorov-Smirnov test.

Distribution	Value of the test statistic	Critical region at the 5% significance level
Cramer-von Mieses test		
Exponential	$\omega^2 = 0.643$	
Weibull	$\omega^2 = 0.040$	$\omega^2 > 0.462$
Kolmogorov-Smirnov test		
Exponential	$D = 0.134$	
Weibull	$D = 0.046$	$D > 0.125$
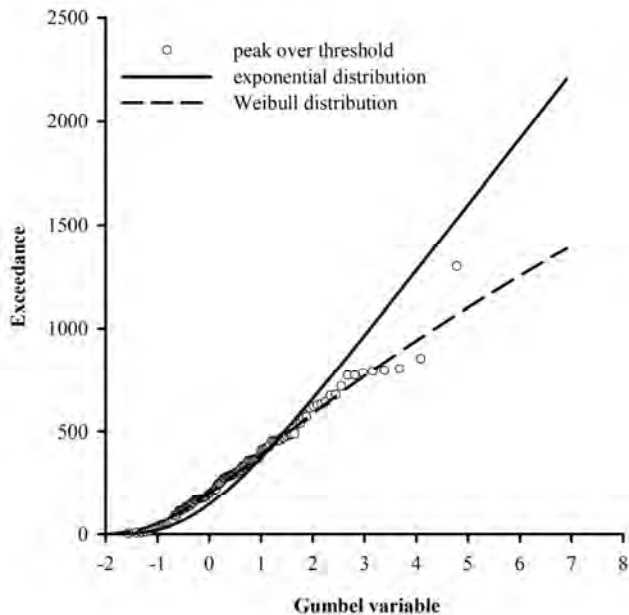
Fig. 6. Distribution of exceedances of meteo-droughts over the threshold of $Z_b = 450$ day°C

The distribution of the maximum meteo-drought in the growing season is obtained by combining the distributions of a number of exceedances and magnitude of exceedances over the threshold. For the Budapest data in this paper, the binomial-Weibull and Poisson-Weibull distribution combinations are used, since the exponential distribution was rejected by the goodness-of-fit tests. The

derived distribution of the maximum of meteo-drought is compared to the empirical distribution of the observed annual maxima. Since there were also years with no meteo-droughts lasting at least 25 days, the conditional probability model in Eq.(12) was used to establish the empirical distribution of the annual maximum meteo-droughts. The empirical and two theoretical distributions of maximum meteo-drought for Budapest are shown in *Fig. 7*, while the results of the goodness-of-fit tests are given in *Table 5*. Although the binomial distribution is a better fit for the number of exceedances, both combinations yield very similar distributions of the maximum meteo-drought in the growing season. The greatest differences between the binomial-Weibull and Poisson-Weibull models are smaller than 5 years for the return periods.
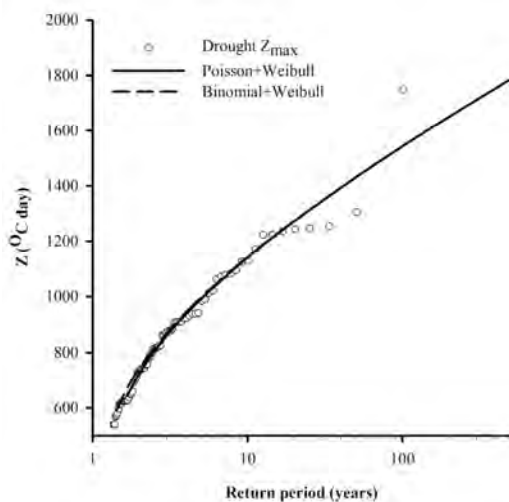
Fig. 7. Distribution of the maximum meteo-drought in the growing season in Budapest

Table 5. Goodness of fit results for the maximum meteo-droughts in the growing season in Budapest

Distribution	Value of the test statistic	Critical region at the 5% significance level
Cramer-von Mieses test		
Poisson+Weibull	$\omega^2 = 0.022$	$\omega^2 > 0.462$
Binomial+Weibull	$\omega^2 = 0.060$	
Kolmogorov-Smirnov test		
Poisson+Weibull	$D = 0.039$	$D > 0.136$
Binomial+Weibull	$D = 0.065$	

514

3.2. Design meteo-droughts

A prerequisite for the construction of design meteo-droughts are the distributions of maximum drought duration (D) and maximum mean air temperature during the drought (T). To obtain these two distributions, the POT method is applied in the same manner as for the meteo-droughts. The adopted threshold for the duration is $D_b = 25$ days, and for the mean air temperature it is $T_b = 9.5$ °C. The binomial-Weibull and the Poisson-Weibull combinations are used as theoretical distributions (*Figs. 8* and *9*). Again, the differences between the two models are negligible.
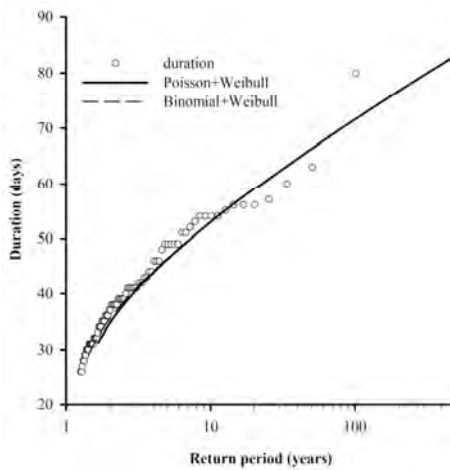
Fig. 8. Distribution of drought duration for droughts longer than 25 days
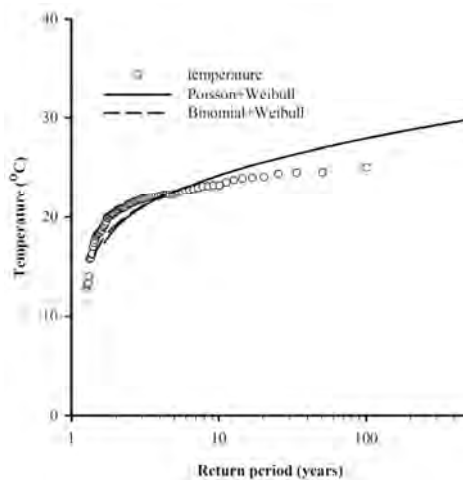
Fig. 9. Distribution of the mean air temperature during droughts longer than 25 days

Finally, the binomial-Weibull distribution combination is adopted for the maximum meteo-droughts, for the maximum drought duration, and for the maximum mean air temperature. As seen in previous figures, differences between the binomial-Weibull and the Poisson-Weibull distribution combinations are minimal. Since the binomial distribution follows the number of exceedances slightly better than the Poisson distribution does, the binomial-Weibull distribution is adopted.

With the adopted theoretical distributions, design meteo-droughts for return periods of 10, 20, 50, and 100 years are determined and presented in *Table 6* as explained in Section 2.4.

Table 6. Synthetic meteo-droughts for Budapest

R (years)	10	20	50	100
D_R (days)	53.0	59.0	66.3	71.6
T_c (°C)	21.6	21.6	21.6	21.5
T_R (°C)	24.3	25.6	27.0	28.0
D_c (days)	47.0	49.7	53.0	55.2
D_d (days)	49.9	54.2	59.3	62.9
T_d (°C)	22.9	23.5	24.1	24.5
Z_R (days°C)	1142.7	1273.1	1430.9	1542.9

In *Table 6*, D_d, T_d, and Z_R denote design drought duration, mean temperature, and their product, respectively; another notation is explained in *Fig. 1*.

Graphical representation of synthetic meteorological drought with a return period of 100 years is shown in *Fig. 10*.
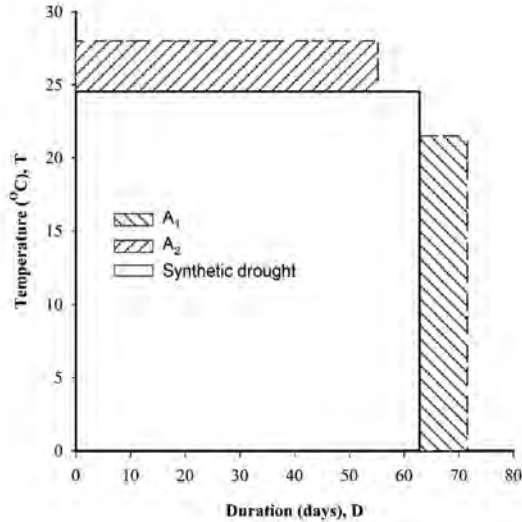
Fig. 10. Synthetic meteo-drought of the 100-year-return period

4. Conclusion

This paper analyzes the phenomenon of occurrence of meteorological droughts during the growing season for a meteorological station in Budapest, with droughts defined as the product of dry period duration and mean air temperature during the drought. The peak-over-threshold (POT) method was applied for estimating the theoretical distributions of the maximum meteorological drought, dry period duration, and the mean air temperature during the drought. This method gives probabilistic estimation of extreme droughts over the growing season, and it is not intended to produce estimations for specific months. The droughts with a duration longer than 25 days are considered and a value of 450 day°C is adopted as a threshold value for meteorological drought. This threshold does not eliminate all droughts from the spring and late summer months, especially those with long duration times, and it is merely a parameter in the final distribution of meteo-droughts.

The results indicate that the POT models combining binomial or Poisson distribution for the number of exceedances with the Weibull distribution for the magnitude of exceedances are the most suitable models for describing this phenomenon for this meteorological station. Based on the adopted theoretical distributions of meteorological droughts, dry period duration and mean air temperatures, synthetic meteorological droughts for return periods of 10, 20, 50, and 100 years are determined. Although the design drought, as the product of

drought duration and mean temperature, can occur under different combinations of two factors, representative design drought duration and mean temperature are also proposed for each return period. Such a formulation of the meteorological droughts can be useful for agricultural management. The methodology can be applied for any choice of the growing season definition and thresholds pertinent for particular crops.

The methodology is demonstrated in this paper with the droughts defined using the precipitation threshold of 5 mm/day. As there is no general definition of droughts and thresholds to be used for definition of the drought, these definitions could be very different depending on the application of the method, e.g., for different crops. We selected this threshold arbitrarily in order to demonstrate the methodology. On the other hand, the methodology focuses on the extreme events, and as such, it deals only with the extreme droughts regardless of the initial threshold used for drought definition.

To get a complete picture of the occurrence and distribution of meteorological drought over a wider region, it is necessary to analyze data from other meteorological stations as well.

References

Blanka, V., Mezősi, G., and *Meyer, B.*, 2013: Projected changes in the drought hazard in Hungary due to climate change. *Időjárás 117*, 219–237.

CLIMATE DATA SERIES / BUDAPEST [WWW Document], Orsz. Meteorológiai Szolg. URL http://owww.met.hu/eghajlat/eghajlati_adatsorok/bp/Navig/201_EN.htm (accessed 6.15.17).

Fabian, Đ., 2015: Stohastička analiza suša u Vojvodini. Građevinski fakultet Subotica, Subotica. (In Serbian)

Fabian, J. and *Zelenhasic, E.,* 2016: Modelling of Meteo-Droughts. *Water Res. Manage. 30*, 3229–3246. https://doi.org/10.1007/s11269-016-1342-6

Gabrić, O., Janjikopanji, Đ., Plavšić, J., and *Fabian, Đ.,* 2017: Statistical Analysis of Meteo-Droughts for Sremska Mitrovica and Kikinda. In: Conference proceedings. Presented at the 5th International Conference Contemporary Achievements in Civil Engineering, Faculty of Civil Engineering Subotica, University of Novi Sad, Subotica, pp. 601–612.

Kiss, A. and *Nikolić, Z.,* 2015: Droughts, Dry Spells and Low Water Levels in Medieval Hungary (and Croatia) I: The Great Droughts of 1362, 1474, 1479, 1494 and 1507. *J. Environ. Geogr. 8.,* 11–22. https://doi.org/10.1515/jengeo-2015-0002

Mishra, A.K. and *Singh, V.P.,* 2010: A review of drought concepts. *J. Hydrol. 391*, 202–216. https://doi.org/10.1016/j.jhydrol.2010.07.012

Plavšić, J., 2007: Flood risk analysis using the discrete stochastic processes (PhD). University of Belgrade, Faculty of Civil Engineering, Belgrade.

Rácz, L., 1999: Climate History of Hungary Since 16th Century: Past, Present and Future. *Discussion Papers 28,* 5–158

Sen, Z., 2015: Applied Drought Modeling, Prediction, and Mitigation. Elsevier, Amsterdam and Oxford.

Sheskin, D., 2004: Handbook of parametric and nonparametric statistical procedures. Chapman & Hall/CRC, Boca Raton. https://doi.org/10.4324/9780203489536

Todorovic, P., 1970: On Some Problems Involving Random Number of Random Variables. *Ann. Math. Stat. 41,* 1059–1063. https://doi.org/10.1214/aoms/1177696981

Todorovic, P. and *Zelenhasic, E.,* 1970: A Stochastic Model for Flood Analysis. *Water Res. Research 6,* 1641–1648. https://doi.org/10.1029/WR006i006p01641

Vukmirović, V. and *Petrović, J.,* 1998: An example of statistical analysis of drought variables, in: FRIEND AMHY Low Flows Expert Meeting. Presented at the FRIEND AMHY Low Flows Expert Meeting, Belgrade, 67–74.

Vukmirović, V. and *Petrović, J.,* 1997: Flood flow analysis using renewal processes, in: UNESCO IHP-V Technical Documents in Hydrology. Presented at the Annual FRIEND-AMHY meeting, 159–169.

Wilhite, D.A., Svoboda, and *M.D.,* 2000: Drought early warning systems in the context of drought preparedness and mitigation. Proceedings of an Expert Group Meeting, Early warning systems for drought preparedness and drought management. 1–16.

IDŐJÁRÁS

The variability and trends of monthly maximum wind speed over Iran

Sohrab Ghaedi

Shahid Chamran University of Ahvaz
Khuzestan province, 6137873397Ahvaz, Iran

Author E-mail: S.ghaedi@scu.ac.ir

Abstract— The maximum wind speed trends over Iran were analyzed based on the data recorded at 49 synoptic stations in Iran, including at least 40 years of data. The regions with maximum winds in Iran are most often seen in the Zagros Mountain. The nonparametric Mann–Kendall test at 95 % level of significance was used to survey whether there is a trend for the maximum wind speed data. Sen's slope estimator was also used to determine the magnitude of the trends. The results reveal that the rate of positive trend is much higher than the negative trend and, in some months, it reaches more than 57% throughout the territory of Iran. Line slope is positive in 86.7% of the country's area. The increasing wind speed can have significant negative impacts on installations and structures, erosion, human health, evapotranspiration, and wind energy.

Key-words: maximum wind, trend, Mann-Kendall test, Sen Slope estimator, Iran

1. Introduction

Climate system is a complex set of elements and factors whose interaction leads to fluctuations or changes in the system. Many studies on climate change have been done on only one of the climatic elements. Many changes, variations, and trends are not the result of one element alone, and are the result of interaction of several climatic elements and factors (*Tuller*; 2004). Wind speed indicates the

impact of different elements influencing one another. Therefore, the study of wind speed trends can reveal climate changes. Wind is not only a reflection of the atmospheric general circulation characteristics, but it is also a source of climatic renewable energy. (*Liu*; 2000).

According to the report of the Intergovernmental Panel on Climate Change (IPCC), global warming has resulted in an increase of natural disasters such as floods, droughts, storms, etc. in the world (*IPCC*; 2014). Storms and maximum winds are among the most devastating natural disasters. Windstorms cause more than half of the economic loss associated with natural disasters in Europe (*Munich*; 2007). *Ulbrich et al*. (2013) believe that windstorms have been the most costly natural hazard in Europe. Long-term variations in near-surface wind speed have a marked impact on a variety of applications including wind energy, building construction, coastal erosion, and evaporation rates, among others (*Troccoli et al.*; 2012). To achieve optimal design balance between safety and design costs, must be accurately estimated extreme wind speeds (*Chiou et al*.; 2012).

Research regarding changes in maximum wind speeds at the national level is important for the sustainable utilization of wind energy and the mitigation of disasters caused by extreme winds. This research is also useful to estimating the cost of electricity generating from wind, wind industry planning and grid maintenance (*Ying et al.*; 2013). In general, the results of studies regarding the trends of winds, maximum winds, gusts, and storms can be classified into three categories. Most of this research indicates a decrease in their trends.

Vautard et al. (2010), using data from 822 weather stations in the northern mid-latitudes, showed that surface wind speeds a drop of between 5% to 15% during a thirty-year period (1979 – 2008). A statistically significant decline was also reported between 1980 and 2005, dropping 5% (equivalent to 0.02 ms^{-1} per year) across the network. Negative trends are similarly found in the PRECIS-Re data in the UK by *Hewston* and *Dorling* (2011). *McVicar et al*. (2012) analyzed 148 studies reporting surface wind speed trends from across the globe, and found that the average trend was –0.014 ms^{-1} for studies with more than 30 sites observing data for more than 30 years. *Ying et al*. (2013) found that the annual and seasonal maximum wind speed, the frequency of gale days, and the wind speed in the troposphere and lower stratosphere declined from 1956 to 2004 (especially in winter) in China. *Azorin-Molina et al*. (2014) analyzed wind speed trends in the Iberian Peninsula and found a slight downward trend for the annual mean wind speed of −0.016 ms^{-1} per decade for 1961–2011 and −0.010 ms^{-1} per decade for 1979–2008. *Baule* and *Shulski* (2014) at several locations in the Beaufort/Chukchi Sea coastal region of the Arctic found negative trends in wind speed at several locations, particularly at locations in Alaska. *Romanic′ et al*. (2015) reported statistically significant negative trends of the Koshava wind speeds and wind activity observed at all five weather stations, which have been more pronounced for wind speeds above 5 ms^{-1}. *Brazdil et al*. (2016) surveyed the variability of maximum wind gusts in the Czech Republic and found statistically

significant decreases (deepest in November and in autumn), with the exception of spring (for stations above 300 m) and summer. *Minola et al.* (2016) studied near-surface wind speed trends in Sweden and found downward trends of −0.06 and −0.14 ms^{-1} per decade for annual mean wind speed of periods 1956–2013 and 1979–2008, respectively. *Laapas* and *Venalainen* (2017) found a negative trend in the analysis of monthly mean and maximum wind speed time series in Finland during 57 years.

Other have achieved positive and negative trends in the regions in their studies.

Yan et al. (2002) found an increasing trend of 0.2 ms^{-1} per decade, which had prevailed over the ocean, in contrast to a decreasing trend of -0/1 m s^{-1} per decade prevailing over continental Europe in summer. *Bronnimann et al.* (2012) studied extreme winds at northern mid-latitudes since 1871, and noticed that the annual 98th percentile of wind speed exhibits changes towards more extreme winds in the North Atlantic storm track region (or a pole-ward shift), decreasing wind extremes over the northern subtropics (especially China), and an equator-ward shift of the Pacific storm track. *Klink* (2015) analyzed seasonal patterns and trends of the fastest 2-min winds at coastal stations in the conterminous USA and concluded, there were positive trends in winter, spring, and summer, while negative trends are frequent in autumn.

Some studies indicate an increase in their trends: *Kruger et al.* (2010) surveyed 94 weather stations in South Africa and reported average annual maximum wind gusts having increased by +0.09 ms^{-1} in a decade. In Switzerland, *Usbeck et al.* (2010) estimated the increase of maximum gust wind speeds and severe winter storm damages in both amount and frequency from 1858 to 2007. *Fujii* (2007) found in Japan that 10 min mean wind speed greater than 20ms^{-1} increased 1.5-fold from 1976–1985 to 1996–2005. He also reported the incidence of wind speed greater than 35 ms^{-1}.

As to the variability of wind speeds, several explanations have been given including decreases in horizontal atmospheric pressure gradients (*Guo et al.*; 2010), increased surface roughness surrounding the observed sites (*Vautard et al.;* 2010), natural climatic variability (*Pirazzolli* and *Tomasin*; 2003), time period chosen for analysis (*Troccoli et al.;* 2012), and influences of changes in the observing instrumentation/firmware (*Pryor et al.;* 2009).

The aim of this paper is to present a comprehensive analysis of monthly and annual maximum wind peak trend in Iran based on instrumental measurements with respect to their spatiotemporal trends.

2. Data and methodology

Iran is located in the southwestern of Asia (25–39°N, 44–63 °E) and consists most of the Iranian Plateau. Persian Gulf and the Oman Sea are situated in the southern

of Iran and the Caspian Sea in the north (Fig. 1). This country is one of the world's most mountainous countries, with its landscape dominated by rugged mountain ranges and populous western and northern part is the most mountainous, with ranges such as the Zagros and the Alborz Mountains (*Rahimzadeh et al.,* 2011).
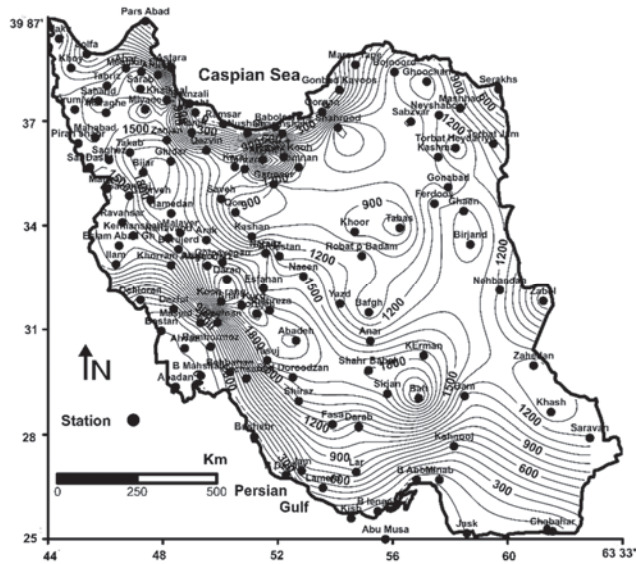
Fig. 1. Position and elevation of stations

The monthly maximum wind speed is the highest wind speed observed in the period of every month, and is measured for every station, along with the associated month of occurrence. The first few Iranian meteorological stations have been launched since 1951. Although the number of stations has gradually increased during the time, the statistical period in many of them is short, thus reducing the accuracy of the trend statements. In this study, the researcher observed wind speeds measured at the standard 10-meter height at 49 stations across Iran run by the meteorological organization in the variability period of 1951–2015. Therefore, the selected stations had a history of at least 40 years of data.

Since the data from the stations represent points rather than areas, the simple Kriging interpolation method is used to generalize point data to the area. There are several methods for interpolation among which Kriging is one of the most commonly used method in climatology (*Cellura*, 2008; *Li et al.,* 2016). The Kriging method provides the best unbiased linear estimation which the weights of the sample values is estimated based on the variogram model. (*Moral*, 2010).

2.1. Classification and zoning of maximum wind

A cluster analysis on annual average of maximum wind showed that Iran can be classified into four regions. The value of maximum wind average varies between 8 and 20.77 ms^{-1}. A discontinuous strip from the northwest to the southeast, located on the Zagros Mountains, and an area in the northeast show the severest maximum winds. The lowest wind speed was observed in a discontinuous strip from the southwest to the southeast and on a relatively extensive region in the northeast. *Fig. 2* represents the classification of annual average of maximum winds over Iran.
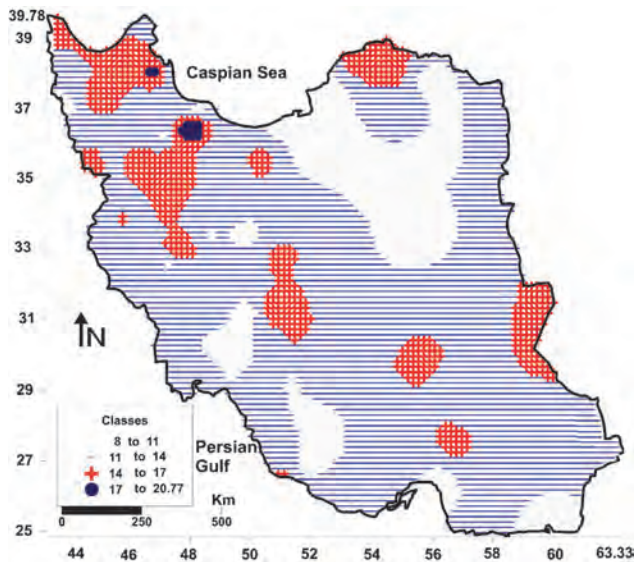
Fig. 2. Classification of annual average of maximum winds over Iran.

2.2. Monthly trends

Table 1 represents the areas with their percentage of the monthly and annual maximum wind speed trends. According to these values, the trend of the maximum wind speed over Iran is seen in all conditions: neutral, positive, and negative. The most frequent case is related to no trend situation, which varies in percentage from 42.3 (May) to 85.2 (December). The percentage of areas with negative trends in most months is very low, with the highest ones in June and July, and even in January, March, April, September, November, and December there is no point with a negative trend. The area with a positive trend is much higher than negative. This is observed in many areas of the country with a monthly average

of about 38.3%. Annual average shows that in more than half of Iran's territory, the maximum wind speed is incremental. The highest ones are observed from May to August and the lowest trends are seen from September to February. Spreading of the area with positive trend in the warm months shows that either the gradient of pressure in these months is increased or the amount of roughness is decreased.

Table 1. Percentage of areas with monthly and annual maximum wind speed trends

	Jan	Feb	Mar	Apr	May	Jun	Jul	Aug	Sep	Oct	Nov	Dec	Ann
Negative trend	0.0	0.1	0.0	0.0	0.2	1.2	1.8	0.7	0.0	0.3	0.0	0.0	0.9
No trend	83.0	69.0	57.0	47.8	42.3	46.0	61.2	49.1	65.0	65.4	65.0	85.2	41.0
Positive trend	17.0	30.9	43.0	52.2	57.5	52.8	37.0	50.2	35.0	34.3	35.0	14.8	58.1

Fig. 3 presents the spatial distribution of monthly maximum wind speed in the territory of Iran. "Red plus" and "blue line" symbols have been used to show positive and negative trends, respectively. According to *Table 1*, the trend is positive in 17% of the area of Iran in January. Discontinuous regions of Zagros and Alborz Mountains, the southern coasts of the Caspian Sea, and the central, northeastern, and eastern regions of the country show a positive trend. In this month there is no negative trend in any part of the country. In February, the magnitude of the positive trend and the extent of the regions with a negative trend is increased. During this month, in addition to the regions that showed positive trends in January, other areas in the northwest and Jask also show a positive trend, while negative trend can be seen only in the northwest. The positive trend increases dramatically in March and covers about 43% of the territory of Iran. This is due to the increasing positive trend in the northwest and the center. Like in January, negative trend can't be observed at any station. In April, the areas with a positive trend are increased, but this increase has been in the central and eastern regions. Northwestern areas have experienced a decrease. The extent of the regions with a negative trend is lower than 1% in the central region of the country. The highest positive trend is related to May. Exactly in this month, there is an area with a negative trend in the southeast. After May, the area of the positive trend gradually decreases until it falls to the lowest value in December. Of course, this decline is in the negative trend and the area of regions without trend is incremental. An increase in the negative trend was seen only in the southeast and a 4.7% decrease in the positive trend along with slight changes in the regions is the difference between June and May. The highest negative trend area is related to July (1.8%), but the extent of positive trend has decreased. In August, limited

areas in the center show a negative trend, and a slight positive trend increase is observed compared to the previous month. No region in the country shows a negative trend in September. In this month, two long strips from the southwest and west parts of the country to the northeast and north, and regions in the east show a positive trend. In October, a positive trend is observed in more scattered areas, compared to September, in areas of Zagros, Alborz, northern and central parts of the country. A negative trend covering limited areas in the southeast. Long strips in around of Iran from southwest to east, north, and northwest regions, and a part in the central area of Zagros are observed with a positive trend in November. The minimum positive trend area is related to December, which is seen in scattered regions of the Zagros Mountain, southern Caspian, the northeastern and the eastern parts of the country. Also, not any part of the country show a negative trend in this month.

Overall, from January to May, the extent of the positive trend is increased and then from May to December, it is gradually decreased.
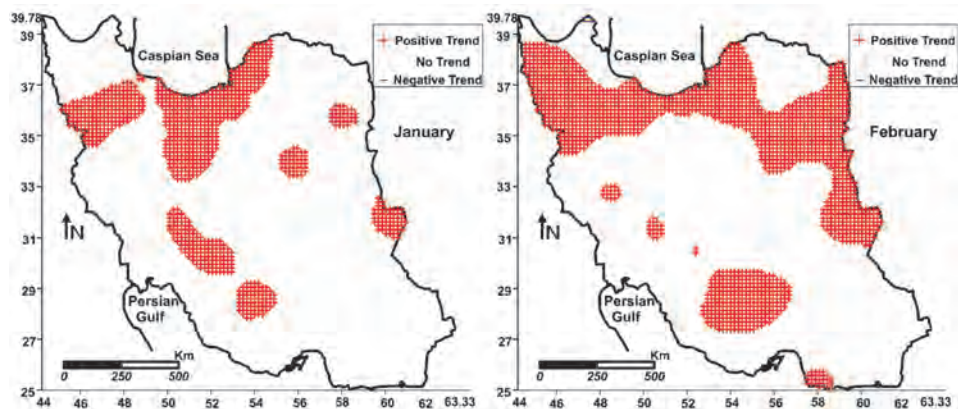
Fig. 3. Spatial distribution of monthly maximum wind speed trends over Iran during the studied period.
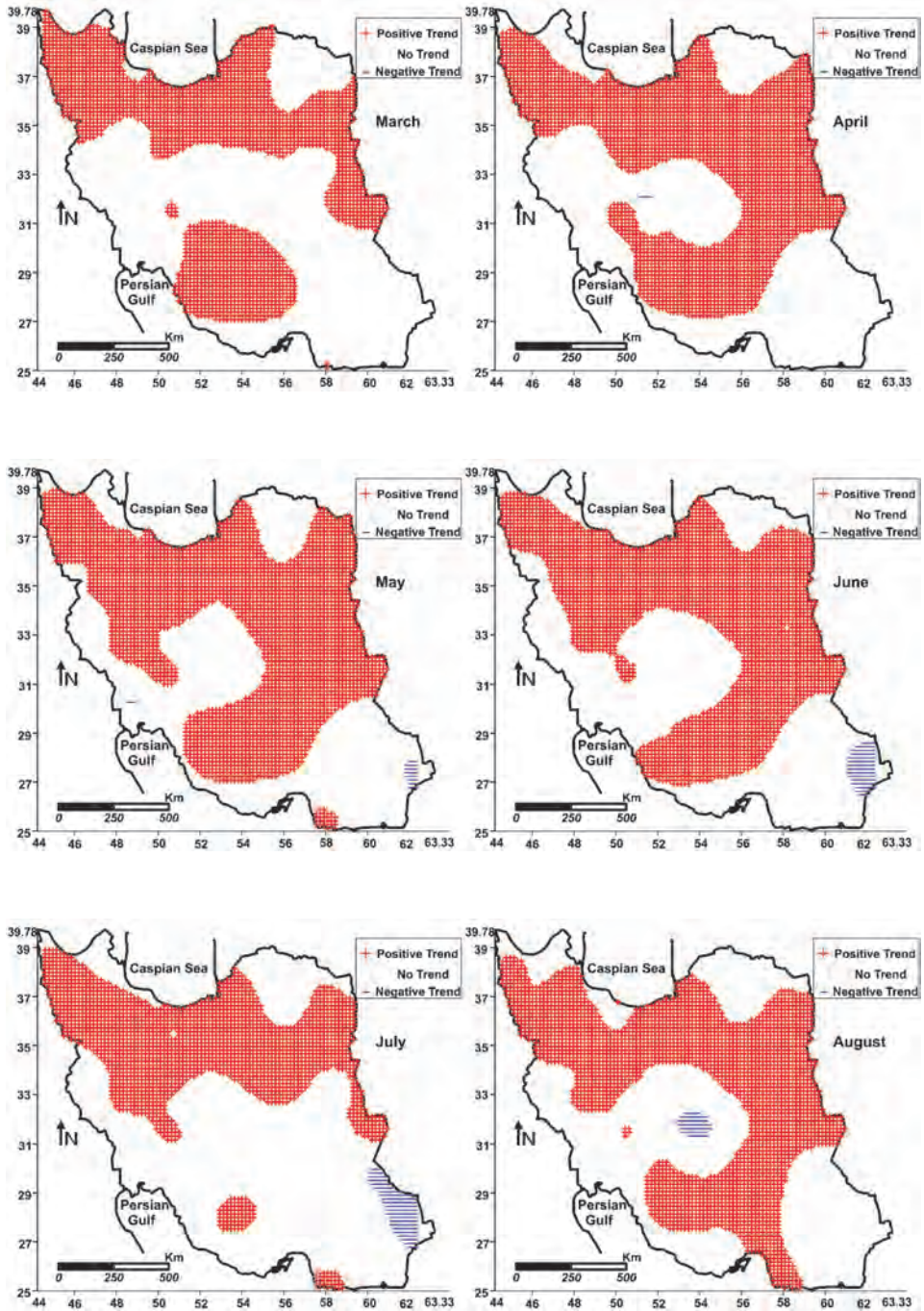
Fig. 3.(continued)
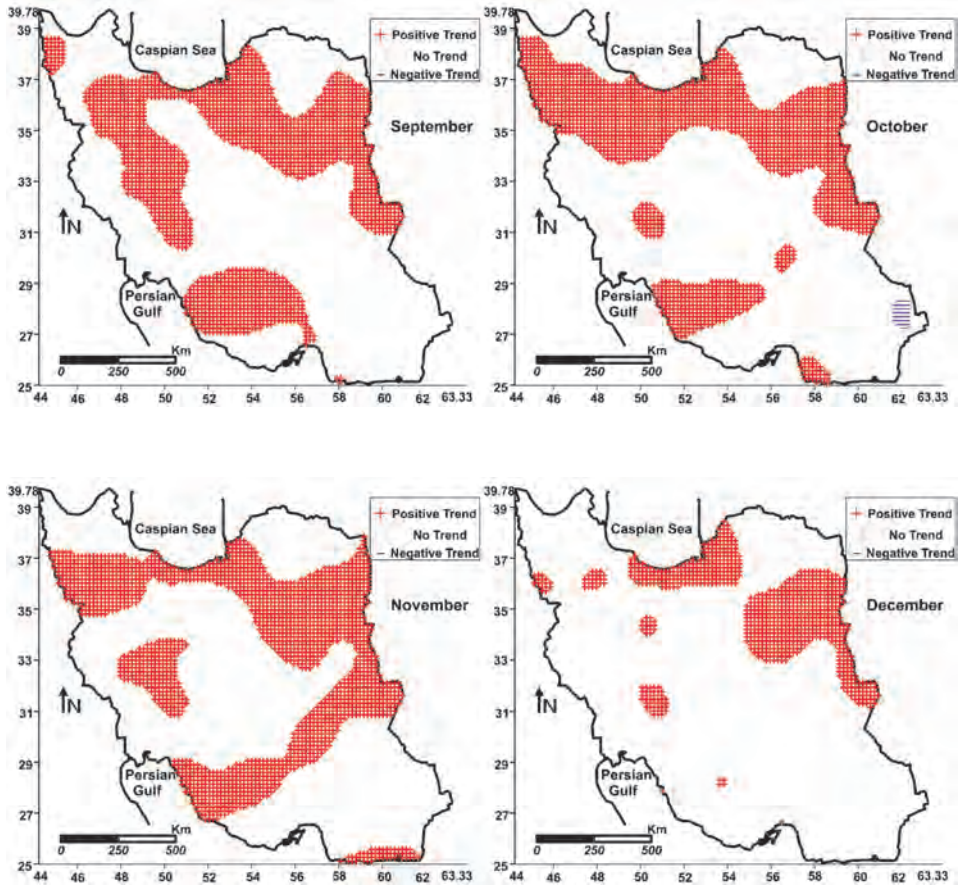
Fig. 3. (continued)

Fig. 4 shows the annual trend of the maximum wind speed and the elevation contours of the stations. 58.1% and 0.9% of the area of the country are associated with positive and negative trends, respectively. The area with the highest positive trend is seen in the continuous regions from south to north with an area in the center, around which there is no trend. Negative trends are located in the southeastern and central parts of the country. Positive and negative trends do not match with specific elevations. Therefore, the trends do not follow the elevation contours, and the positive trends include regions from lower than zero to higher than 2500 m regions with positive trend including more than half of the country except for regions in the center, southwest to west, south, southeast, and northeast. Negative trends are seen in the southeast and central regions of the country.
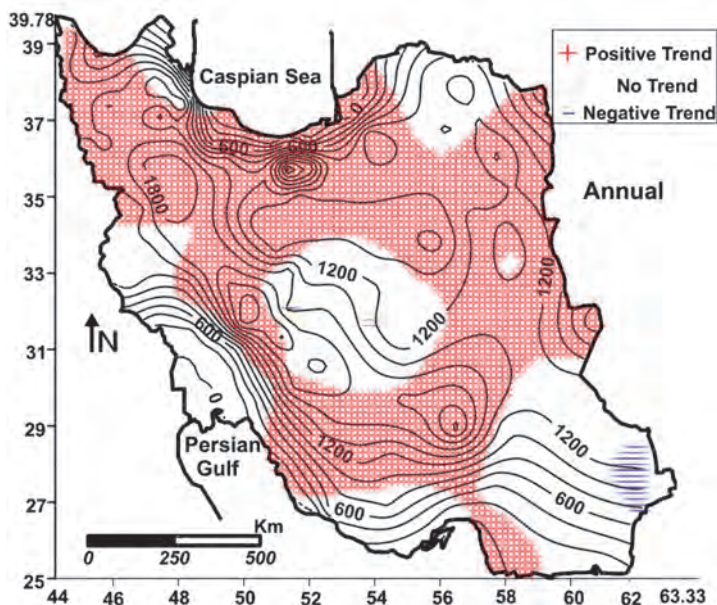
Fig. 4. Spatial distribution of annual maximum wind speed trends over Iran during the studied period.

In so far as the Mann-Kendall test can only identify trends and their directions in which the line slope is not known, the Sen Slope estimator was used to calculate the line slope. The line slope of the maximum annual wind speed is presented in *Table 2*. Positive and negative slopes were seen in 86.7% and 13.3% of the areas in the country, respectively. Negative slope regions are located as scattered points in the center and the corners of the country. The most extensive regions with a negative slope are seen in the southeast and southwest areas. The highest positive slope is related to Zabul station (in the eastern part of the country, Sistan and Baluchestan province) by 0.155 in each year, and the highest negative slope is related to the Kish station (in the southern part of the country, an Island in the Persian Gulf) by –0.035 in each year. The pressure gradient between the altitudes in the northeastern part of Iran and the low pressure of Pakistan cause the 120-day wind in Sistan. This wind blow during June to September. Zabul is located in the direction of these severe seasonal winds. Kish is one of the most important tourism island of Iran which located in the Persian Gulf. The decreasing of wind speed show that pressure gradient has decreased between this island and the surrounding regions (*Fig. 5*).

530
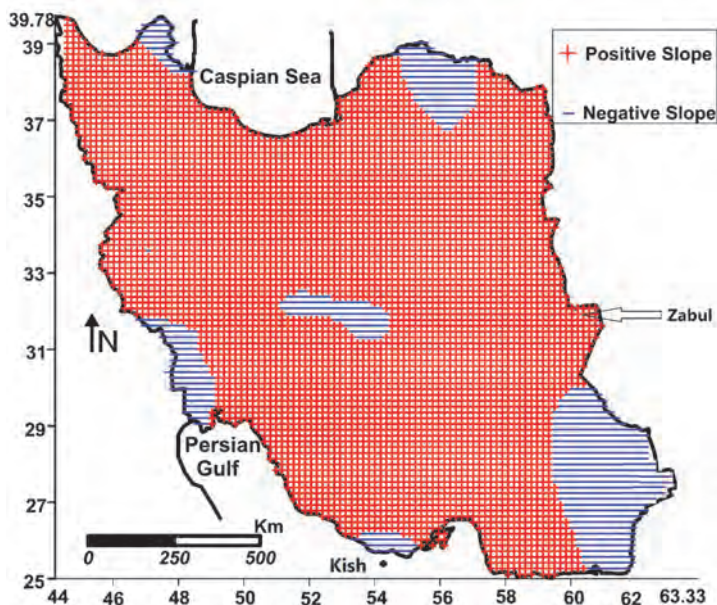
Fig. 5. Spatial distribution of annual maximum wind speed slope line over Iran during the studied period.

Table 2. Statistics from stations with the highest positive and negative line slopes

Station	Mean slope	Min 99%	Max 99%	Min 95%	Max 95%	beta
Zabul	0.155	0.096	0.208	0.112	0.192	2.7816
Kish	-0.035	-0.103	0.029	-0.087	0.009	2.8038

3. Conclusion

Global warming and climate change have caused disturbances in the planet's systems such as increasing maximum winds, storms, and gusts. The increasing maximum winds and gusts can increase losses to human. The value of maximum wind average varies between 8 to 20.77 ms^{-1} in different parts of Iran. The lowest wind speed is observed in the southern and southeastern parts of the country and

the highest is observed in Manjil and Ardebil (more than 17 ms^{-1}). This is true for the discontinuous parts of the Zagros Mountain as a belt extending from northwest to southeast, and a relatively small region in the east of the Caspian Sea. The investigation of monthly and annual maximum wind speeds indicates that all the three states of positive, negative, and no trend can be seen in Iran. The most prevalent state is related to no trend, which changes between 42.3% (annual) and 85.2% (December). The percentage of the area with positive trend changes between 57.5% (annual) and 14.8% (December). The area with negative trend is very insignificant (less than 2%). The line slope of the annual maximum winds is presented in *Table 2*. Positive and negative slopes are seen in 86.7% and 13.3% of the areas of the country. Negative slope regions are located as scattered points in the center and the corners of country. The most extensive regions with a negative slope are seen in the southeastern and southwestern parts of the country.

Any effective factor on pressure gradient and roughness can change the speed of winds and gusts. Drying of the country's water areas, including lakes and lagoons, has increased the temperature in these areas and has increased their pressure gradient with regions surrounding them (like the Urmia Lake and the Bakhtegan Lake). Destruction of forests in the Zagros Mountain and in the northern part of the country has led to decreasing the roughness, and the result is an increase in the wind speed. On the other hand, the temperature increase in the high pressure regions has led to a decrease in the pressure gradient as well as in the wind speed (southeastern area). In the centra and eastern regions, the occurrence of dust has decreased the wind speed. Broadly speaking, there are different reasons for each region in Iran due to specific environmental conditions. These cases of increased maximum wind speed have strong negative impacts on installations and structures, erosion, human health, evapotranspiration, and wind energy, therefore, necessary measures are obligatory to be taken to reduce the negative consequences.

References

Azorin-Molina, C,. Vicente-Serrano S. M., McVicar T. R., Jerez S., Sanchez-Lorenzo A., López-Moreno J. I., Revuelto J., Trigo R. M., Lopez-Bustins J. A., and Espirito-Santo F., 2014: Homogenization and Assessment of Observed Near-Surface Wind Speed Trends over Spain and Portugal, 1961–2011. J. climate 27, 3692–3712. https://doi.org/10.1175/JCLI-D-13-00652.1

Baule, W.J. and Shulski, M.D., 2014: Climatology and trends of wind speed in the Beaufort/Chukchi Sea coastal region from 1979 to 2009. Int. J. Climatol. 34, 2819–2833. https://doi.org/10.1002/joc.3881

Brazdil, R., Hostynek, J., Reznickova, L.R., Zahradnicek, P., and Tolasz, R., 2016: The variability of maximum wind gusts in the Czech Republic between 1961 and 2016. Int. J. Climatol 37, 1961–1978, https://doi.org/10.1002/joc.4827

Bronnimann, S., Martius, O., von Waldow, H, Welker C, Luterbacher, J, Compo, G.P., Sardesmukh, P.D., and Usbeck, T., 2012: Extreme winds at northern mid-latitudes since 1871. Meteorol. Z. 21, 13–27. https://doi.org/10.1127/0941-2948/2012/0337

Cellura, M., Cirrincione, G., Marvuglia, A., and Miraoui A., 2008: Wind speed spatial estimation for energy planning in Sicily: Introduction and statistical analysis, *Renew. Energy. 33,* 1237–1250. https://doi.org/10.1016/j.renene.2007.08.012

Chiou, P., Miao, W., and Ho, T.C., 2012: The Annual Maximum Wind Speed at Pisa Airport in Italy, *Int. J. Environ. Sci. Develop. 3,* 258–262. https://doi.org/10.7763/IJESD.2012.V3.227

Fujii, T., 2007: On geographical distributions and decadal changes of the annual maximum wind speeds caused by typhoons in Japan. *J. Nat. Disaster Sci. 26,* 267–277 (in Japanese with an English abstract).

Guo, H., Xu, M., and Hu, Q., 2010: Changes in near-surface wind speed in China: 1965–2005. *Int. J. Climatol. 31,* 349–358. https://doi.org/10.1002/joc.2091

Hewston, R. and Dorling, S.R., 2011: An analysis of observed daily maximum wind gusts in the UK. *J. Wind Eng. Ind. Aerodyn. 99*, 845–856. https://doi.org/10.1016/j.jweia.2011.06.004

IPCC, 2014: Synthesis report. Contribution of working groups I, II and III to the Fifth Assessment Report of the Intergovernmental Panel on Climate Change [Core Writing Team, R.K. Pachauri and L.A. Meyer (Eds.)]. IPCC Geneva Switzerland.

Klink K., 2015: Seasonal patterns and trends of fastest 2-min winds at coastal stations in the conterminous USA. *Int. J. Climatol. 35,* 4167–4175. https://doi.org/10.1002/joc.4275

Kruger, A.C., Goliger, A.M., Retief, J.V., and Sekele, S., 2010: Strong wind climatic zones in South Africa. *Wind Struct.13*, 37–55. https://doi.org/10.12989/was.2010.13.1.037

Laapas, M. and Venalainen, A., 2017: Homogenization and trend analysis of monthly mean and maximum wind speed time series in Finland. 1959–2015. *Int. J. Climatol. 37*, 4803–4813. https://doi.org/10.1002/joc.5124

Li, X., Meshgi, A., and Babovic, V., 2016: Spatio-temporal variation of wet and dry spell characteristics of tropical precipitation in Singapore and its association with ENSO. *Int. J. Climatol. 36*, 4831–4846. https://doi.org/10.1002/joc.4672

Liu, X.N., 2000: The homogeneity test on mean annual wind speed over China. *J. Appl. Meteorol. Sci. 11*, 27–34. (In Chinese).

McVicar, T.M ., Roderick, M.L. Donohue, R.J. Li, L.T. Van Niel, T.G. Thomas, A. Grieser, J. Jhajharia, D. Himri, Y. Mahowald, N.M. Mescherskaya, A.V. Kruger, A.C. Rehman, S., and Dinpashoh, Y., 2012: Global review and synthesis of trends in observed terrestrial near-surface wind speeds: Implications for evaporation. *J. Hydrol. 416–417*, 182–205. https://doi.org/10.1016/j.jhydrol.2011.10.024

Minola, L., Azorin-Molina, C., and Chen, D., 2016: Homogenization and assessment of observed near-surface wind speed trends across Sweden. 1956–2013. *J. Climate 29,* 7397–7415. https://doi.org/10.1175/JCLI-D-15-0636.1

Moral, F.J., 2010: Comparison of different geostatistical approaches to map climate variables: application to precipitation. *Int. J. Climatol. 304*, 620–631. https://doi.org/10.1002/joc.1913

Munich, R.E., 2007: Zwischen Hoch und Tief — Wetterrisiken in Mitteleuropa, Edition Wissen. Publication of the Munich Re, Order Number, 302-05481, www.munichre.com (In German)

Pirazzolli, P.A. and Tomasin, A., 2003: Recent near-surface wind changes in the central Mediterranean and Adriatic areas. *Int. J. Climatol.238,* 963–973. https://doi.org/10.1002/joc.925

Pryor, S.C., Barthelmie, R.J., Young, D.T., Takle, E.S., Arritt, R.W., Flory, D., Gutowski, W.J, Nunes, A., and Roads, J., 2009: Wind speed trends over the contiguous United States. *J. Geophys. Res. Atmosphere 114* D14. https://doi.org/10.1029/2008JD011416

Rahimzadeh, F., Noorian, A.M., Pedrama, B.M., and Michael, C.K., 2011: Wind speed variability over Iran and its impact on wind power potential: a case study for Esfahan Province. *Meteorol. Appl. 182,* 198–210. https://doi.org/10.1002/met.229

Romanic, D.C., uric, M., Jovicic, I., and Lompar, M., 2015: Long-term trends of the 'Koshava' wind during the period 1949–2010. *International J. Climatol. 352*, 288–302. https://doi.org/10.1002/joc.3981

Troccoli, A., Muller, K., Coppin, p., Davy, R., Russell, C., and Hirsch, A.l., 2012: Long-term wind speed trends over Australia. *J. Climate 25*, 171–184. https://doi.org/10.1175/2011JCLI4198.1

Tuller, S.E., 2004: Measured wind speed trends on the west coast of Canada. *Int. J. Climatol. 24,* 1359–1374. https://doi.org/10.1002/joc.1073

Ulbrich, U., Leckebusch, G.C., and *Donat, M.G.,* 2013: Windstorms, the most costly natural hazard in Europe. Natural Disasters and Adaptation to Climate Change.. Cambridge University Press: Cambridge. UK.

Usbeck, T., Wohlgemuth, T., Dobbertin, M., Pfister, C., Burgi, A., and *Rebetez, M.*, 2010: Increasing storm damage to forests in Switzerland from 1858 to 2007. *Agric. Forest Meteorol.150*, 47–55. https://doi.org/10.1016/j.agrformet.2009.08.010

Vautard, R., Cattiaux, J., Yiou, P., Th´epaut, J.N., and *Ciais, P.,* 2010: Northern Hemisphere atmospheric stilling partly attributed to an increase in surface roughness. *Nat. Geosci. 3,* 756– 761. https://doi.org/10.1038/ngeo979

Yan Z., Bate S., Chandler R E., Isham V., and *Wheater H.,* 2002: An Analysis of Daily Maximum Wind Speed in Northwestern Europe Using Generalized Linear Models. *J. Climate 15,* 2073–2087. https://doi.org/10.1175/1520-0442(2002)015<2073:AAODMW>2.0.CO;2

Ying, J., Yong, L., and *Zongci, Z.*, 2013: Maximum wind speed changes over China. *Acta Meteorology Sinica, 27*, 63–74. https://doi.org/10.1007/s13351-013-01

IDŐJÁRÁS

Hydrological role of Central European forests in changing climate –review

Zoltán Gribovszki, **Péter Kalicz**, **Michael Palocz-Andresen***, **Dóra Szalay**, and **Tünde Varga**

University of Sopron
Bajcsy-Zs. u. 4, 9400 Sopron, Hungary

*Corresponding Author E-mail: palocz-andresen.michael@uni-sopron.hu

Abstract— Climate change exerts one of the most relevant impacts on hydrological processes by altering precipitation patterns and evapotranspiration processes. Forests, the terrestrial ecosystems with the highest water demand, will likely be the most influenced by the changing water regime. The study aims to outline the vital role forests play in the global water cycle, a role that increases as climate change intensifies. The deforestation that has occurred in recent years is a main trigger of global climate change, one that negatively affects climate-sensitive areas. The study focuses on the importance of crown and litter interception as well as the manner in which climate change alters these. We also present some results for forest and groundwater relations in Hungary and the impact of forests on runoff during extreme weather conditions.

Key-words: forest hydrology, climate change, interception, groundwater, runoff

1. Introduction

Forest vegetation currently covers 37% of global land surface and is known for its high carbon-absorbing capacity. Nevertheless, recent practices – primarily changes in land use – have accelerated deforestation considerably with forest cover loss reaching 29.7 million hectares (73.4 million acres) globally in 2016 (*Weisse* and *Goldman*, 2017). Agricultural land expansion causes about 80% of

forest cover loss, while industrial activity accounts for the remainder 20% (*UNFCCC*, 2007). This forest loss is one of the driving factors behind climate change, contributing as much as 10 to 30% to global greenhouse gas emissions each year (*Johnson*, 2009; *RA*, 2017; *Schrope*, 2009). The changing climate causes a feedback loop and negatively impacts climate-sensitive areas, especially forests (*Szép*, 2010).

In addition, forests possess many additional features that intensively affect the climate and the water cycle. The characteristics of precipitation transformed by forest vegetation greatly influence the amount of water available for runoff and recharge, but also influence concentration time, as in the case of flood wave formation processes. Forests generally reduce the negative impacts of floods as water drainage in undisturbed forest-covered areas tends to be of high quality (*Baird* and *Wilby*, 1999).

Researching hydrological behavior in an ecosystem with such a significant influence on water circulation is also important in assessing climate change effects, because the quantity and quality of available water resources will become a bottleneck in the future.

The main objective of this paper is to summarize relevant research results in forest hydrology and climate change, focusing specifically on water-related problems in Hungary. Special emphasis is put on the analysis of interception and groundwater relations of the forests.

2. Forest hydrology

A portion of the rain that falls onto a forested area simply moistens the vegetation and then evaporates back into the atmosphere. This is called interception (crown interception), which is usually divided into two parts: storage capacity and evaporation during the precipitation event. Some precipitation makes its through the crown or flows down stem and reaches the forest litter surface on the ground, where it remains, filling the storage capacity of the forest floor. This is known as litter interception. The remaining water infiltrates into the forest soil and contributes to subsurface water reservoirs. Precipitation that does not completely infiltrate the soil creates surface runoff; see *Fig. 1*.
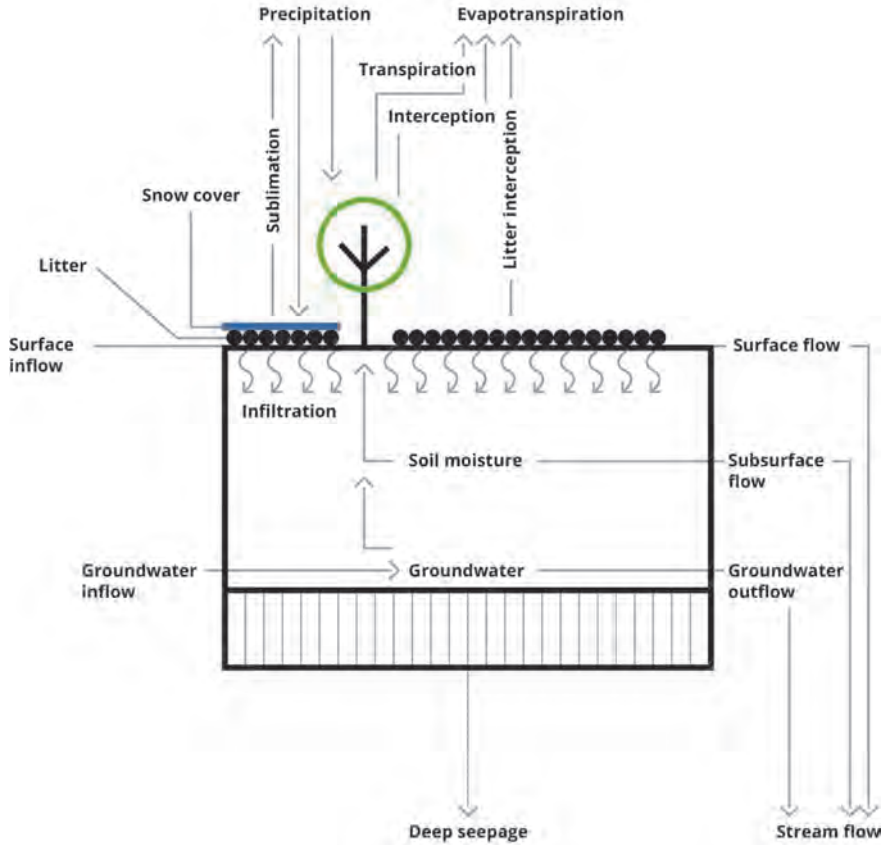
Fig. 1. Water balance of the forest.

The water balance of the forest can be characterized by considering the quantities of incoming, used, temporarily stored, and exiting water:

$$P + p + Rin_{s,gw} - I - T - Rout_{s,gw} = dS, \qquad (1)$$

where P is the liquid and the solid macro precipitation (measurable by normal Helman-type ombrometer like rain and snow); p is the liquid and the solid micro precipitation (like dew, frost, rime, and mist precipitation [fog drip]); $Rin_{s,gw}$ is the inflow (surface and subsurface); dS is the storage change of water in the area; I is the interception (crown and ground litter); T is the transpiration from the vadose zone and groundwater; and $R_{s,gw}$ is the outflow (surface and subsurface).

2.1. Effects of forests on the amount of macro and micro precipitation

Forests receive the largest amount of water intake from macro precipitation. Its varying volume and distribution due to climate change significantly impacts the biological production and structure of typical forest types. The modifying effect of forests on macro precipitation is quite disputed (*Rácz*, 1981).

The micro-precipitating effect of the forest can be significant, especially in mountainous terrains, where mist precipitation (fog drip) and rime can lead to horizontal precipitation. This effect translates into about 30% of the macro precipitation depending on forest stand characteristics. This value can be 1–3 times higher in mountainous areas than it is in lowland areas. This effect happens in the Hungarian Great Plain during the winter and reduces interception loss (*Szőnyi*, 1966, 1967; *Hazslinszky*, 1976).

2.2. Kinds of interception and their relation to climate change

As stated earlier, one part of the precipitation remains in the crown and evaporates, while another, perhaps seemingly insignificant part, is absorbed by leaves. This temporarily stored and quickly evaporating precipitation amount is called interception (*Delfs*, 1955). The interception loss usually varies between 10% and 40% depending on the forest ecosystem (*Dingman*, 2001); it is a vital factor and the first stage in the hydrological cycle of forests (*Savenije*, 2004).

Normally, interception means crown interception. However, total interception loss (I) is the sum loss of crown interception (E_{su}) and litter interception (E_s):

$$I = E_{su} + E_s. \tag{2}$$

Whether interception loss plays an additional or substitutional role or not is an open question currently. In the dormant period, interception is an incoming factor of evaporation. In the vegetation period, interception evaporation has an advantage over transpiration because stomatal resistance does not regulate interception evaporation; thus, transpiration continues at a lower level. According to the latest research, interceptive evaporation is many times higher than the rate of transpiration, but replaces transpiration only for short periods (*Dingman*, 2001). Interceptive evaporation is around three times higher (*Stewart*, 1977) than the transpiration rate under the same conditions.

Negative interception is possible under certain, specific circumstances. In these cases, forests can adsorb humidity from the air. This process is known as condensed horizontal precipitation, which may reach 30% of precipitation depending on tree stand characteristics. This phenomenon mainly occurs at forest edges, and its importance decreases further into the internal areas of the forest. In

some places, the condensed horizontal precipitation significantly reduces the interception loss (*Rácz*, 1981; *Ward* and *Robinson*, 1975).

Snow interception loss is one of the least known factors in the water balance equation of forests. Research in coniferous forests has estimated that interception loss may reach 20–50% of precipitation. The storage of snow (both the mass and the duration of the storage) is ten times higher than it is for rain. However, most hydrological models treat snow interception in a rather simplified form (*Lundberg* and *Halldin*, 2001).

2.2.1. Crown interception

The difference between crown interceptions of different forest stands in Hungary can be summarized as follows (*Járó*, 1980):

– The average interception of coniferous forests is 5% higher than the interception of deciduous forests.

– Crown precipitation retention amounts to 1/3 of the precipitation on average, usually along the dry forest edge, in typical climatic conditions in Hungary.

– The precipitation retention level of forest stands with a multi-layered canopy is higher than those of with one-layer canopy.

Considering the different crown interception losses (*Table 1*) the changes in interception show a growing tendency depending on the age of the stands (*Járó*, 1980). Subsequently, higher interception losses must be considered by the same canopy closure in the older stands because of the growing evaporation surface.

Precipitation distribution also influences the amount of interception. Years involving the same annual precipitation amounts may have fewer large precipitation events; this reduction of rainy days decreases the sum of annual interception. Using a daily time-step interception model, *Kalicz et al.* (2017) compared the present and future interception totals of a beech forest in the Sopron Hills and projected, that the current 30% crown interception level would decline to 27–28% by the end of the twenty-first century.

Table 1. Results of interception studies on Hungarian forests (interception expressed as a percentage of the annual precipitation)

Forest type	Interception [%]	Source
Turkey oak – Sessile oak	22.3	*Szabó* (1979)
Sessile oak	25	*Führer* (1984)
Hybrid poplar clones	25	
Hornbeam –Turkey oak	27	
Turkey oak	27.5	*Járó* (1980)
Linden	28	
Hybrid poplar clones	29	
Black locust (young)	30	
Beech (young)	30.9	*Kucsara* (1998)
Black locust (old)	31	*Járó* (1980)
Northern red oak	33	
Beech (unmanaged)	39.7	*Koloszár* (1981)
Larch	34	
Scots pine (young)	35	*Járó* (1980)
Balck pine (young)	36	
Scots pine (old)	37	
Spruce (old)	37	*Führer* (1984)
Eastern white pine	36	
Hornbeam-Scots pine	37	*Járó* (1980)
Douglas fir	38	
Black pine (old)	39	
Spruce (young)	41.6	*Kucsara* (1998)
Spruce (middle age)	40.5	*Kucsara* (1998)
Beech (managed)	47 28 29.7	*Járó* (1980) *Führer* (1984) *Koloszár* (1981)

2.2.2. Litter interception

Litter cover significantly influences the root zone water balance by retaining precipitation, thereby preventing it from entering the root zone and potentially reducing the amount of absorbable water. At the same time, litter also prevents the drying of the soil.

Litter positively influences the root zone water balance during decomposition. *Table 2* contains some representative data for the amount of litter interception collected from different climate regimes and forest stands.

Table 2. Litter interception in different forest stands as a percentage of the annual precipitation

Forest type	Litter interception [%]	Region	Source
	1–5%	Eastern United States	*Helvey* and *Patric* (1965)
Deciduous	2-5% in the summer time and 3.5% in the winter time	Eastern United States	*Helvey* and *Patric* (1965)
Sessile oak	5–7%	Sopron, Hungary	*Zagyvainé et al.* (2014)
Sessile oak	8% in the summer time and 16% in the winter time	Hungary	*Führer* (1994)
Mixed oak	8–12%	Himalayas	*Pathak et al.* (1985)
Beech	34%	Western Europe	*Gerrits et al.* (2006)

Litter interception of 1–5% of annual rainfall has been detected in the United States. In the eastern part of United States, this loss generally does not exceed the limit of 50 mm/year. For deciduous species, litter interception is 2–5% of the precipitation in summer and 3.5% in winter (*Helvey* and *Patric*, 1965). For coniferous species, litter interception losses increase from 2% to 4% in aging stands that are between 10 and 60 years old (*Helvey*, 1967).

Studies in other climatic conditions show a higher value of litter interception than previously mentioned. The litter interception of sessile oak forest stands is 5–7% of the annual precipitation in the western part of Hungary (*Zagyvainé et al.*, 2014). In the Himalaya region, 8–12% of the throughfall precipitation was detected in mixed oak forest (*Pathak et al.*, 1985). One of the greatest litter interception values (34%) was measured as a western European beech forest (*Gerrits et al.*, 2006). Litter interception of a sessile oak forest in Hungary was 8% of the precipitation in summer and 16% in winter (*Führer*, 1994).

Litter storage capacity, which is a key factor for litter interception size, is proportional to the mass of litter per unit area (*Putuhena* and *Cordery*, 1996; *Row*e, 1955). This fact was confirmed in *Zagyvainé et al.* (2013), which considered spruce, beech, and oak stands. The maximum water holding capacity of the litter per unit weight was independent from the tree species and could be characterized as 2.1–2.2 l/kg. Naturally, forests with larger litter masses can retain

more water due to the differences in dry weight. The calculated storage capacities for 1 m² forest area are the following: 2.3 l/m² for beech, 4.1 l/m² for spruce, and 1.8 l/m² for sessile oak (*Zagyvainé et al.*, 2013).

2.3. *Transpiration and transpiration factors*

Active water release, i.e., transpiration, is essential for maintaining plant production. Plants lose significantly more water than that is required for them to build biomass and transport nutrients from the soil to the leaves (*Madas*, 1980). Transpiration is actually an evaporation process controlled by similar factors. Evaporation can only occur when water is available and can be defined as the process where liquid water is transformed into a gaseous state. Meadows and forests have differing transpiration and evaporation surfaces. The evaporation and transpiration surface of a forest is usually larger, and the surface resistance plays a more important role in the process (*Lee*, 1980). Forests possess a higher roughness and leaf area index, both of which determine transpiration constraints when compared to other land cover forms. Both roughness and leaf area index increase the transpiration when adequate water is available. On the other hand, the forest root depth is higher, and deeper soil possesses a higher capacity for water storage. Thus, forests are less vulnerable to water stress caused during longer dry periods than other vegetation covers generally are. However, longer dry periods can significantly endanger forests as well and decrease their survival and regeneration potential.

The transpiration water use amount for the forest biomass production per year can be calculated using the following equation:

$$AT = ABP \cdot TC \,, \tag{3}$$

where *AT* is the annual transpirational water use of the forest, *ABP* is the annual biomass production, and *TC* is the transpiration coefficient, which is the amount of transpirational water required per unit of produced biomass.

As a result, the weight of the annual increment, the weight of the annual crown, and the weight of the annual root biomass are proportional to the annual transpirational water used. In the equation, the multiplication factor is the amount of water required for unit biomass formation. This is called the transpiration coefficient (*TC*), the inverse of which is generally referred to as water use efficiency (*WUE*):

$$TC \ (1/WUE) = \frac{T}{BP} \,. \tag{4}$$

According to Eq. (4), the amount of transpirational water (*T*) required to form one gram of biomass (*BP*) of different tree species can be seen in *Table 3*.

Table 3. Transpirational water use of various forest stands (based on *Polsters*' results; *Járó*, 1981)

Species	Amount of required transpirational water to form 1 g biomass (g)	Annual maximum transpirational water consumption of main tree species (mm/year)
Beech	169	188
Hornbeam		163
Sessile oak		267
Pedunculate oak	344	441
Turkey oak		317
Black Locust		279
Birch	317	
White Willow		646
Hybrid poplar	520	680
Domestic poplar	585	800
Scots pine	300	205
Black pine		185
Spruce	231	148
Larch	257	

Table 3 shows that light demanding wood species require larger water amounts to produce one unit of biomass, while shade-tolerant wood species require a smaller water amounts, because they utilize water far more efficiently (*Madas*, 1980).

According to Eq. (3), the transpiration coefficients of different stands multiplied by the sum of the dry weight of the annual growth, leaf, and root, presents the annual transpirational water consumption of forest stands. Based on the water consumption equation, the maximum water consumption per year for stands of main tree species can be calculated, for example, as a unit per hectare in mm (*Table 3*).

In terms of forest water use in Hungary, forests in semi-humid areas containing species such as beech and spruce show less transpirational water demand than forests in semi-arid environments containing common oak and native poplars (*Járó*, 1981). Consequently, the forests at the xeric limit in the Hungarian Great Plain generally have a higher transpirational water demand. However, some species with low transpirational water demands – such as Scotch pine, black pine, and black locust – also occur in the dry climate conditions that characterize the Great Plain region.

2.3.1. Forest groundwater relations

The most studied topic of the past twenty years has been the interaction of forests and groundwater at the Hungarian Great Plain.

Forest evapotranspiration (both transpiration and interception) is generally higher than the evapotranspiration of the neighboring grasslands because of the enhanced LAI (leaf area index) and the greater root depth that woody vegetation within forests possess. These differences are characteristic for the relatively dry climate of the Hungarian Great Plain where precipitation is generally inadequate to support woody vegetation; consequently, trees only survive arid periods if they can access groundwater resources (*Ijjász*, 1939).

The groundwater level can be detected throughout the year under forests (if the trees are able to reach it). It is deeper under forests than under grasslands, but the difference between these two vegetation covers is bigger during the growing season in the Hungarian Great Plain (*Ijjász*, 1939).

The groundwater level was on average 0.8–1.1 m deeper under a middle-aged pine forest in the Danube-Tisza sand plateau region than it was in the surrounding, non-forested areas (*Major*, 2002). The actively growing black pine forest had a mean annual evapotranspiration (ET) rate of 712 mm year^{-1}. On average, this forest used 130 mm more water than it received as annual precipitation.

Gribovszki et al. (2012) compared the groundwater balance of two neighboring plots, an oak forest and a pasture. The study found the water level to be 0.44 m lower in the oak forest than it was under the pasture, whereas the groundwater uptake for the oak forest was more than twice as much as it was for the pasture during the extremely dry summer of 2012. Both results point to a significantly deeper groundwater level under forest vegetation. The larger amount of forest groundwater use does not work in a parallel fashion for salt uptake; therefore, salts accumulate in the soil and also in the groundwater. The salt content of the groundwater is slightly greater under the forest than it is under a pasture. The measured differences pose no problem for forest vegetation productivity and vitality, but the climate change induced salt accumulation can be a long-term effect. Afforestation can also contribute to salt accumulation in soils; see *Fig. 2*.
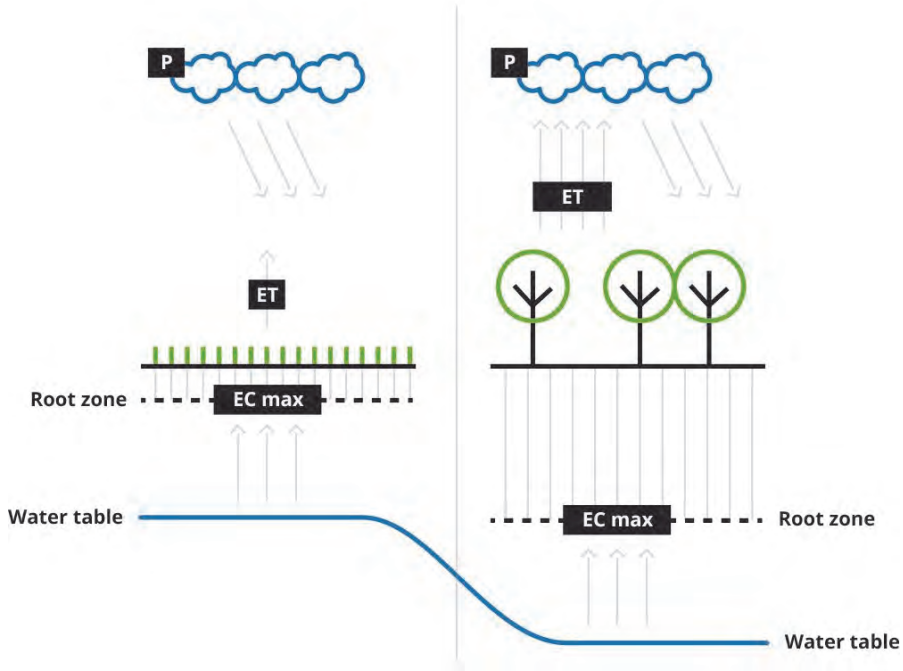
Fig. 2. Impact of forest vegetation on the water and salt balance by a shallow groundwater site (hypothetical model) (after *Szabó et al*., 2012). ET is the evapotranspiration, P is the precipitation.

In addition to vegetation type, soil type and layering also affect the groundwater uptake. Unfortunately, research is related to forest and groundwater relations focused mostly on sandy areas; therefore, the effect of soil parameters cannot be discussed in this paper.

Complex hydrological studies on forest water balance components in Hungary are rare.

The water balance of different land using forms in the northeastern part of the Hungarian Great Plain (Nyírség) was analyzed by *Móricz et al.* (2012). The study considered a dry (2007) and a wet growing season (2008). The lowland common oak forest showed approximately 30% higher evapotranspiration (758 mm) than the neighboring fallow (623 mm) on the yearly scale. The difference was more significant (threefold) for the groundwater use of different vegetation types (oak: 243 mm, fallow: 85 mm). Groundwater consumption was close to 60% of the total transpiration of the oak forest and approximately 30% of the fallow plot. Groundwater consumption was approximately 40% less during the wetter growing season than during the drier growing season despite the deeper

groundwater level during the dry period. Consequently, vegetation in both the oak and fallow forests use available groundwater resources.

Remote sensing broadens our possibilities to map and analyze the spatial heterogeneity of landscape unit hydrology, including forests, which are important landscape elements from hydrological point of view.

Evapotranspiration (determined by linear transformation of the MODIS: Moderate Resolution Imaging Spectroradiometer daytime land surface temperature) in the Danube-Tisza sand plateau region of the Hungarian Great Plain was analyzed by *Szilágyi et al.* (2012). The largest ET – 505 mm year^{-1} – according to land cover occurred over deciduous forests. The regional annual precipitation was 550 mm, which shows that in some locations ET amounts are estimated to be larger than precipitation amounts.

These groundwater discharge areas are overlapped by forest areas in many regions. Often the dense and deep root system of forests can tap the shallow groundwater level, which leads to a high evapotranspiration rate that frequently exceeds the precipitation rate. The average annual evapotranspiration for forests is 620 mm year^{-1} in groundwater discharge areas, which is about 70–80 mm more than the mean annual regional precipitation rate. This negative water balance can be maintained if forests create a local depression in the water table and induce a groundwater flow that is directed toward to the forest itself.

2.4. *Surface runoff and flood peak reduction*

Hydrological studies focusing on streamflow differences between forested and non-forested areas influenced by climate change are scarce in Hungary.

As an example, *Gribovszki et al,* (2006) analyzed rainfall and runoff time series of two neighboring small mixed forested catchments (100% forest cover) in western Hungary in the dry year of 2001 and found, that only 7–10% of the annual precipitation (606 mm) was streamflow, while evapotranspiration remained a dominant part (90–93%) of the annual simple water balance.The average annual evapotranspiration in this forested region was 615 mm (85%), while the yearly average precipitation was 726 mm from 2000 to 2008 (*Kovács,* 2011).

Kalicz et al. (2012) evaluated the runoff data sets of three different subcatchments (forested [HAZ], countryside [BAN], and urban [TESCO]) around Sopron, Hungary. They concluded that specific peak discharges of floods in urban areas induced by major rainfall events exceed those in a forested drainage basin by as much as two magnitudes.
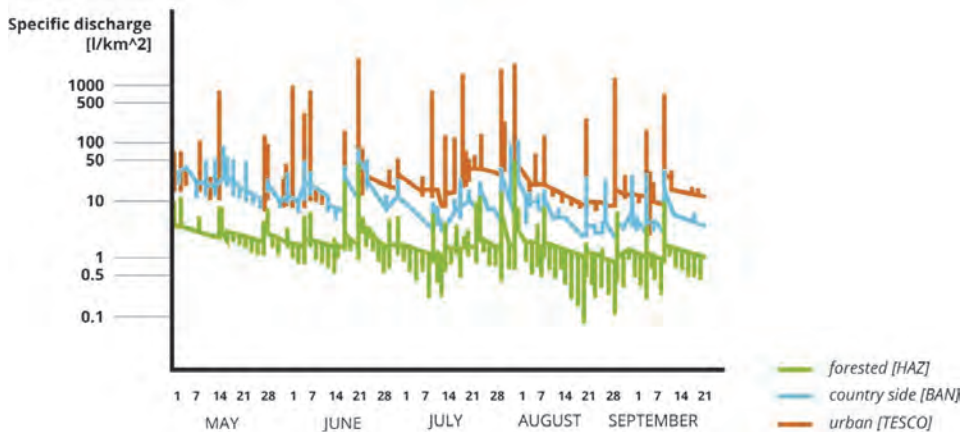
Fig. 3. Comparison of streamflow (specific discharges) for some characteristic subcatchments in Sopron neighborhoods.

3. Concluding remarks

Since forests ecosystems have the most complex hydrological cycle, they will likely be the most influenced by the changing water regime. In the following we summarize the possible changes in the forest water balance elements regarding climate change.

The evapotranspiration of forests (both transpiration and interception) is generally higher than that of other non-woody vegetation due to higher LAI and root depth.

Changes in precipitation distribution due to climate change, such as the increasing frequency of heavy precipitation events, reduces interception loss. This effect increases the amount of water available for transpiration and runoff. Otherwise, the rising temperature coupled with a larger leaf area index induces a higher transpiration if adequate water is present. This increases storage capacity and interception loss.

The greater water demand of forests is most obvious in areas where rainfall alone is insufficient to maintain woody vegetation, but where trees are able to reach groundwater sources through roots. Utilization of this possibility allows forests to survive dry periods. Nonetheless, dry periods that last several years can significantly endanger the survival and regeneration of forests.

Impacts on the water absorption of forests will become increasingly prevalent in a drier climate as long as forest root systems can reach water resources (the soil moisture content of the deeper soil layers or the groundwater). However, forests in these areas will be at great risk once these resources are

exhausted. The possible disappearance of these forests is especially problematic in river basins, where forests play a key hydrological role in reducing the amount of surface runoff and the extension of time of concentration in case of floods.

Extreme weather conditions such as large storms will likely be more frequent and more intense due to human-induced climate change. Forests could significantly mitigate the adverse effects of heavy rainfall-related greater surface runoff.

Driven by rising temperatures, increasing transpiration demand in the future will likely induce an enhanced groundwater uptake by plant communities. Eventually, this could lead to the lowering of the groundwater table and significant salt accumulation. If this occurs, the existence of groundwater-dependent forest communities in these areas is questionable, since the root structures of younger forests probably will not be able to reach the additional water source. One possible option to satisfy the demand of groundwater dependent forests is to supply them with water through other means such as river flood waves.

References

Baird, A.J. and *Wilby, R.L.* (eds), 1999: Eco-hydrology, Plants and water in terrestrial and aquatic environments. Taylor & Frances, London, New York.
https://doi.org/10.1046/j.1365-2745.2000.00526-2.x

Delfs, I., 1955: Die Niederschlagzurückhaltung im Walde /Interzeption/. Mitteilungen des Arbeitskreises "Wald und Wasser". Koblenz 2. (In German)

Dingman, S.L., 2001: Physical Hydrology (2nd edition). Prentice Hall.

Führer, E., 1994: Csapadékmérések bükkös, kocsánytalan tölgyes és lucfenyves ökoszisztémában. *Erdészeti Kutatások 8*4, 11−35. (In Hungarian)

Gerrits, A. M. J., Savenije, H. H. G., Hoffmann, L., and *Pfister, L.*, 2006: Measuring forest floor interception in a beech forest in Luxembourg. *Hydrol. Earth Sys. Sci. Discus. 3*, 2323–2341. https://doi.org/10.5194/hessd-3-2323-2006

Gribovszki, Z., Balog, K., Fodor, N., Szabó, A., and *Tóth, T.*, 2012: Impact of lowland forests on water table in shallow groundwater areas of the Hungarian Great Plain. Hydrocarparth International Conference, Catchment processes in regional hydrology: from experiment to modelling in Carpathian drainage basins, Sopron, Hungary, 28-30 October 2012, Conference CD, p. 7. ISBN 978-963-334-069-1.

Gribovszki, Z., Kalicz, P., and *Kucsara, M.*, 2006: Streamflow Characteristics of Two Forested Catchments in Sopron Hills. Acta Silv. Lign. Hung. 2, 81-92.

Hazslinszky, T., 1976: Az erdő szerepe a hidrológiai körfolyamatban. *Vízügyi Közlemények 2*, 295–301. (in Hungarian)

Helvey, J.D. and *Patric, J.H.*, 1965: Canopy and litter interception of rainfall by hardwoods of eastern United States. *Water Resour. Res. 1,* 193-206.https://doi.org/10.1029/wr001i002p00193

Helvey, J.D., 1967: Interception by eastern white pine. *Water Resour. Res.* 1, 723–729. https://doi.org/10.1029/wr003i003p00723

Ijjász E., 1939: A fatenyészet és az altalajvíz, különös tekintettel a nagyalföldi viszonyokra. *Erdészeti Kísérletek 42*, 1–107. (In Hungarian)

Járó, Z., 1980: Intercepció a gödöllöi kultúrerdei ökoszisztémában. *Erdészeti kutatások 73*, 7–17. (In Hungarian)

Járó, Z., 1981: A hazai erdők vízfogyasztása. *Agrártudományi közlemények 40*, 353–356. (In Hungarian)

Johnson, T., 2009: Deforestation and Greenhouse-Gas Emissions. Council on Foreign Relation [online]. in<https://www.cfr.org/backgrounder/deforestation-and-greenhouse-gas-emissions>[quoted on February 12, 2018]

Kajtár, L. and *Vörös, Sz.*, 2004: Risk-Based Modelling of Air Conditioning Systems in Hungary. ROOMVENT 2004: 9th Internaitonal Conference on Air Distribution in Rooms. 2004.09.05-2004.09.08., Coimbra, Portugália, 236–237.

Kalicz, P., Erős, M., Gribovszki, Z., Markó, G., and *Primusz, P.,* 2012: A soproni Rák-patak egy városi szakaszának hidrológiai és hidrodinamikai vizsgálata. In (Eds. A*lbert L., Bidló A., Jancsó T., Gribovszki Z.*) Városok öko-környezetének komplex vizsgálata a nyugat-dunántúli régióban. Nyugat-magyarországi Egyetem Kiadó, Sopron. (In Hungarian)

Kalicz, P., Herceg, A., Kisfaludi, B., Csáki, P., and *Gribovszki, Z.,* 2017: Canopy interception variability in changing climate. *Geophys. Res. Abs. 19*: Paper EGU2017-14894. EGU General Assembly 2017. 2017.04.23 -2017.04.28. Bécs, Ausztria.

Koloszár, J., 1981: Természetes erdei ökoszisztémák és a csapadék. Erdő és víz, VEAB, 75–88. (In Hungarian)

Kovács, Á.D., 2011: Tó- és területi párolgás becslésének pontosítása és magyarországi alkalmazásai. PhD Thesis. TUB, Budapest. (In Hungarian)

Kucsara, M., 1998: Az erdő csapadékviszonyainak vizsgálata. *Vízügyi Közlemények 3*, 456–475. (In Hungarian)

Madas, A., 1980: Az erdőgazdálkodás hatása és jelentősége az árvizek kialakulására. Erdő és víz. Workshop Sopron. Veszprém, 12–22. (In Hungarian)

Major, P., 2002: Síkvidéki erdők hatása a vízháztartásra. *Hidrológiai Közlöny 82*, 319–324. (In Hungarian) https://doi.org/10.1136/bmj.324.7333.319

Móricz N., Mátyás C., Berki I., Rasztovits E., Vekerdy Z., and *Gribovszki Z.*, 2012: Comparative water balance study of forest and fallow plots. *Forest-Biogeosci. Forestry 5(4),* 188-196. [online] in<http://www.sisef.it/iforest/contents?id=ifor0624-005>[quoted on August 2, 2012] https://doi.org/10.3832/ifor0624-005

Lee, R., 1980: Forest Hydrology. Columbia University Press, New York.

Lundberg, A. and *Halldin, S.*, 2001: Snow interception evaporation. Review of measurement techniques, processes, and models. *Theor. Appl. Climatol. 70*, 117–133. https://doi.org/10.1007/s007040170010

Pathak, P.C., Pandey, A.N. and *Singh, J.S.,* 1985: Apportion of rainfall in central Himalayan forests (India). *J. Hydrol. 76*, 319–332. https://doi.org/10.1016/0022-1694(85)90140-4

Putuhena, W. and *Cordery, I.,* 1996: Estimation of interception capacity of the forest floor. *J. Hydrol. 180*, 283–299. https://doi.org/10.1016/0022-1694(95)02883-8

RA, 2017: Rainforest Alliance. What is the Relationship Between Deforestation and Greenhouse Gas Emissions? [online].in<https://www.rainforest-alliance.org/articles/relationship-between-deforestation-greenhouse-gas-emissions>[quoted on February 12, 2018]

Rácz, J, 1981: Az erdő szerepe a vízgyűjtő területek vízháztartásában. Erdő és víz, VEAB, 23–29. (In Hungarian)

Rowe, P.B. 1955: Effects of forest floor on disposition of rainfall in pine stands. *J. For. 53*, 342–355.

Savenije, H.G. 2004: The importance of interception and why we should delete the term evapotranspiration from our vocabulary. *Hydrol. Proc. 18*, 1507-1511. https://doi.org/10.1002/hyp.5563

Schrope, M., 2009: When money grows on trees. Nature Reports *Climate Change 3*, 101–103. https://doi.org/10.1038/climate.2009.78

Szabó, M., 1979: Egy cseres-tölgyes erdő („Síkfőkút projekt") víz és ásványanyag forgalma. Candidate dissertation. Budapest, Hungary. (In Hungarian)

Szabó, A, Kiss, K., Gribovszki, Z., and Tóth, T., 2012: Erdők hatása a talaj és altalaj sóforgalmára, valamint a talajvíz szintjére. *Agrokémia és Talajtan. 61*, 195-209. (In Hungarian) https://doi.org/10.1556/Agrokem.60.2012.1.14.

Szép, T., 2010: A klímaváltozás erdészeti ökonómiai vonatkozásai. *Doktori (PhD) értekezés.* Nyugat-magyarországi Egyetem. 175.

Szilágyi J., Kovács Á., and *Józsa J.*, 2012: Remote sensing based groundwater recharge estimates in the Danube-Tisza Sand Plateau region of Hungary. *J. Hydrol. Hydromech. 60*, 64–72. https://doi.org/10.2478/v10098-012-0006-3

Szőnyi, L., 1966: Erdészeti hidrológiai megfigyelések a mátrafüredi kísérleti vízgyűjtőben. *Erdészeti Kutatások 62*, 202–213. (In Hungarian)

Szőnyi, L., 1967: Az erdő hatása a víz levonulására. *Az Erdő 9,* 411–414. (In Hungarian)

Stewart, J.B., 1977: Evaporation from the wet canopy of a pine forest. *Water Resour. Res. 13*, 915–921. https://doi.org/10.1029/wr013i006p00915

Weisse, M. and *Goldman, E. D.,* 2017: Global Tree Cover Loss Rose 51 Percent in 2016. World Resource Institute. in<http://www.wri.org/blog/2017/10/global-tree-cover-loss-rose-51-percent-2016>[quoted onApril 12, 2018]

Zagyvainé Kiss, K.A., Kalicz, P., and *Gribovszki, Z.*, 2013: Az erdei avar tömege és víztartó képessége közötti összefüggés. *Erdészettudományi közlemények 3*, 79−88. (In Hungarian)

Zagyvainé Kiss, K. A., Kalicz, P., Csáfordi, P., and *Gribovszki, Z.*, 2014: Forest Litter Interception Model for a Sessile Oak Forest. *Acta Silv. Lign. Hung. 10*, 91–101. https://doi.org/10.2478/aslh-2014-0007

Ward, R.C. and *Robinson, M.*, 1975: Principles of hydrology, third edition. McGraw-Hill Book Company Europe 3, 54–70.

IDŐJÁRÁS

A new index for climate change evaluation – An example with the ALADIN and RegCM regional models for the Balkans and the Apennines

Valery Spiridonov and **Rilka Valcheva***

National Institute of Meteorology and Hydrology (NIMH)
66, Tsarigradsko Shose blvd Sofia 1784, Bulgaria

* Corresponding Author e-mail: Rilka.Valcheva@gmail.com

Abstract— A new index for climate change assessment has been introduced. It is a ratio between the number of cases from a future period and the cases of a control experiment (reference period) falling within a predefined interval of the reference period. By "case" we mean the value of a meteorological element that meets certain conditions. Additionally, its conservation is a necessary condition for reducing the risk of losing a reliable signal of the modeled variability of future climate when applying bias correction methods (BCM's). The spatial distribution of this index is presented by using two regional climate models, ALADIN and RegCM4, over an area including the Balkan and Apennine Peninsulas. The assessment is performed for the average monthly temperature and precipitation. Both models have similar indices in broad areas. In winter, spring, and summer this refers to temperature and in spring and summer to rainfall.

Key-words: climate change, new index, ALADIN, RegCM4, bias correction

1. Introduction

For assessment of climate change by numerical model experiments, we usually consider differences (tendencies) between the future and a reference (control) period. Thus, to a certain extent, the systematic error of the simulations is

compensated. This difference can be added to actual observations to obtain future values. In some papers this method is mentioned as "delta change" approach (*Teutschbein et al.*, 2011). Later, this method will be described. Although, the models are deterministic, their results are often postprocessed by statistical methods as random processes. There are two main reasons for applying the statistical approaches. The first one is statistical downscaling when the climate model grid resolution is quite coarse. This is usually the case with global climate models. "Downscaling" is a method of obtaining high-resolution climate or climate change information from relatively coarse-resolution global climate models (GCMs). The dynamical downscaling is achieved through regional climate models (RCM), such as RegCM and ALADIN. Statistical downscaling methods cover regression-type models including both linear and non-linear relationships established between the output of the model and a more dense set of local observations (*Mearns et al.*, 1999; *Huth,* 1999). In addition to achieving a finer resolution, some of these methods also eliminate systematic errors (biases). This gives the idea to change the results of dynamical downscaling to match observations. Numerous methods for such modification are known as "bias correction methods" (BCMs). This procedure is necessary in many cases, when we use climate model results as input data for other impact models such as hydrological, agricultural (*Navarro-Racines et al.*, 2015; *Haerter et al.,* 2015), and air quality models. In this case, it is necessary to use the daily values from the output of dynamic models. Consequently, the output of dynamic models must be adjusted to match the statistical structure of daily observations. An example of this is the so-called "drizzle" problem (*Dai*, 2006). By this terminology the trend of the climate models to precipitate too frequently at reduced intensity is denoted. Such an input for hydrological models makes them unusable. The term "bias correction" includes much more transformation than the simple removing of bias between model results and observations. The transformation of the model results from the so-called control or reference experiment (run) is used to match them to the observing data or other data considered as reference, for example to re-analyses. It is assumed that if the output of the model differs from observations in the same reference period, there will be a false signal in the future simulations. The applied techniques can be summarized by defining a "transfer function" between observed and reference (control) values, so that the obtained probability density function (pdf) (or cumulative density function cdf) corresponds to the measured data for the reference period or to the data considered as reference. Then, this "transfer function" is applied to the results obtained for the future period. Gaussian kernel (*Sippel et al.*, 2016) and gamma distribution (*Piani et al.*, 2010) as cumulative density function can be used. The distribution of Weibull is often applied to the wind. Various methods are used, such as "multiple linear regression", "analogue methods", "local intensity scaling", and "quantile mapping". After all, the result could be described as transformation of the probability density function or

cumulative distribution function. The multiple linear regression method has a linear transfer function, but others may or may not have that property. If we denote pdf as S, the linearity means that after applying the linear transfer function $F(a,b)$, the new pdf (or S') should obey on the relation $S' = a*S + b$, where a and b are constants. The simplest case is when $a = 0$. In this case S moves at distance b from its original position. Most of these methods are included in the software developed in *Cattaneo et al.* (2015). In *Deque* (2007) another method is described which is similar to quantile mapping.

There are no observations in the future, so we have to rely on the assumption of correct extrapolation of these methods in the changing climate. As noted in *Ehret et al.* (2012): "however, in the context of CCIS (Climate Change Impact Studies), the definition of bias is not as strict: it varies with the scope of the studies and is often used in a general sense for addressing any deviation of interest (e.g., with respect to mean, variance, covariance, length of dry spells, etc.) of the model from the corresponding "true" value ". A critical analysis and review of the most commonly used methods can be found in *Maraun* (2016).

Here, we propose a way to avoid the risk of losing a reliable climate change signal when using some BCM's. Some may lead to the loss of an otherwise properly predicted change. As it is mentioned in *Grillakis et al.* (2017): "However, it is well known that quantile mapping may significantly modify the long-term statistics due to the time dependency of the temperature bias". In many BCM's, the different meteorological fields are treated independently. That may lead to some discrepancies. For example, hydrological impact models require assessment of evaporation and evapotranspiration. This means consistency between changes in temperature, wind, and solar radiation. The separate correction loses the relationships between them. As noted in *Hagemann et al.* (2011): "Some more uncertainties have occurred over several dry regions and seasons, especially for precipitation. Here, any projected changes in discharge and their subsequent impact on water resources have to be carefully considered, with and without using bias corrected GCM data" In *Dosio* (2016) a possible distortion of the climate change signal is noted: "The mean climate change is conserved by bias adjustment only if the bias is constant, which is not the case for the RCMs' results over large part of Europe". Here the effect of bias correction on a number of climate indices from the Expert Team on Climate Change Detection and Indices (ETCCDI) have been investigated. In *Pierce et al.,* (2015) it is mentioned: "The quantile mapping and cumulative distribution function transform can significantly alter the global climate model's mean climate change signal, with differences of up to 2 °C and 30% points for monthly mean temperature and precipitation, respectively". Different approaches to BCM's attempt to avoid potential drawbacks. Preservation of the originally modeled long-term signal in the mean, the standard deviation and higher and lower percentiles of temperature is investigated in *Grillakis et al.*

(2017). A method for reducing errors in the models' simulation of variance as a function of frequency is proposed in *Pierce et al.* (2015). In *Switanek et al.* (2017), instead of quantile mapping, a scaled distribution mapping technique is developed. The question to be answered is "to what extent a certain bias correction method can be applied, and in which area it can be applied".

2. Definition and properties of the proposed C-index for climate change evaluation

The values of any meteorological element obtained through a reference (30-year-long) period simulation, have various statistical distributions for each grid point of the model. The future period simulation (again 30 years) leads to a new distribution for each grid points. Let X_R be the number of cases from the reference period that belong to an interval of a set of values ($\delta1$, $\delta2$). Let X_F be the number of cases from the future period that fall within the same interval from the reference period. The ratio

$$C = X_F / X_R \tag{1}$$

is another possible measure of climate change at each grid point. This ratio will be called "C-index". When $C < 1$, the number of cases from the future period are less than those from the reference period for the defined interval, and when $C \geq 1$ the number of cases from the future period are maintained or increased with regard to the reference period cases for the same interval. For example, the number of cases above a certain value during the reference period are compared to the cases of the future period. This measure has a "relativistic" meaning, i.e., how the future weather would look like for the observer from the reference (control) simulation period.

According to this definition, the necessary condition for any bias correction method, which should not cause distortion of pdf or cdf is that the value of C (whatever it is) should not change. In other words, if B is the "transfer function" mentioned above, then

$$B(X_F) / B(X_R) = X_F / X_R = C \tag{2}$$

is the necessary condition that is valid only for the defined interval of C-index. This is a partial answer to the question raised above.

The conservation of C depends on the bias correction method (BCM). We will show that the linear transformation ("linear transfer function") does not change this ratio. If the transfer function is non-linear, this feature is not guaranteed, but there may be an interval in which the C-index remains unchanged. Another possibility is to approximate the non-linear function by a piecewise linear function.

Let the values of an element (temperature, precipitation, etc.) from the future period fall within a certain interval before the transformation:

$$X1_R < X_F < X2_R ,\qquad(3)$$

where $X1_R$ and $X2_R$ determine the interval of interest from the reference period in which the cases X_F from the future period fall. We will prove that for any linear transformation:

$$Y = AX + B,\qquad(4)$$

for which, when $A \geq 0$ the future cases falling within this range are preserved, i.e.:

$$AX1_R +B < AX_F + B < AX2_R + B .\qquad(5)$$

Let us consider the left inequality and assume the opposite,

$$AX1_R +B \geq AX_F + B,\qquad(6)$$

or

$$A(X1_R - X_F) \geq 0.\qquad(7)$$

When $A > 0$, we get $X1_R \geq X_F$, which contradict to Eq. (3). In the same way, the correctness of the right part of Eq. (5) is proved. Once this is true for all of the cases, it is also true for the ratio of their sum C. The particular case, $A = 0$, is when probability density function (pdf) is only "moved" on the X-axis.

The proposed index is an indicator, which signs if the signal from the control run to the future one is changed by the applied "bias correction" method.

One important question is how stable the value of C i.e., the ratio X_F / X_R is. This depends on the inherent errors of the model (for example, as a result of accepted parameterizations, approximation of equations, etc.). The following equation Eq. (8) shows that if the error is proportional to the value of X, the ratio between the reference and the future simulation does not change. The "drizzle" effect mentioned above actually is an error of the magnitude of rainfall rates simulated by the model *Dai* (2006) and *Sun et al.* (2006). The error component proportional to the magnitude does not affect the C-index.

Let k be the error coefficient, then:

$$(X_F + k X_F) / (X_R + k X_R) = X_F(1+ k) / X_R(1+ k) = X_F / X_R .\qquad(8)$$

Note, that this index is determined separately for each point of the model's grid. So, instead of fixed thresholds, it is possible to have different intervals at each grid point. This will be illustrated in the next example.

3. Example with an interval defined by standard deviation σ and mean μ

We will illustrate the C-index by looking at the change of the number of cases falling within a certain interval ($\delta 1=\mu-\sigma$; $\delta 2=\mu+\sigma$). The C-index is determined by the ratio of the number of cases of the future period and the reference period falling within this range defined by the mean μ and the standard deviation σ of the reference period.

About 68% of values drawn from the Gaussian distribution are within one standard deviation σ away from the mean μ. Let the cases falling within this interval be considered as "normal", and the cases outside it as "extreme". When $C \geq 1$, more cases of the future period fall within this interval, i.e., in this definition the future period becomes "more normal" from the point of view of the "referent period simulation observer", and this change will not seriously affect the environment, but it is possible to have more cases of "extreme" weather outside this interval. When $C < 1$, it means that less cases from the future period fall in the interval defined by the reference period, i.e., this can be considered as a sensitive climate change. The smaller the C, the greater the change.

Simulation results with the regional model ALADIN forced with boundary conditions from the ARPEGE global (A1B scenario) and RegCM4.4.5 regional climate models (*Giorgi et al.,* 2012) forced with boundary conditions from the HadGEM2-ES global climate model (Hadley Centre Global Environment Model – Earth-System version 2, *Collins et al.*, 2011) according to the RCP45 scenario (*Thomson et al.*, 2011) were used. Both models have a resolution of 20 km. In *Figs. 1* and *2,* the C-index distribution of the temperature value from ALADIN and RegCM4 models by seasons (winter - DJF; spring – MAM; summer – JJA; and autumn – SON) is shown. Areas with $C \geq 1$ are marked in red ($C>1$) and orange ($C=1$) (actually, where the weather is "usual"). For $C<1$, the color gradation is by intervals of 0.2. In *Figs. 1a* and *2a,* temperature tendencies with ALADIN and RegCM4 models are shown, i.e., the difference between the future and reference periods by seasons in degrees Celsius (°C). For the 2021–2050 period the warming trend is notable throughout the whole year for both models, especially during the JJA season. Similarly, in *Figs. 3* and *4,* the C-index distribution of precipitation values for both models is presented, while in *Figs. 3a* and *4a,* the tendencies for precipitation calculated by the two models are shown (in %). Both models show less precipitation in summer (JJA) and more precipitation in spring (MAM).

556
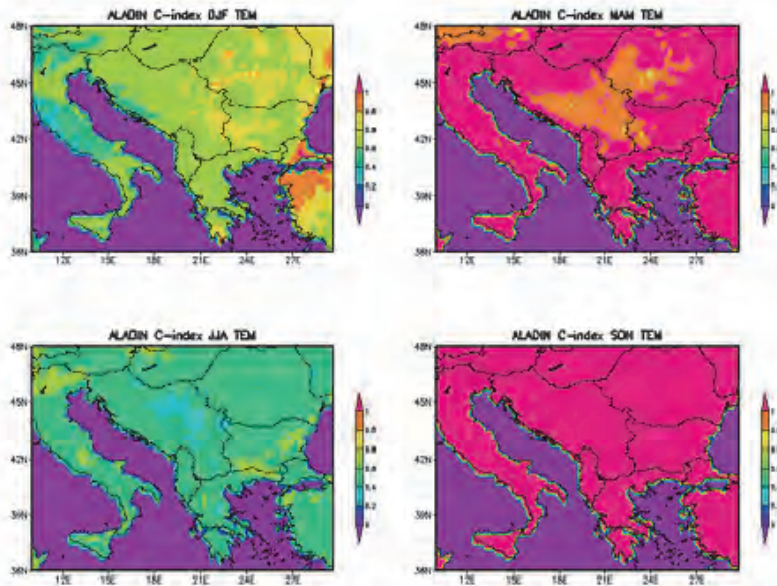
Fig. 1. Temperature C-index distribution from ALADIN model simulation for reference (1975–2004) and future (2021–2050) periods by seasons (winter - DJF; spring - MAM; summer - JJA; autumn - SON).
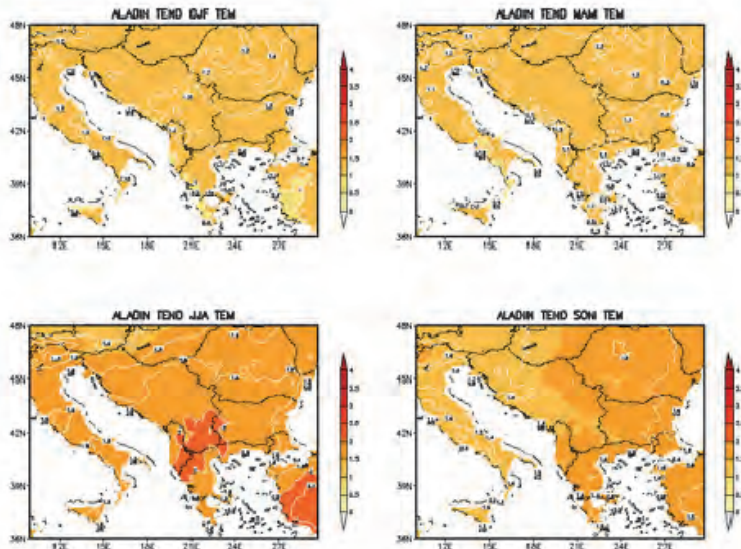
Fig. 1a. Temperature tendencies with ALADIN model - difference between future (2021–2050) and reference (1975–2004) periods by seasons (winter - DJF; spring - MAM; summer – JJA; autumn - SON) in °C.

557
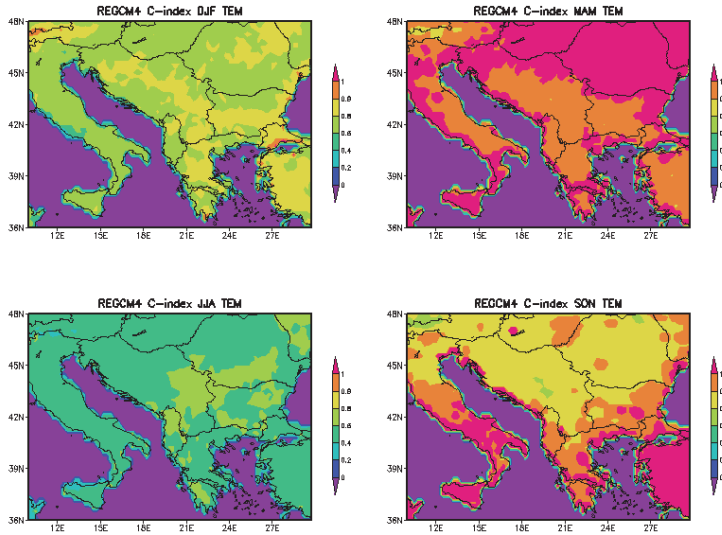
Fig. 2. Temperature C-index distribution from RegCM4 model simulation for the reference (1975-2004) and future (2021-2050) periods by seasons (winter - DJF; spring - MAM; summer - JJA; autumn - SON).
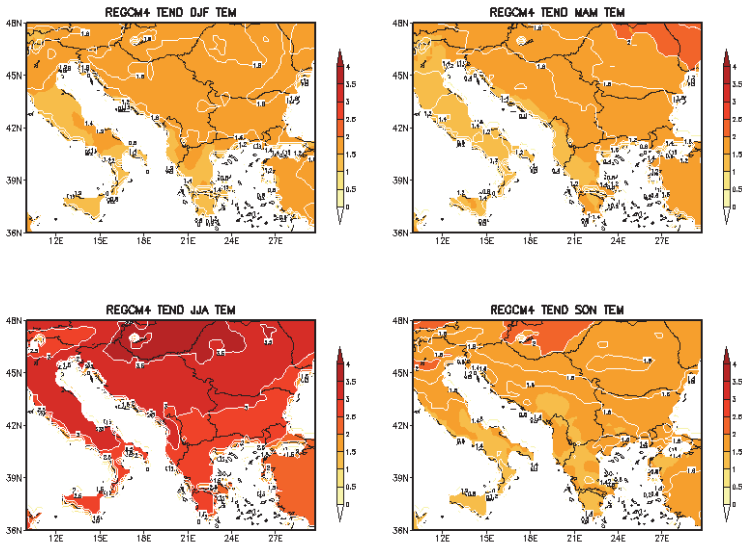
Fig. 2a. Temperature tendencies with RegCM4 model - difference between future (2021-2050) and reference (1975-2004) periods by seasons (winter - DJF; spring - MAM; summer - JJA; autumn - SON) in °C.
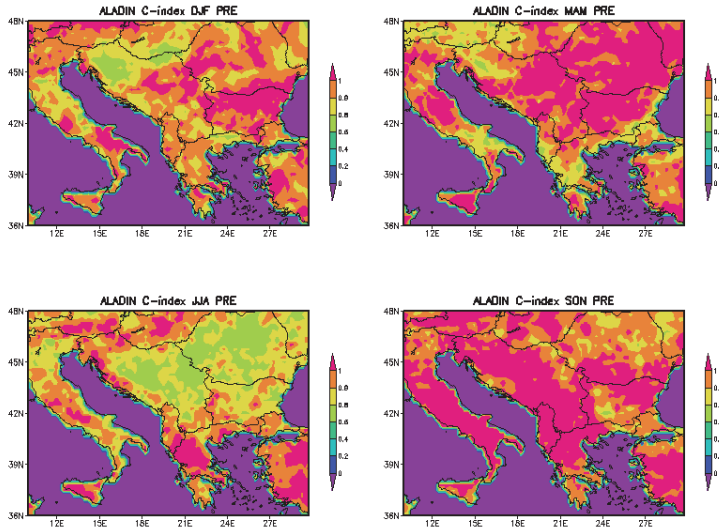
Fig. 3. Precipitation C-index distribution from ALADIN model simulation for reference (1975–2004) and future (2021-2050) periods by seasons (winter - DJF; spring - MAM; summer - JJA; autumn - SON).
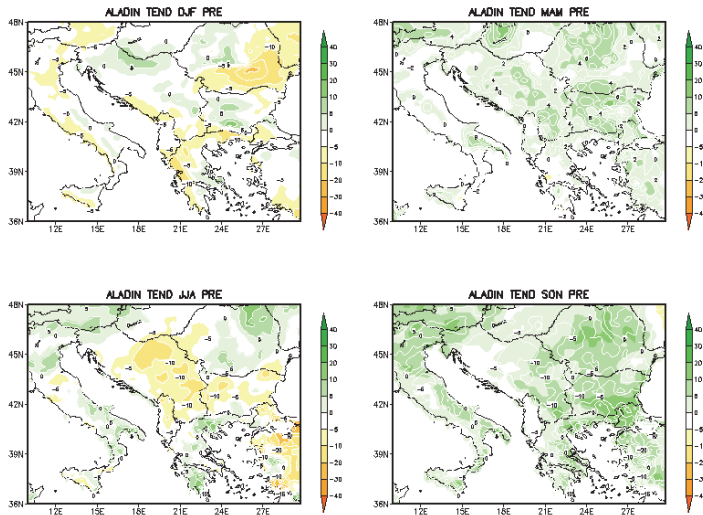
Fig. 3a. Precipitation tendencies with ALADIN model - difference between future (2021–2050) and reference (1975-2004) periods by seasons (winter - DJF; spring - MAM; summer - JJA; autumn - SON in %.

559
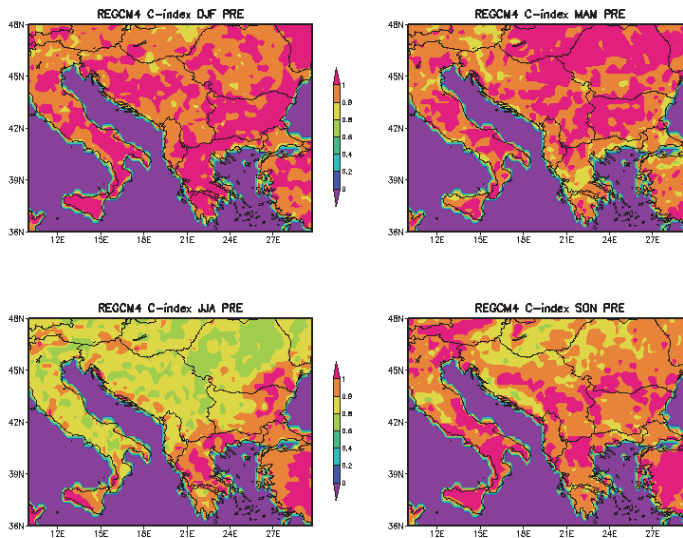
Fig. 4. Precipitation C-index distribution from RegCM4 model simulation for reference (1975–2004) and future (2021-2050) periods by seasons (winter - DJF; spring - MAM; summer - JJA; autumn - SON).
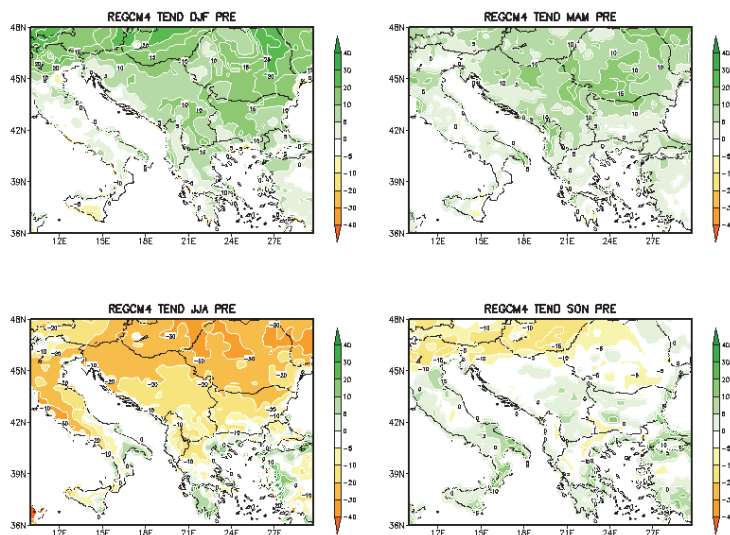
Fig. 4a. Precipitation tendencies with RegCM4 model - difference between future (2021–2050) and reference (1975-2004) periods by seasons (winter - DJF; spring - MAM; summer - JJA; autumn - SON) in %.

560

For both models, the biggest changes, i.e., large areas with small values of the C-index occur during the summer season. For the RegCM model,temperature C-index maps (*Fig. 2*) show small values ($C < 1$) in winter and summer over the whole area and small C-index in autumn over a significant area in the northern part of the modeled domain. In spring, $C \geq 1$ over the whole area. The RegCM precipitation C-index spatial distribution maps (*Fig. 4*) show small C-index ($C < 1$) in summer (especially in the northern part of the domain). In winter and spring, the RegCM precipitation C-index (*Fig. 4*) is equal to or more than 1 over a significant part of domain. For the ALADIN model, precipitation C-index distribution maps (*Fig. 3*) show small C-index in summer over the central and north-eastern parts of the domain, where the model shows the biggest changes in precipitation. These examples illustrate the added value of applying the C-index as a measure of climate change. If the tendencies are small (e.g., zero) and the σ of the future climate simulation is greater than the σ of the reference period, then the C-index may be much smaller than 1 (significant change). The opposite situation is when the value of the index is about 1 (relatively small change in climate in the sense of preserving or increasing the number of cases falling within the specified interval), and the trend is significant. In this regard, we would like to draw attention to two specific cases. The first one occurs in the spring season on the RegCM4 temperature (*Fig. 2a*) and C-index temperature distribution maps (*Fig. 2*). It is shown that in the northeastern part of the domain, where temperature warming is above 2 °C, the C-index distribution is more than 1. The other case occurs in the autumn season on the ALADIN temperature (*Fig. 1a*) and C-index temperature distribution maps (*Fig. 1*), where in the northeastern parts of the domain, the temperature warming is also about 2 °C, while the corresponding C-index is greater than 1. If the interval ($\mu - \sigma; \mu + \sigma$) is considered as an interval of cases with "normal" temperature or precipitation, the increasing of their number in the future is not considered as a dangerous climate change. This means, that in these cases ($C \geq 1$) the future temperature changes will not affect the potential impact on the environment, regardless temperature warming, but it is possible to have more cases of extreme weather there. In fact, pdf deforms to higher or smaller values, remaining in the same interval. Choosing another interval can lead to other values of the C-index and even to a change in the direction of the inequality.

In some areas the differences between the tendencies of models may look more or less significant than the differences between the C-index, for example, the temperature in the models for the summer season. The reason is in the effect of combination between σ and μ. Despite of tendencies, because of re-distribution, a bigger or smaller number of cases falls in the interval defined by the mean and sigma of the referent period. The differences between the μ of a future run and the μ of the control (reference) run may be compensated by a smaller σ of the future period and vice versa. The reason for this is that the

C-index is sensitive to changing the distribution of cases from the future period to the reference. When this change is the same for both models, then their C-indices coincide. If the expected trends for the two models are the same, but the changes in the distributions are significant, then the C-indices differ significantly. This is the added value of this index for climate change assessment.

For better understanding of the relationship between the C-index and the tendencies, the standard deviation of the past period is shown in *Figs. 5a* and *6a* for temperature and in *Figs. 5b* and *6b* for precipitation for both models, which is actually in connection with the width of the selected interval. The change of standard deviation – the ratio between the future (2021–2050) and reference (1975–2004) periods is presented in *Figs. 7a* and *8a* for temperature and in *Figs. 7b* and *8b* for precipitation.

Figs. 5a and *6a* show temperature standard deviation distribution (in °C) from ALADIN and RegCM models, respectively, for the reference period 1975–2004 by seasons (winter - DJF; spring – MAM; summer – JJA; autumn - SON). Both models show the biggest temperature σ in spring (MAM) and autumn (SON) seasons between 3.5° and 5°C. In winter (DJF), the σ values are between 0.8° and 1.6 °C for the ALADIN model and between 1.2° and 2.7 °C for RegCM. In summer (JJA), the temperature standard deviation for ALADIN is between 1.2° and 1.8 °C and between 1.2° and 2.4 °C for RegCM, respectively.

In *Figs. 5b* and *6b,* precipitation standard deviation distribution (in mm) from ALADIN and RegCM models, for the reference period 1975–2004 by seasons (winter - DJF; spring – MAM; summer - JJA; autumn - SON) is shown. Precipitation standard deviation distribution from the ALADIN model is between 10 and 30 mm in all seasons, while the RegCM standard deviation values are between 20 and 60 mm.

The changes of values of σ from the reference (1975–2004) to the future (2021–2050) periods are presented in *Figs. 7a, 7b, 8a,* and *8b*.
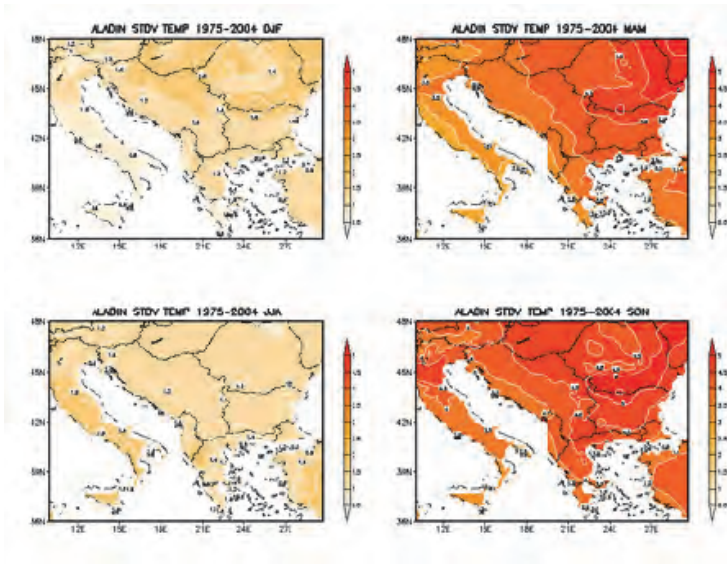
Fig. 5a. Standard deviation of temperature (in °C) from the ALADIN model for the reference period 1975-2004 by seasons (winter - DJF; spring - MAM; summer - JJA; autumn - SON)
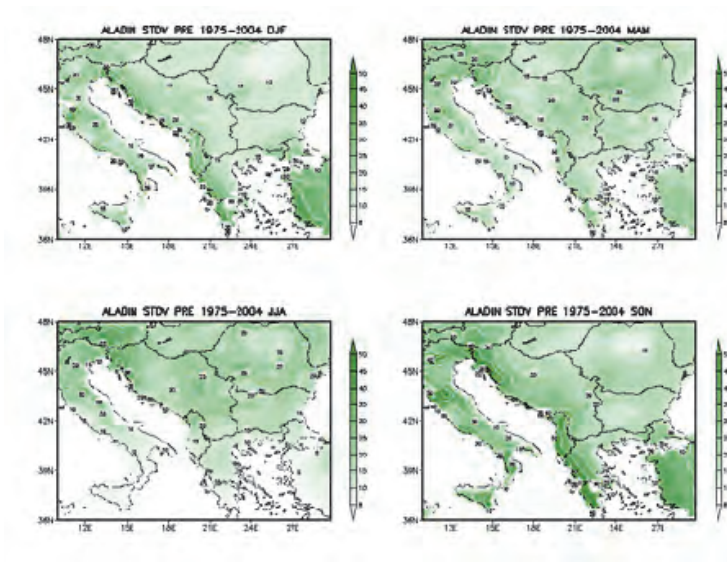
Fig. 5b. Standard deviation of precipitation (in mm) from the ALADIN model for the reference period 1975-2004 by seasons (winter - DJF; spring - MAM; summer - JJA; autumn - SON).
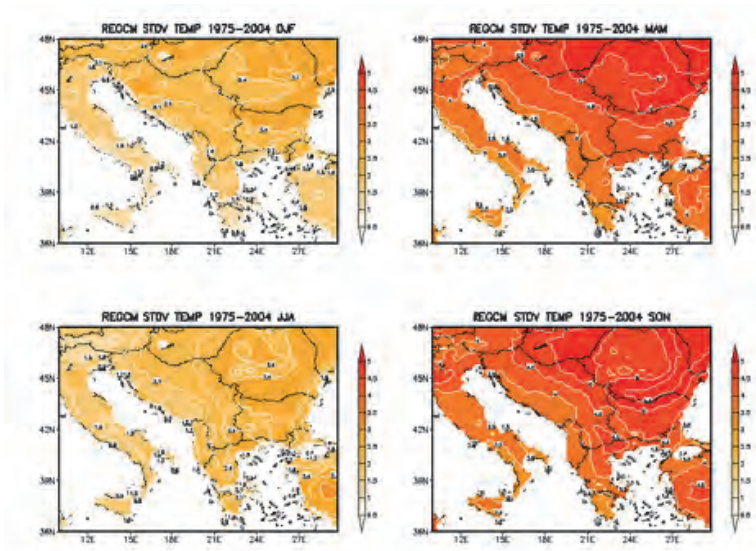
Fig. 6a. Standard deviation of temperature (in °C) from the RegCM4 model for the reference period 1975-2004 by seasons (winter - DJF; spring - MAM; summer - JJA; autumn - SON).
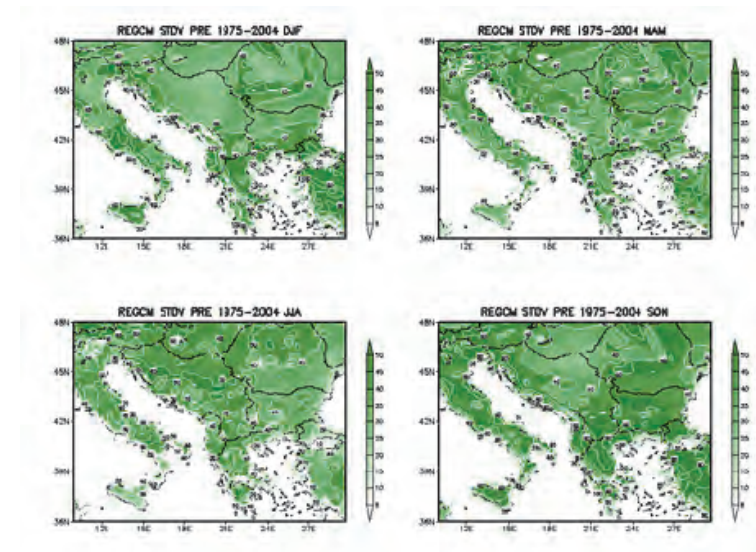
Fig. 6b. Standard deviation of precipitation (in mm) from the RegCM4 model for the reference period 1975-2004 by seasons (winter - DJF; spring - MAM; summer - JJA; autumn - SON).
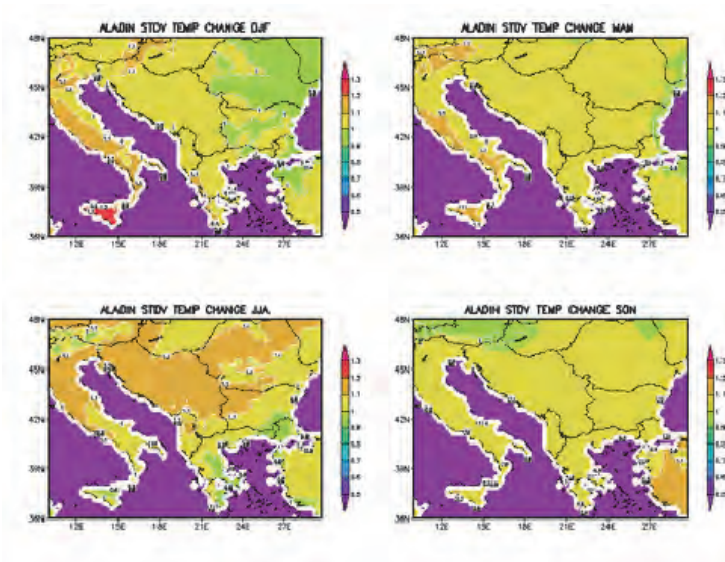
Fig. 7a. Temperature standard deviation change (in °C) from the ALADIN model – the ratio between future (2021–2050) and reference (1975–2004) periods by seasons (winter - DJF; spring - MAM; summer - JJA; autumn - SON).
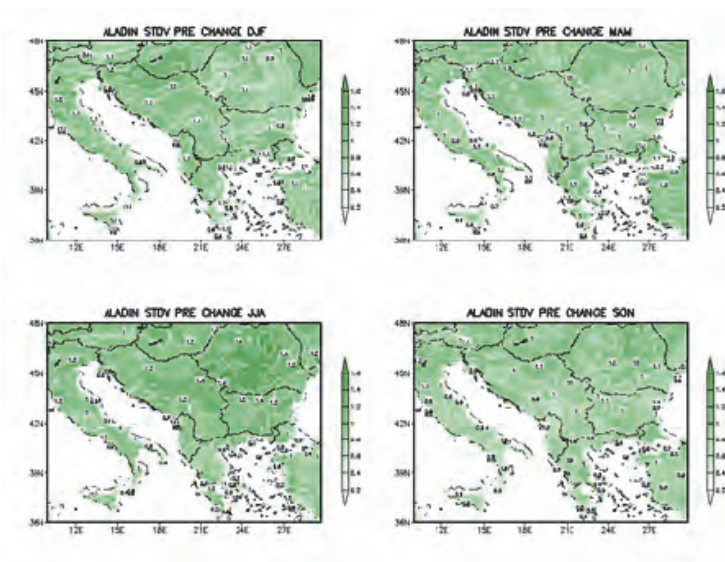
Fig. 7b. Precipitation standard deviation change (in mm) from the ALADIN model – the ratio between future (2021–2050) and reference (1975–2004) periods by seasons (winter - DJF; spring - MAM; summer - JJA; autumn - SON).
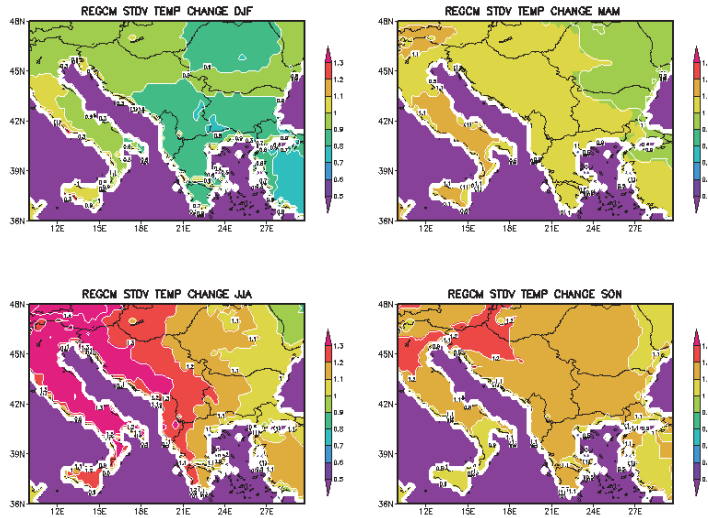
Fig. 8a. Temperature standard deviation change (in °C) from the RegCM4 model – the ratio between future (2021–2050) and reference (1975–2004) periods by seasons (winter - DJF; spring - MAM; summer - JJA; autumn - SON).
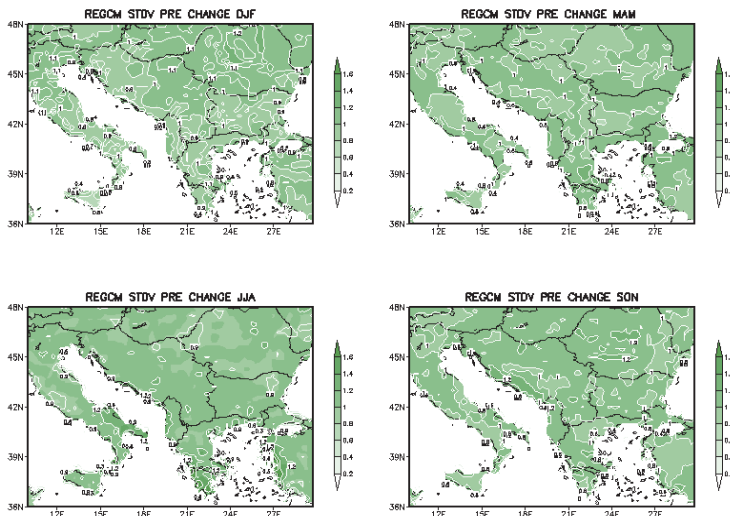
Fig. 8b. Precipitation standard deviation change (in mm) from the ALADIN model – the ratio between future (2021–2050) and reference (1975–2004) periods by seasons (winter - DJF; spring - MAM; summer - JJA; autumn - SON).

In *Figs. 7a* and *8a*, the temperature standard deviation change (in °C) from ALADIN and RegCM models is shown – the ratio between the σ of future (2021–2050) and the σ of the reference (1975–2004) periods by seasons (winter - DJF; spring - MAM; summer - JJA; autumn - SON). The biggest change in temperature standard deviation occurs in summer (JJA) between 1.0° and 1.2 °C for ALADIN, where temperature changes are the biggest (*Fig. 1a*), $C < 1$ (*Fig. 1*) and the temperature standard deviation is small (*Fig. 5a*). In JJA and SON for RegCM model the temperature standard deviation change is between 1.0° and 1.3 °C, and 1.1° and 1.3 °C, respectively, where the C-index is small (*Fig. 2*) and temperature changes are the biggest (*Fig. 2a*).

In *Figs. 7b* and *8b*, precipitation standard deviation change (in mm) from ALADIN and RegCM models is shown – the ratio between the σ of future (2021–2050) and the σ of the reference (1975–2004) periods by seasons (winter - DJF; spring – MAM; summer - JJA; autumn - SON). Both models show that the precipitation standard deviation change is between 0.4 and 1.4 mm in all seasons. The biggest precipitation σ change from the RegCM model is in summer (JJA) and autumn (SON), where precipitation changes are the biggest (*Fig. 4a*) and $C < 1$ (*Fig. 4*). The biggest precipitation σ change from the ALADIN model is in summer (JJA) which corresponds to $C < 1$ (*Fig. 3*) and to a decrease of the summer precipitation (*Fig. 3a*).

4. Example with two BCMs

A very simple but useful method of bias correction is the "delta change" method. Let μ_{ref} and μ_f be the average of N cases obtained from the reference and future periods for temperature or precipitation. Let X_i ($i = 1, N$) are the corresponding series of observations. The corrected range of temperature for the future is:

$$Y_i^{cor} = X_i + (\mu_f - \mu_{ref}). \tag{9}$$

For the precipitation, relative changes are considered:

$$Y_i^{cor} = X_i * (\mu_f / \mu_{ref}). \tag{10}$$

For averages, we find:

$$(\textstyle\sum Y_i^{cor})/N = \mu'_f = (\textstyle\sum X_i^c)/N + (\mu_f - \mu_{ref}) = \mu_o + (\mu_f - \mu_{ref}) \tag{11}$$

or

$$\mu'_f = \mu_o + (\mu_f - \mu_{ref}). \tag{12}$$

For precipitation, respectively, we find:

$$\mu'_f = \mu_o * (\mu_f / \mu_{ref}). \qquad (13)$$

Obviously, both transformations are linear and they conserve the C-index, as proved above. The trends are sufficient to assess the extent of climate change as a whole in the area of integration, and together with the C-index they can be used as coordinates to analyze the original signal from the models. Additionally, as mentioned in *Maraun* (2016), the delta change method is a useful benchmark for bias correction. Indeed, this method imposes the trend towards the actually measured sequence of cases. There is no "transfer" function as in other BCMs. This is the reason to introduce a reversed analogue, using the sequence from the future period.

Let μ_o be the average obtained from the observation (temperature or precipitation). The corrected range of temperature for the future is:

$$Y_i^{cor} = Y_i + (\mu_o - \mu_{ref}), \qquad (14)$$

and for precipitation it is:

$$Y_i^{cor} = Y_i * (\mu_o / \mu_{ref}). \qquad (15)$$

For averages, we find:

$$(\textstyle\sum Y_i^{cor})/N = \mu'_f = (\textstyle\sum Y_i)/N + (\mu_f - \mu_{ref}) = \mu_f + (\mu_o - \mu_{ref}), \qquad (16)$$

or

$$\mu'_f = \mu_f + (\mu_o - \mu_{ref}) = \mu_o + (\mu_f - \mu_{ref}). \qquad (17)$$

For precipitation respectively we find:

$$\mu'_f = \mu_f * (\mu_o / \mu_{ref}) = \mu_o * (\mu_f / \mu_{ref}). \qquad (18)$$

The reason for naming this method as a "reverse delta change" (RDC) is that the dependencies between the mean values for both methods have identical equations as it was proved.

Now, the transfer functions are:

$$(\mu_o - \mu_{ref}) \text{ and } (\mu_o / \mu_{ref}), \qquad (19)$$

so the transformations are linear. As a second method we will consider the quantile mapping (QM).

To illustrate the application of both methods and the dependence of the C-index on them, we will use observations from Cherni Vrah, the highest peak in the Vitosha Mountains. The synoptic station was established in 1935. At that time it

was the highest mountain station. There has been no interruption of the observations, and the measurement method has been retained so far. There are no influences from industrial and urban changes or replacement, unlike at other stations.

The transfer functions defined by the Quantile-Quantile plots are shown in the next figures. To find a more general relationship between the observed and modeled data, we do not divide them into seasons. We assume that a certain observed value corresponds to a given modeled value regardless of the season. This assumption is justified by the results below. In *Figs. 9a* and *9b,* the transfer functions for temperature and precipitation from the ALADIN simulation are in the top right corners of the plots. The same is in *Figs. 10a* and *10b*, but for RegCM.
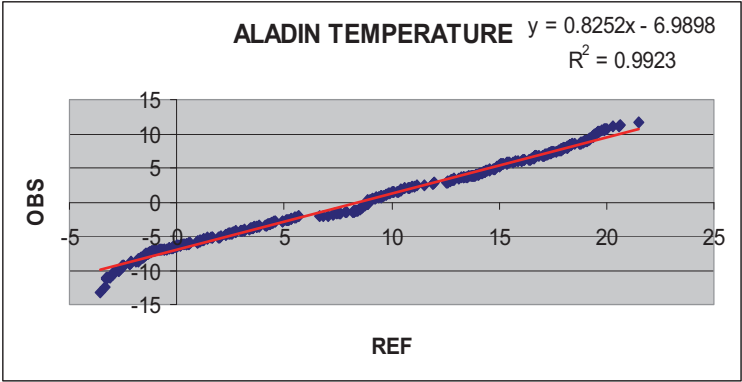
Fig. 9a. Quantile-Quantile plot comparing the distribution of observed (Cherni Vrah station) and modeled (ALADIN) temperature data for the period 1975–2004. The transfer function for temperature from the ALADIN simulation is in the top right corner of the plot.
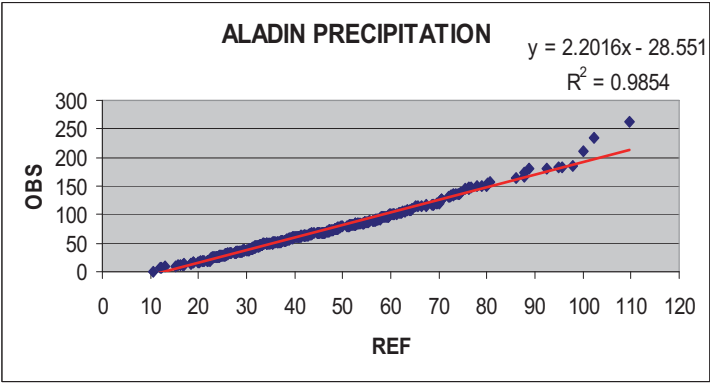
Fig. 9b. Quantile-Quantile plot comparing the distribution of observed (Cherni Vrah station) and modeled (ALADIN) precipitation data for the period 1975–2004. The transfer function for precipitation from the ALADIN simulation is in the top right corner of the plot.
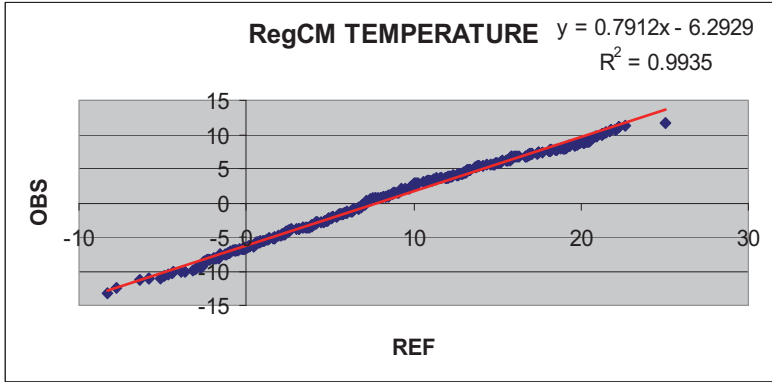
Fig. 10a. Quantile-Quantile plot comparing the distribution of observed (Cherni Vrah station) and modelled (RegCM4) temperature data for the period 1975–2004. The transfer function for temperature from the RegCM4 simulation is in the top right corner of the plot.
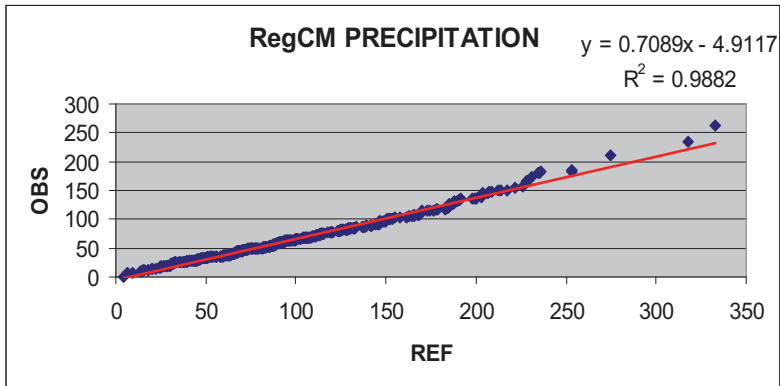
Fig. 10b. Quantile-Quantile plot comparing the distribution of observed (Cherni Vrah station) and modelled (RegCM4) precipitation data for the period 1975–2004. The transfer function for precipitation from the RegCM4 simulation is in the top right corner of the plot.

As it can be seen, linear functions approximate very well the main part of the quantiles. The C-index should be determined before and after applying the BCM, i.e., the transfer functions should be applied to the original data from the reference

run according to Eq. (2). Then it happens, that all cases are in this linear part at certain intervals (mean ± standard deviation). The results of these methods are presented in *Table 1* for temperature and in *Table 2* for precipitation.

Table 1. Mean, standard deviation, and C-index before (μ, σ, and C-index) and after (μ', σ' and C-index') applying BCMs (RDC – reverse delta change; QM – quantile mapping) for temperature by using ALADIN and RegCM4 models.

	μ	σ	C-index	μ'	σ'	C-index'
ALADIN RDC	8.741668	7.500746	0.9839572	0.2236101	7.500748	0.9839572
ALADIN QM	8.741668	7.500746	0.9839572	0.2238232	6.189616	0.9839572
RegCM RDC	8.236060	7.827411	0.9627907	0.2236048	7.827417	0.9627907
RegCM QM	8.236060	7.827411	0.9627907	0.2234672	6.193053	0.9627907

Table 2. Mean, standard deviation, and C-index before (μ, σ, and C-index) and after (μ', σ', and C-index') applying BCMs (RDC – reverse delta change; QM – quantile mapping) for precipitation by using ALADIN and RegCM4 models.

	μ	σ	C-index	μ'	σ'	C-index'
ALADIN RDC	43.83639	17.93699	1.024096	67.95747	27.80694	1.024096
ALADIN QM	43.83639	17.93699	1.024096	67.95921	39.49014	1.024096
RegCM RDC	102.7887	55.78205	0.9433199	67.95747	36.87967	0.9433199
RegCM QM	102.7887	55.78205	0.9433199	67.95520	39.54397	0.9433199

In the tables μ, σ, C-index, μ', σ', and C-index' are the mean, the standard deviation, and the C-index before and after applying the BCM. The significant changes in the mean values are mainly due to the distance between the grid points of the models and the station location as well as the topography in model points. We used the closest point (the models have different grids) without any interpolations. The BCM should overcome these discrepancies. Any method for localization will add its own error. We can see that in the results, after these different corrections, the mean values are almost identical. For the temperature, the differences between σ and σ' after using the RDC for any of the models are

insignificant. The standard deviations of temperature and precipitation have similar values after applying both methods for both models. Indices C do not change as expected. Their values for temperature are practically identical for both models. For the precipitation they are on both sides of the benchmark "1".

Another example of using the proposed index is the overall assessment of climate change in the integration domain by means of graphs in the coordinate system of the trend and the C-index. In *Figs. 11a, 11b, 12a,* and *12b* examples are given for temperature and precipitation from ALADIN and RegCM, respectively. The values in the grid points are placed in tendencies–C-index coordinate system.
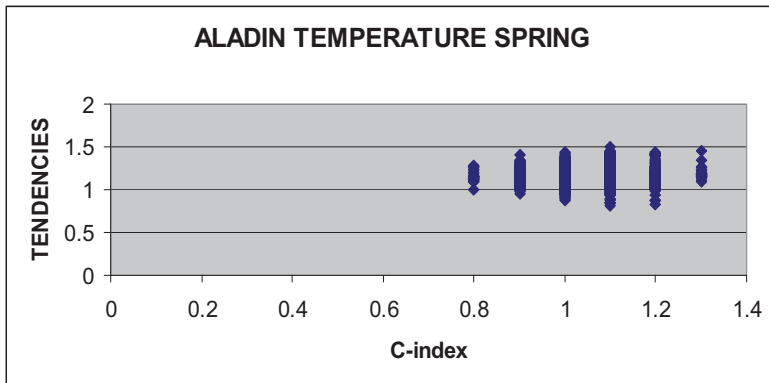
Fig. 11a. Tendencies–C-index chart of temperature during the spring season for the ALADIN model.
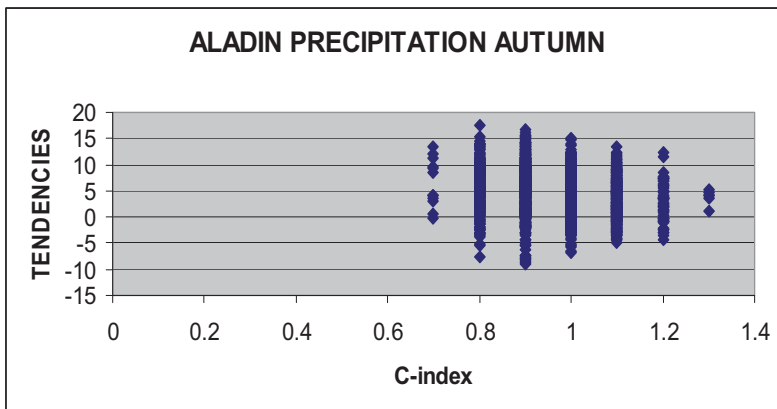
Fig. 11b. Tendencies–C-index chart of precipitation during the autumn season for the ALADIN model.
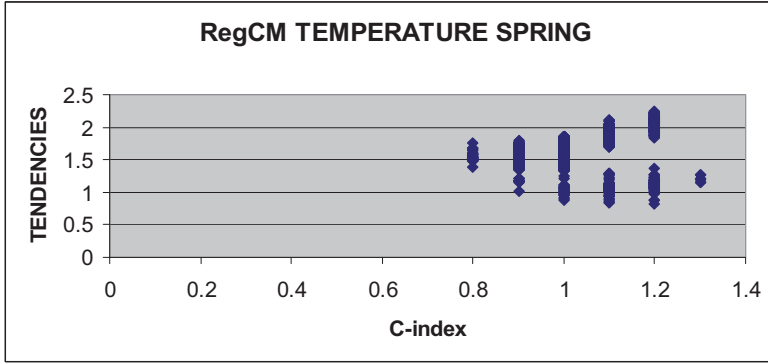
Fig. 12a. Tendencies–C-index chart of temperature during the spring season for the RegCM4 model.
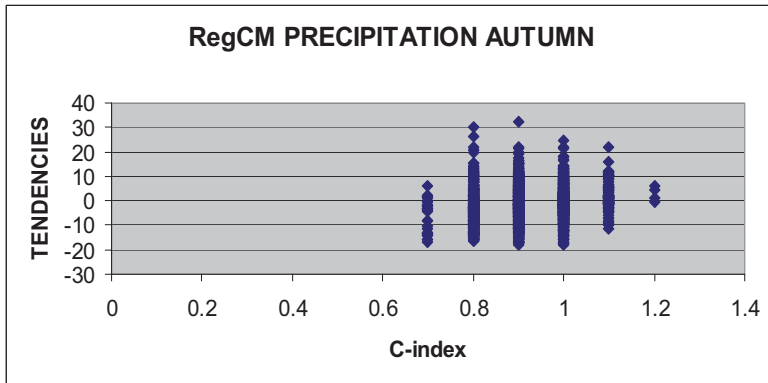
Fig. 12b. Tendencies–C-index chart of precipitation during the autumn season for the RegCM4 model.

Both models have significant munber of cases with C ≥ 1, i.e., these cases remain or are moved within the interval determined by the reference simulations. In spring, ALADIN shows tendencies mainly in the interval 1 – 1.5 °C. RegCM predicts two areas with different temperature tendencies. The first one have tendencies in the interval 1.5 – 2.3 °C and the second one in interval 0.3 – 1.5 °C. Positive rainfall trends in autumn are up to 20% for ALADIN and RegCM. Negative rainfall trends are 10% for ALADIN and up to 20% for RegCM. Generally speaking, RegCM is warmer and drier than ALADIN during these seasons, but both models have a significant number of cases with C ≥ 1, especially for the temperature. Similar diagrams make analyses easier than using maps.

5. Conclusion

All ETCCDI indices analyzed in *Dosio* (2016) are various measures for assessing climate change. The proposed C-index provides two options. The first is to assess the structure of climate change in the future period from the point of view of an "observer" of the climate in the control (reference) period. The other option is to keep the index when applying the "transfer function" as a requirement not to lose the original climate change signal.

From the examples above, it can be seen that in both models there are large areas with the same C-index, determined by the interval $(\mu - \sigma; \mu + \sigma)$. If a bias correction method is applied, the distribution of C-index should be the same, i.e., the figures shown above should remain the same.

The C-index can be defined for each interval $(\delta1, \delta2)$ of different meteorological elements or indices. Within this range, the properties mentioned above will be retained. This index can be considered as a measure of "climate change" at this interval. The smaller the index, the bigger the change in the climate. Another possibility is to use it as an indicator for changing the signal of the model. If the index changes, the logic of the model simulations will be lost. Then the future climate after bias correction will look differently for the "observer" from the reference period.

The determination of the interval depends on the analysis to be made. In the examples presented here, we followed the assumption that the extreme weather is outside the range defined by the mean and standard deviation. If the goal is to assess the change above or below some threshold, then we must take into account the distribution error in the reference period. For example, many models are colder during the reference period and a priori defined threshold may not exist. This indicates an other fact, that should be taken into account. As mentioned in *Dosio* (2016): "Results show that absolute-threshold indices are largely affected by bias adjustment, as they depend strongly on both the present mean climate value (usually largely biased in the original RCMs) and its shift under climate change". The stability of the proposed index depends not only on the error of the model (the linear component has no impact on the index as shown above) but also on the number of cases falling in the chosen interval. A small number will lead to its instability. Methods providing the automatic presence of a significant number of cases, such as using standard deviation, are suitable for determining a stable index.

References

Cattaneo, L., Rillo, V., Manzi, M.P., Villani, V., and Mercogliano, P., 2015: Clime: climate data processing in GIS environment. CMCC Research Papers RP0257.

Collins, W.J., Bellouin, N., Doutriaux-Boucher, M., Gedney, N., Halloran, P., Hinton, T., Hughes, J., Jones, C.D., Joshi, M., Liddicoat, S., Martin, G., O'Connor, F., Rae, J., Senior, C., Sitch, S., Totterdell, I., Wiltshire, A., and Woodward, S., 2011: Development and evaluation of an Earth-system model – HadGEM2. *Geosci. Model Dev. Discuss. 4*, 997–1062. https://doi.org/10.5194/gmdd-4-997-2011

Dai, A., 2006: Precipitation Characteristics in Eighteen Coupled Climate Models. *J. Climate 19*, 4605–4630. https://doi.org/10.1175/JCLI3884.1

Deque, M., 2007: Frequency of precipitation and temperature extremes over France in an anthropogenic scenario: Model results and statistical correction according to observed values. Glob. *Planet. Change 57*, 16–26. https://doi.org/10.1016/j.gloplacha.2006.11.030

Dosio, A., 2016: Projections of climate change indices of temperature and precipitation from an ensemble of bias-adjusted high-resolution EURO-CORDEX regional climate models. *J. Geophys. Res. Atmos. 121*, 5488–5511. https://doi.org/10.1002/2015JD024411

Ehret, U., Zehe, E., Wulfmeyer, V., Warrach-Sagi, K., Liebert, J., 2012: Should we apply bias correction to global and regional climate model data? *Hydrol. Earth Syst. Sci. Discuss 9*, 5355–5387. https://doi.org/10.5194/hessd-9-5355-2012

Giorgi, F, Coppola, E, Solmon, F, Mariotti, L, Sylla, MB, Bi, X, Elguindi, N, Diro, GT, Nair, V, Giuliani, G, Turuncoglu, UU, Cozzini, S, Güttler, I, O'Brien, TA, Tawfik, AB, Shalaby, A, Zakey, AS, Steiner, AL, Stordal, F, Sloan, LC and Brankovic, C, 2012: RegCM4: Model description and preliminary tests over multiple CORDEX domains. *Climate Res.* 52, 7–29. https://doi.org/10.3354/cr01018

Grillakis, M.G., Aristeidis G. Koutroulis, Ioannis N. Daliakopoulos, and Ioannis K. Tsanis, 2017: A method to preserve trends in quantile mapping bias correction of climate modeled temperature. *Earth Syst. Dynam. 8*, 889–900. https://doi.org/10.5194/esd-8-889-2017

Haerter, J.O., B. Eggert, C. Moseley, C. Piani and P. Berg, 2015: Statistical precipitation bias correction of gridded model data using point measurements. *Geophys. Res. Lett. 42*, 1919–1929. https://doi.org/10.1002/2015GL063188

Hagemann, S., Chen, J.O. Harter, J. Heinke, D. Gerten, and C. Piani, 2011: Impact of a statistical bias correction on the projected hydrological changes obtained from three GCMs and two hydrology models. Journal of Hydrometeorology. https://doi.org/10.1175/2011JHM1336.1

Huth, R., 1999: Statistical downscaling in central Europe: evaluation of methods and potential predictors. *Clim. Res*. 13, 91–101. https://doi.org/10.3354/cr013091

Maraun, D., 2016: Bias Correcting Climate Change Simulations - a Critical Review. *Curr. Clim. Change R*ep. https://doi.org/10.1007/s40641-016-0050-x

Mearns, L.O., Bogardi, I., Giorgi, F., Matyasovszky, I., and M. Palecki, 1999: Comparison of Climate Changes Scenarios Generated from Regional Climate Model Experiments and Statistical Downscaling. *J. Geophys. Res. 104*, 6603–6621. https://doi.org/10.1029/1998JD200042

Navarro-Racines, C.E., Tarapues-Montenegro, J.E., and Ramirez-Villegas, J.A., 2015: Bias-correction in the CCAFS-Climate Portal: A description of methodologies. Decision and Policy Analysis (DAPA) Research Area. International Center for Tropical Agriculture (CIAT). Cali, Colombia.

Piani, C., Haerter, J.O., and Coppola, E., 2010: Statistical bias correction for daily precipitation in regional climate models over Europe. *Theor. Appl. Climatol. 99*, 187–192. https://doi.org/10.1007/s00704-009-0134-9

Pierce, D.W., Cayan, D.R., Maurer, E.P., Abatzoglou, J.T., and Hegewisch K.C., 2015: Improved bias correction techniques for hydrological simulations of climate change. J. Hydrometeorol. 16, https://doi.org/10.1175/JHM-D-14-0236.1

Sippel, S., F.E.L. Otto, M. Forkel, M. R. Allen, B.P. Guillod, M. Heimann, M. Reichstein, S. I. Seneviratne, K. Thonicke, and M.D. Mahecha, 2016: A novel bias correction methodology for climate impact simulations. *Earth Syst. Dynam. 7*, 71–88. https://doi.org/10.5194/esd-7-71-2016

Sun, Y., S. Solomon, A. Dai, and *R.W. Portmann,* 2006: How often does it rain? *J. Climate 19*, 916–934. https://doi.org/10.1175/JCLI3672.1

Switanek, M.B., Peter A. Troch, C.L. Castro, A. Leuprecht, H.-I Chang, R. Mukherjee, and *E.M.C. Demaria*, 2017: Scaled distribution mapping: a bias correction method that preserves raw climate model projected changes. *Hydrol. Earth Syst. Sci. 21*, 2649–2666. https://doi.org/10.5194/hess-21-2649-2017

Teutschbein, C., Wetterhall, F., and *Seibert, J.,* 2011: Evaluation of different downscaling techniques. *Clim Dynam.37,* 2087–2105. https://doi.org/10.1007/s00382-010-0979-8

Thomson, A.M., Calvin, K.V., Smith, S.J., Kyle, G.P., Volke, A., Patel, P., Delgado-Arias, S., Bond-Lamberty, B., Wise, M.A., Clarke, L.E., and *Edmonds, J.A.,* 2011: RCP4.5: a pathway for stabilization of radiative forcing by 2100. *Climatic Change 109*, 77–94. https://doi.org/10.1007/s10584-011-0151-4

IDŐJÁRÁS

VOLUME 123 ∗ 2019

EDITORIAL BOARD

BUDAPEST, HUNGARY

AUTHOR INDEX

TABLE OF CONTENTS

I. Papers

SUBJECT INDEX

INSTRUCTIONS TO AUTHORS OF *IDŐJÁRÁS*

The purpose of the journal is to publish papers in any field of meteorology and atmosphere related scientific areas. These may be

- research papers on new results of scientific investigations,
- critical review articles summarizing the current state of art of a certain topic,
- short contributions dealing with a particular question.

Some issues contain "News" and "Book review", therefore, such contributions are also welcome. The papers must be in American English and should be checked by a native speaker if necessary.

Authors are requested to send their manuscripts to

Editor-in Chief of IDŐJÁRÁS
P.O. Box 38, H-1525 Budapest, Hungary
E-mail: journal.idojaras@met.hu

including all illustrations. MS Word format is preferred in electronic submission. Papers will then be reviewed normally by two independent referees, who remain unidentified for the author(s). The Editor-in-Chief will inform the author(s) whether or not the paper is acceptable for publication, and what modifications, if any, are necessary.

Please, follow the order given below when typing manuscripts.

Title page should consist of the title, the name(s) of the author(s), their affiliation(s) including full postal and e-mail address(es). In case of more than one author, the corresponding author must be identified.

Abstract: should contain the purpose, the applied data and methods as well as the basic conclusion(s) of the paper.

Key-words: must be included (from 5 to 10) to help to classify the topic.

Text: has to be typed in single spacing on an A4 size paper using 14 pt Times New Roman font if possible. Use of S.I.

units are expected, and the use of negative exponent is preferred to fractional sign. Mathematical formulae are expected to be as simple as possible and numbered in parentheses at the right margin.

All publications cited in the text should be presented in the *list of references*, arranged in alphabetical order. For an article: name(s) of author(s) in Italics, year, title of article, name of journal, volume, number (the latter two in Italics) and pages. E.g., *Nathan, K.K.,* 1986: A note on the relationship between photo-synthetically active radiation and cloud amount. *Időjárás 90,* 10–13. For a book: name(s) of author(s), year, title of the book (all in Italics except the year), publisher and place of publication. E.g., *Junge, C.E.,* 1963: *Air Chemistry and Radioactivity.* Academic Press, New York and London. Reference in the text should contain the name(s) of the author(s) in Italics and year of publication. E.g., in the case of one author: *Miller* (1989); in the case of two authors: *Gamov* and *Cleveland* (1973); and if there are more than two authors: *Smith et al.* (1990). If the name of the author cannot be fitted into the text: *(Miller,* 1989); etc. When referring papers published in the same year by the same author, letters a, b, c, etc. should follow the year of publication. DOI numbers of references should be provided if applicable.

Tables should be marked by Arabic numbers and printed in separate sheets with their numbers and legends given below them. Avoid too lengthy or complicated tables, or tables duplicating results given in other form in the manuscript (e.g., graphs). *Figures* should also be marked with Arabic numbers and printed in black and white or color (under special arrangement) in separate sheets with their numbers and captions given below them. JPG, TIF, GIF, BMP or PNG formats should be used for electronic artwork submission.

More information for authors is available: journal.idojaras@met.hu